1

Solid State Electrochemistry I: Thermodynamics and Kinetics of Charge Carriers in Solids

Joachim Maier

Max-Planck-Institut für Festkörperforschung, Heisenbergstraße 1, 70569 Stuttgart, Germany. E-mail: s.weiglein@fkf.mpg.de

I. INTRODUCTION

This contribution deals with thermodynamics and kinetics of charge carriers in solids in the case of zero or non-zero electrical or chemical driving forces. It does not intend to repeat well-known electrochemical principles, however, it intends to underline the special situation in solids by, on one hand, emphasizing characteristic aspects due to the solid nature, but on the other hand, stressing the common and generalizing aspects of the picture whenever it appears necessary. This also implies that specific solid state aspects (such as structural details, anisotropies or strain effects) are neglected whenever their influence is not indispensable for the understanding.

The present contribution does not include solid state techniques to measure electrochemical parameters, nor does it consider applications of solid state electrochemistry. Such topics will be dealt with in a second part which will appear separately.[1]

In the traditional electrochemical community solids have a long tradition, however, almost exclusively from the stand-point of electronic processes. Careful studies have been performed in order to understand the behavior of metallic or semi-conductive electrodes in contact to liquid electrolytes in great detail. Ionic processes are mostly considered to occur "outside" the solid, i.e., on its surfaces or in the fluid phases adjacent. More recently, in particular in conjunction with applications such as lithium batteries or fuel cells the ionic conductivity and the appearance of mixed ionic electronic conductivity within the solid state is more and more appreciated, but even in "modern" electrochemical textbooks one hardly finds any specific mention of the ionic charge carriers in solids, which are the ionic point defects. On the other hand, such considerations are in the focus of entire solid state communities which, however, vastly concentrated on solid electrolytes. Recently and again triggered by electrochemical applications such as batteries, fuel cells, sensors or chemical filters, interfacial processes are more and more getting to the fore in the field of solid state ionics. Hence, treatments that try to combine and generalize relevant aspects and concepts are desired. The contribution does not aim to be exhaustive, it concentrates on issues being particularly relevant in this context. It can partly rely on and refer to a variety of excellent existing reviews[2-22] and in particular on a comprehensive monograph that appeared recently.[23,24]

II. SOLIDS VS. LIQUIDS

If a liquid is reversibly cooled below the melting point, the solid, i.e., a three-dimensional giant molecule ("3D polymer") forms, characterized by a long range order. So-formed crystals exhibit strict periodicity. While, in the case of liquids, structural configurations fluctuate in space and time, glasses as "frozen liquids" or other amorphous solids show also fluctuations but essentially only with respect to the position coordinate.

There is neither a sharp demarcation in the treatment of solids compared to molecular units, nor is there a strict demarcation in the treatment of different bonding types. It is Schrödinger's (or Dirac's) equation that describes the bonding situation in all cases. Nonetheless, it proves meaningful to use "ad hoc" classifications.

In some cases the bond strength between the "monomers" (intermolecular forces) is weak and molecular crystals are formed, in others the intermolecular forces are not at all saturated within the monomer and no real distinction between inter- and intramolecular forces can be made, as is the case in typical ionic crystals, covalent crystals or metal crystals. In the latter two cases the orbitals of the bonding partners severely overlap forming comparatively wide bands in which the electrons are delocalised. In the case of metals (e.g. Na) the topmost non-empty band is only partially filled also in the thermal ground state, and the outer electrons are nearly freely mobile. In the case of typical covalent crystals (such as Si), at $T = 0$ K the topmost non-empty band is completely filled, the electrons therein immobile, and the bands of higher lying unoccupied levels separated by a substantial gap (which corresponds to the energy distance between the bonding and anti-bonding level in the two-atom problem). Those electrons can also be thought to be situated between the bonding partners. In the case of ionic crystals (e.g. NaCl) the bonding electrons are affiliated with orbitals of the electronegative partners only. Hence orbitals of the anionic partner usually form the highest occupied band while orbitals of the cationic partner form the lowest unoccupied band. (This is at least so in the case of main group elements. In a variety of transition metal oxides, e.g., both valence and conduction bands refer to the cationic states.) Owing to poor interaction of the atoms of the same kind the bands are quite narrow. (In this context it is also worthy of mention that — according to Mott — too large a distance between atoms prevents sufficient orbital overlap and delocalization.[25,26])

As well known from semiconductor physics, in non-metals electrons are, at finite temperatures, excited from the highest occupied band to the lowest unoccupied band to form excess electrons in the conduction band and electron holes in the valence band. Owing to long-range order each crystal possesses a certain amount of "free" electronic carriers. The mixed conductor which exhibits both ionic and electronic conductivity, will play an important role in this text, since it represents the general case, and pure ionic and electronic (semiconductors) conductors follow as special cases.

Under the conditions we will refer to here (the yield strength is not reached), a potentially applied stress does not change the form (no plastic deformation) during the electrochemical performance or measurements, rather is elastically supported. (The viscosity is virtually infinite; only at very high temperatures and/or extreme driving forces a

creep of the solid becomes possible.) There is no convective flow, and diffusive transport is the decisive mechanism of mass transport. Owing to this, solid-solid contacts frequently exhibit a low degree of perfection.

Under usual conditions at least one sublattice is very rigid and—in the case of interest (in particular when dealing with solid ion conductors)—one sublattice exhibits a significant atomic mobility. The selectivity of the conductivity (cf. also the selective solubility of foreign species) is indeed a characteristic feature of solids.

A paramount role is played by point defects;[1,2] the configurational entropy gained by their presence allows them to be present even in thermodynamical equilibrium; they have their counterpart in liquids and will be considered explicitly in the next chapter.

Further characteristic solid state properties following from the high bond strength compared to kT, are the anisotropies of structure and properties (transport coefficients e.g. are tensors) as well as the occurrence of higher-dimensional defects such as dislocations and internal boundaries.

Grain boundaries are a specific feature of the solid state and are typical non-equilibrium defects. Their metastability, however, is often so high and their influence can be so great that it is very necessary to consider them explicitly. In the following text we will refer to them as frozen-in structure elements with zero mobility. Dislocations are usually more mobile and can often be healed out (if they are not constituting grain boundaries); we will neglect them in the following.

While external boundaries are in principle necessary because of mass conservation, their amount, nature and arrangement, and hence the shape, are usually not in equilibrium. (As long as we can ignore the energetic influence of intersections of surfaces, the Wulff-shape represents the equilibrium shape of crystals.[27,28] The Wulff-shape is characterized by a ratio of surface tension and orthogonal distance from the center that is common to every surface plane; as it is only rarely established, we will also consider the shape as frozen-in.) The occurrence of internal interfaces leads to the fact that upon the (usually strictly periodic) atomic structure we have to superimpose the micro-structure which is of rather fuzzy periodicity – if we may use this term at all. Lastly let us come back to the point that sluggish kinetics prevent many materials from adopting the ordered state: In inorganic glasses or many polymers the atomic structure is amorphous. Then, as already stated, structural fluctuations occur in space but under usual conditions

not in time. Let us start with the atomic structure and the ionic charge carriers therein.

III. POINT DEFECTS AS CHARGE CARRIERS

The ionic charge carriers in ionic crystals are the point defects.[1,2,23,24] They represent the ionic excitations in the same way as H_3O^+ and OH^- ions are the ionic excitations in water (see Fig. 1). They represent the chemical excitation upon the perfect crystallographic structure in the same way as conduction electrons and holes represent electronic excitations upon the perfect valence situation. The fact that the perfect structure, i.e., ground structure, of ionic solids is composed of charged ions, does not mean that it is ionically conductive. In AgCl regular silver and chloride ions sit in deep Coulomb wells and are hence immobile. The occurrence of ionic conductivity requires ions in interstitial sites, which are mobile, or vacant sites in which neighbors can hop. Hence a "superionic" dissociation is necessary, as, e.g. established by the Frenkel reaction:

$$Ag_nCl_n + Ag_{n'}Cl_{n'} \underset{\leftarrow}{\rightarrow} (Ag_{n+1}Cl_n)^+ + (Ag_{n'-1}Cl_{n'})^- \qquad (1)$$
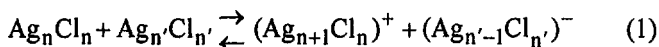
or more concisely in a "molecular notation"

$$2\,AgCl \underset{\leftarrow}{\rightarrow} Ag_2Cl^+ + \Box Cl^- \qquad (2)$$

where it is indicated that a vacancy is formed within the cluster from which Ag^+ is removed.

A major difference of the crystalline state compared with the liquid state, is that the sites are crystallographically defined and need to be conserved in such reactions. In defect nomenclature this crystallographic site is usually given as a lower index, where i denotes the interstitial site which is occupied in $(Ag_{n+1}Cl_n)^+$, or referring to Eq. (2) in the Ag_2Cl^+ unit. In the rock-salt structured AgCl where the Ag^+ ions regularly occupy all octahedral interstices of the close-packed
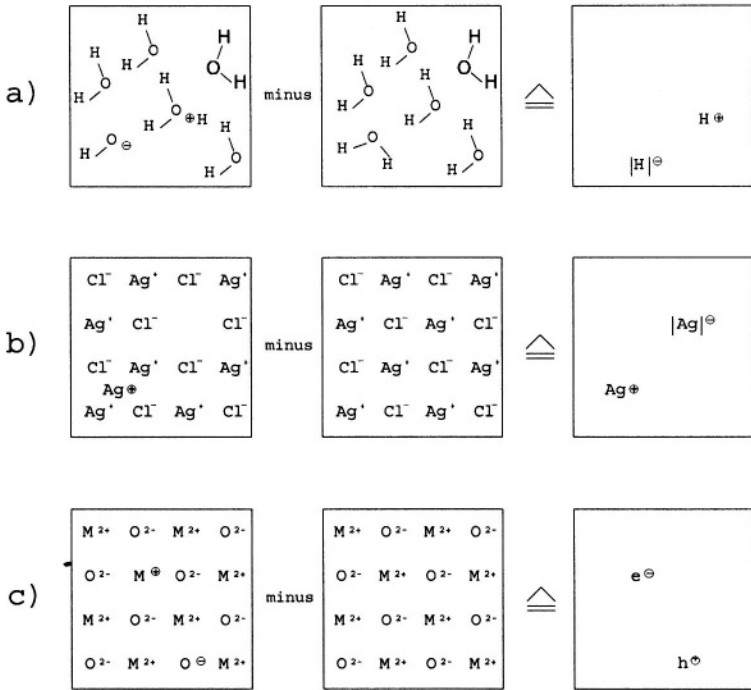
Figure 1. a) If the compositionally unperturbed structure (chemical ground structure) is substracted from the real structure, the point defects shown on the right remain. Naturally each is surrounded by a distorted region (effective radius of the point defect) which affects at least the immediate neighborhood. In the case of fluid phases (see above) this procedure can only be regarded as an instantaneous picture. Owing to the absence of defined sites no distinction is made between various types of defect reactions as is done in the solid state. b) Frenkel disorder is sketched in the second row. c) Third row shows the case of purely electronic disorder. Here the charge carriers are assumed to be localized for the sake of clarity.[20]

chlorine lattice $(n' = 6)$, the interstitial site is the tetrahedral interstice ($n = 4$). Instead of writing $\square$ it is customary to use the symbol $\vee$ (for vacancy).[2]
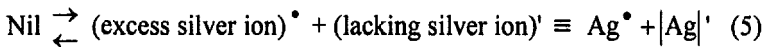
Since the above disorder reaction is restricted to the silver sublattice we can condense Eq. (2) to the even more concise form:

$$Ag^+_{Ag^+} + \vee^0_i \underset{\leftarrow}{\rightarrow} Ag^+_i + \vee^0_{Ag^+} \qquad (3)$$
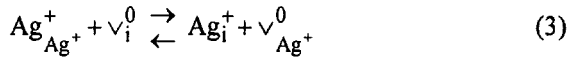
As already considered, the absolute charges do not really matter, the regular Ag-ion, $Ag^+_{Ag^+}$, is not mobile in contrast to the silver vacancy $\vee^0_{Ag^+}$. Hence it is advantageous to refer to relative charges (the structure element $M^{z^\bullet}_{S^{z^r}}$ has the relative charge $z^\bullet - z^r$). Omitting the absolute charges leads to the Kröger-Vink formulation[29]

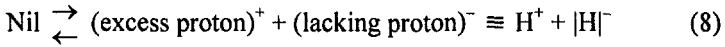$$Ag^x_{Ag} + \vee^x_i \underset{\leftarrow}{\rightarrow} Ag^\bullet_i + \vee'_{Ag} \qquad (4)$$
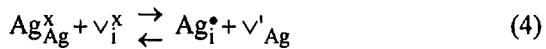
Here the cross denotes the relative charge zero, the prime ' the relative charge -1 and the dot · the relative charge +1. Even though it is the special notation that creates quite an activation barrier to deal with point defect chemistry, it proves extremely helpful, once being familiar with it. Equation (4) denotes the so-called Frenkel reaction in structural element formulation, i.e., in terms of particles that actually constitute the real crystal. Unfortunately, thermodynamics demand strictly speaking the treatment of so-called building elements, elements that you can add to the perfect crystal.[30] The chemical potential of a vacant site, e.g. measures the increase in Gibbs energy on adding a vacancy. However, adding the structure element vacancy $(\vee'_{Ag})$ requires the removal of a lattice constituent (Ag^x_{Ag}). This leads to a complete relative description in which the Frenkel reaction is described by

$$\text{Nil} \underset{\leftarrow}{\rightarrow} (\text{excess silver ion})^\bullet + (\text{lacking silver ion})' \equiv Ag^\bullet + |Ag|' \quad (5)$$

(On the r.h.s. the defects are written in Schottky's building element notation,[30] also used in Fig. 1.) Equation (5) is obtained by subtracting 2AgCl from Eq. (2) or bringing the regular constituents in Eq. (4) to the right hand side: Obviously $(\text{excess silver ion})^\bullet \equiv (Ag^\bullet_i - Ag^x_{Ag})$ and
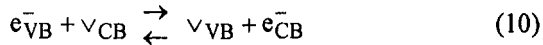
(lacking silver ion)$' \equiv \vee'_{Ag} - Ag^{x}_{Ag}$ are the entities for which chemical potentials can be rigorously defined.

The treatment in terms of excess and lacking particles is the key to defect chemistry. The similarity with "aqueous chemistry" is obvious: We end up with an analogous "disorder" equation (as a snap-shot at a given time) with H_3O^+ and OH^- as "defects" when removing all H_2O from the autoprotolysis reaction:

$$2\,H_2O \underset{\leftarrow}{\overset{\rightarrow}{}} H_3O^+ + OH^- \tag{6}$$

$$H_2O \underset{\leftarrow}{\overset{\rightarrow}{}} H^+ + OH^- \tag{7}$$

$$Nil \underset{\leftarrow}{\overset{\rightarrow}{}} (\text{excess proton})^+ + (\text{lacking proton})^- \equiv H^+ + |H|^- \tag{8}$$

(compare Eq. 6 with Eq. 2; Eq. 7 with Eqs. 3 and 4; and Eq. 8 with Eq. 5). Here we still can use absolute charges since the ground state is uncharged.
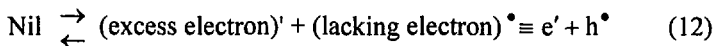
The analogous situation is met if we excite an electron from the ground state (electron in the valence band, VB) to an energetically higher position (in the conduction band, CB), e.g. in silicon, according to

$$Si_{Si} + Si_{Si} \underset{\leftarrow}{\overset{\rightarrow}{}} Si^+_{Si} + Si^-_{Si} \tag{9}$$

$$e^-_{VB} + \vee_{CB} \underset{\leftarrow}{\overset{\rightarrow}{}} \vee_{VB} + e^-_{CB} \tag{10}$$

the symbol $\vee$ denotes here the electronic vacancy (hole). Equation (10) reads in relative charges

$$e^x_{VB} + \vee^x_{CB} \underset{\leftarrow}{\overset{\rightarrow}{}} e'_{CB} + \vee^{\bullet}_{VB} \tag{11}$$

or simpler in building element notation ($e' \equiv e'_{CB} - v^x_{CB}$,

$h^\bullet \equiv v^\bullet_{VB} - e^x_{VB} \equiv |e|^\bullet$)

$$\text{Nil} \; \underset{\leftarrow}{\rightarrow} \; (\text{excess electron})' + (\text{lacking electron})^\bullet \equiv e' + h^\bullet \qquad (12)$$

Equation (12) is independent of any detailed knowledge of the band structure. In AgCl where the valence band is formed by the Cl-p orbitals and the conduction band by the Ag-d orbitals, the detailed formulation of Eq. (12) would read

$$Ag^+ + Cl^- \; \underset{\leftarrow}{\rightarrow} \; Ag^0 + Cl^0 \qquad (13)$$
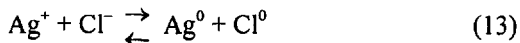
while in PbO, to mention a main group metal oxide (see Fig. 1c), we would have to write

$$Pb^{2+} + O^2 \; \underset{\leftarrow}{\rightarrow} \; Pb^+ + O^- \qquad (14)$$

In the case of transition metal compounds such as **LaMnO$_3$** d-level splitting can be so pronounced that both valence and conduction band are derived from d-orbitals. For **LaMnO$_3$,** e.g. Eq. (12) has to be interpreted as a redox disproportionation

$$Mn^{3+} + Mn^{3+} \; \underset{\leftarrow}{\rightarrow} \; Mn^{4+} + Mn^{2+} \qquad (15)$$
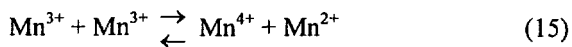
Note that generally bands correspond to hybrids, and attributing bands to certain elements is an approximation. Unlike the electronic "energy" level distribution, the distribution of ionic "energy" levels in crystals (the meaning of which we will consider in the next section) is discrete. In the electronic case we face bands comprising a manifold of narrowly neighbored levels, so that we better speak of a continuous density of states.
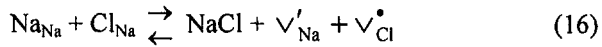
In a fluid system such as water the energy levels can be conceived as smeared out on spatial and time average, while in amorphous solids

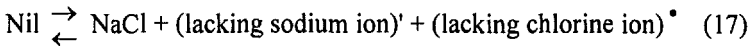the structure fluctuations occur in space but (approximately) not in time (see e.g. Refs.[31-34]).

IV. EQUILIBRIUM CONCENTRATION OF CHARGE CARRIERS IN THE BULK

1. Defect Reactions

A major difference between crystals and fluids refers to the necessity of distinguishing between different sites. So the autoprotolysis in water could, just from a mass balance point of view, also be considered e.g. as a formation of a OH^- vacancy and a H^+ vacancy. In solids such a disorder is called Schottky disorder (S) and has to be well discerned from the Frenkel disorder (F). In the densely packed alkali metal halides in which the cations are not as polarizable as the Ag^+, the formation of interstitial defects requires an unrealistically high energy and the dominating disorder is thus the Schottky reaction
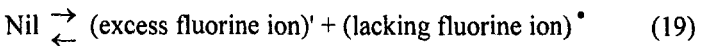
$$Na_{Na} + Cl_{Na} \underset{\leftarrow}{\overset{\rightarrow}{}} NaCl + v'_{Na} + v^{\bullet}_{Cl} \qquad (16)$$

which reads in building element notation

$$Nil \underset{\leftarrow}{\overset{\rightarrow}{}} NaCl + (\text{lacking sodium ion})' + (\text{lacking chlorine ion})^{\bullet} \quad (17)$$

In particular if the anions are as small as F^-, e.g. in CaF_2, we can have Frenkel disorder in the anion sublattice, which is also referred to as anti-Frenkel-disorder ($\overline{\overline{F}}$),
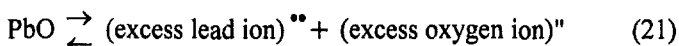
$$F_F + v_i \underset{\leftarrow}{\overset{\rightarrow}{}} F'_i + v^{\bullet}_F \qquad (18)$$

Equation (18) reads in building element notation

$$Nil \underset{\leftarrow}{\overset{\rightarrow}{}} (\text{excess fluorine ion})' + (\text{lacking fluorine ion})^{\bullet} \qquad (19)$$

In addition, there should also be the possibility of having the so-called anti-Schottky reaction ($\overline{S}$) in materials with comparatively loose structures, such as orthorhombic PbO

$$PbO + v_{i(Pb)} + v_{i(O)} \; \underset{\leftarrow}{\rightarrow} \; Pb_i^{\bullet\bullet} + O_i'' \tag{20}$$
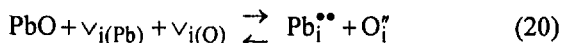
or in terms of building elements

$$PbO \; \underset{\leftarrow}{\rightarrow} \; (\text{excess lead ion})^{\bullet\bullet} + (\text{excess oxygen ion})'' \tag{21}$$

More complex internal defect reactions involve association reactions or doping effects; they will be considered later. (For more extensive treatments of defect chemistry see Ref.[2])

All these reactions leave the 1:1 composition, the "Dalton composition"[23], unchanged. However, according to the phase rule, stoichiometric variations are possible by tuning the chemical potential of one component, e.g. the chlorine partial pressure over AgCl or the oxygen partial pressure over PbO, (or generally n-1 component partial pressures in a n-component multinary, e.g. the O_2 and SrO partial pressures over $SrTiO_3$). The interaction with oxygen may be formulated as:

$$\frac{1}{2}O_2 + v_O^{\bullet\bullet} + 2e' \; \underset{\leftarrow}{\rightarrow} \; O_o \tag{22}$$
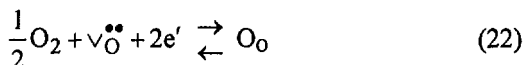
meaning that the oxygen is incorporated on a vacant site as O^{2-} which requires the annihilation of two conduction electrons. Equally the interaction could have been formulated by assuming that two regular electrons are annihilated (and $2h^{\bullet}$ would be formed), or we could have incorporated oxygen ions into interstitial sites. In equilibrium one formulation suffices, since the others follow by reaction combinations. It is advisable to use a formulation in terms of majority carriers. Evidently, Eq. (22) involves the ionic and electronic defects, changes the oxide $MO_{1+\delta}$ into $MO_{1+\delta+\Delta\delta}$ and implies a variation of the mean oxidation numbers. (In ternary systems such stoichiometric changes can occur without involving the electronic budget, e.g. the incorporation of H_2O in NaOH.)

Figure 2. Electronic and ionic disorder in ionic solids and in water in "physical" (top) and "chemical" language (bottom).[20] The coupling of the ionic and electronic Fermi levels takes place via the chemical potential of the neutral components (here: $\tilde{\mu}_{Ag^+} + \tilde{\mu}_{e^-} = \mu_{Ag}$) (see Fig. 3). A further relevant example could be the breaking-up of an ion pair in a polymer.

For a given material all the defect reactions considered so far occur to a greater or lesser extent. It is the problem of the next section to show how the equilibrium concentrations of all defects (including electronic carriers) can be calculated.

2. Equilibrium Defect Concentrations in Pure Compounds

Figure 2 translates the charge carrier formation reaction into an "energy level" diagram for various systems. In fact these levels refer to standard chemical potentials or (in the case of the "Fermi-levels") to full chemical potentials (see e.g. Refs.[3,35]). As long as —in pure materials— the gap remains large compared to RT, the Boltzmann-form of the chemical potential of the respective charge carrier (defect) is valid,

$$\mu_j = \mu_j^o + RT \ln (c_j / c_j^o) \tag{23}$$

independent of the charge carrier situation and also independent of the form of the energy level distributions. If there is a smearing out of the levels or even a band of levels, μ_j^o refers to an effective level, such as the band edges when dealing with the electronic picture. Equation (23) results from a simple combinatorial analysis by assuming a random configurational entropy, and it is the configurational entropy which is the reason why defective states of atomic dimensions (such as vacancies, interstitial sites, excess electrons, holes, H_3O^+, OH^- etc.) are important in thermal equilibrium, i.e., exhibiting non-zero concentrations. Figure 3 shows the coupling of the ionic level picture and the electronic level picture for AgCl via the thermodynamic relation $\mu_{Ag^+} + \mu_{e^-} = \mu_{Ag}$ and hence via the precise position in the phase diagram.

Let us consider an elemental crystal first (with defect d). If N_d identical defects are formed in such a crystal of N identical elements, a local free enthalpy of Δg_d^0 is required to form a single defect, and if interactions can be neglected, the Gibbs energy of the defective crystal (G_p refers to the perfect crystal) is

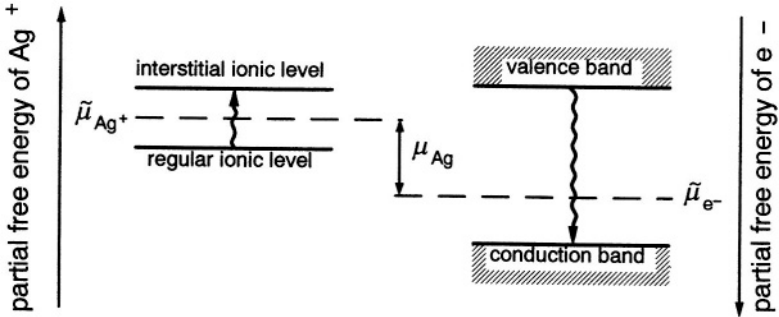$$G = G_p + N_d \Delta g_d^o - k_B T \ln \binom{N}{N_d} \tag{24}$$

Figure 3. Coupling of ionic and electronic levels in AgCl.[36,37] (Reprinted from J. Maier, "Defect chemistry and ion transport in nanostructured materials. Part II. Aspects of nano-ionics." *Solid State Ionics,* **157,** 327-334. Copyright © 2003 with permission from Elsevier.)

(For a description of how Δg^0 can be atomistically computed, the reader is referred to the literature.[18,38-40]) Owing to the infinitely steep decrease of the configurational entropy term (cf. last term in Eq. 24) there is a minimum in G (see Fig. 4) that occurs in our elemental crystal if the
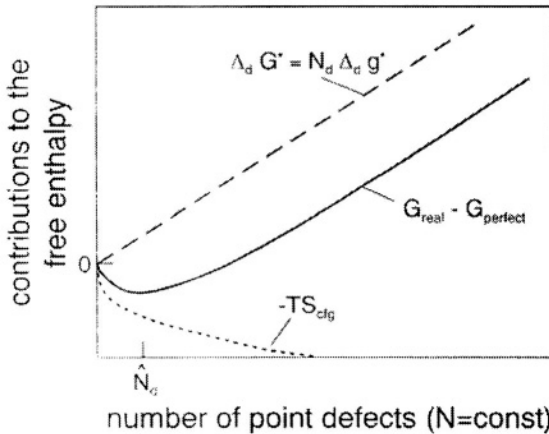
Figure 4. Contributions to the free enthalpy of the solid by defect formation with a constant total number of sites.

chemical potential of d, i.e., $\mu_d \equiv \partial G / \partial (N_d / N_m)$, vanishes, which is given by

$$\mu_d = \mu_d^o + RT \ln \frac{N_d}{N - N_d} \simeq \mu_d^o + RT \ln \frac{N_d}{N} = \mu_d^o + RT \ln \frac{n_d}{n} \qquad (25)$$

Equation (25) follows after differentiation and application of Stirling's formula ($n \equiv N/N_m$, $n_d \equiv N_d/N_m$, N_m = Avogadro's number; $\mu^o = N_m \Delta g^o_d$). It is worthy to note that the strict result (see l.h.s. of Eq. 25) which is formally valid also for higher concentrations, is of the Fermi-Dirac type. This is due to the fact that double occupancy is forbidden and hence the sites are exhaustible similar as it is the case for the quantum states in the electronic problems.

  If we consider a situation in which the levels are broadened to a more or less continuous zone the Fermi-Dirac form given by Eq. (25) l.h.s. is only valid, if we attribute N_d and μ_d^o to an infinitely small level interval (ranging from E_d to $E_d + dE_d$); then in order to obtain the total concentration, the molar density of states $D (E_d)$ has to be considered, and the result for n_d follows by integration:

$$n_d = \int_{\text{zone}} \frac{D (E_d)\, dE_d}{1 + \exp \dfrac{|E_d - \mu_d|}{RT}} \qquad (26)$$

Note that μ_d (Fermi-level) is independent of E_d in equilibrium. Equation (26) has been discussed for a variety of state densities (delta function for point defects in crystals, Gaussian function for charge carriers in an amorphous matrix, parabolic for electronic carriers in ideal band) in Ref.[31] The above considerations can be obviously only applied to situations in which carriers are statistically distributed, i.e., particles in almost empty zones or vacancies (holes) in an almost full zone. The T-dependence of the occupation refers to the thermal excitation from the top occupied zone to the lowest empty zone. In the systems of interest the Fermi-level (μ_d) lies in between these two zones with the absolute distance between μ_d and the neighbored zone edges being great compared to RT. If, without restriction of generality, the almost empty zone is considered and the lower edge of this zone designated as E_d', for all levels more distant from μ_d than E_d' the unity in the denominator of Eq. (26) can be neglected, leading to

$$n_d \approx \bar{n}_d(T)\exp{-\left|E'_d - \mu_d\right|/RT} \tag{27}$$

where by the effective value is given by

$$\bar{n}_d(T) = \int_{\text{zone}} dE_d \left\{ D(E_d)\exp{-\left|E_d - E'_d\right|/RT} \right\} \tag{28}$$

and is usually only a weak function of temperature.[32] Equation (28) as Eq. (26) ignores changes of the parameters with occupation (in semiconductors this is called rigid band model).

 As anticipated above, the Boltzmann-form of the chemical potential results. If n in Eq. (25) is identified with $\bar{n}_d$, the effective value μ_d^o is given by E'_d. As long as we refer to dilute conditions, freedom of normalization is left with respect to the concentration measure (see Eq. 23).

 At this point we do not want to treat the case of high concentrations, since then we also have to include interactions. However, we want to draw the reader's attention to a peculiar point: Thermodynamically μ_d refers to the defect as a building element for which an activity term $N_d/(N-N_d)$ results at high concentrations. Frequently, in the literature structure elements (defective and regular ones) are used in the thermodynamic treatment.[29] Even though not correct a priori, it leads to correct results if they are defined properly, since $x_d \equiv N_d/N$ is the concentration of the defective structural unit and $1 - x_d$ is the concentration of the regular constituent (replaced by the defective one) owing to mass conservation. By applying Boltzmann approximations to both we automatically end up with the Fermi-Dirac correction when we later formulate mass action laws. This is also well known when dealing with Langmuir adsorption. The adsorbed species has the activity $\theta/(1-\theta)$ which can also be expressed as the mass action ratio of occupied (θ) and free sites $(1 - \theta)$.

 Strictly speaking dealing with charged particles requires taking account of the electrochemical potential (already used in Figs. 2 and 3)

$$\tilde{\mu}_d = \mu_d + z_d F\phi \tag{29}$$

which includes the electrical potential ϕ.[41] However, when we deal with bulk problems where ϕ is constant or generally with reactions that are electroneutral at given position, this term cancels.

If one repeats the above statistical derivation for the formation of a pair of defects or for more complicated reactions of the type

$$\text{Nil} \; \underset{\leftarrow}{\overset{\rightarrow}{\rightleftharpoons}} \; \Sigma_j \nu_j A_j \tag{30}$$

Equation (29) is valid for the individual defects as long as interactions and non-random configurational effects can be neglected; hence, mass action laws result

$$\Sigma_j \nu_j \mu_j = 0 = \Sigma_j \nu_j \mu_j^\circ + RT \ln \Pi_j (c_j / c_j^\circ)^{\nu_j} \tag{31}$$

This set of reactions and mass action laws has to be coupled with the electroneutrality reaction

$$\Sigma_j z_j c_j = 0 \tag{32}$$

which is a special case of Poisson's equation for a homogeneous material. Since the mass action laws (dilute) linearly combine the logarithms of the concentrations, we only arrive at simple solutions, if the electroneutrality equation reduces to a proportionality (in the following this case is called Brouwer condition[42]) which is necessarily fulfilled if two (oppositely charged) carriers are in the majority.

Let us explicitly consider an oxide MO and assume that only oxygen defects can be formed to a perceptible extent, then we have to consider the set of internal and external equations given by Table 1. (Note that one disorder reaction is redundant in Table 1.) The free parameters are obviously (i) the temperature which enters the mass action constants (see Table 1) and (ii) the partial pressure P_{X_2} which we also simply term P. (The hydrostatic pressure p is assumed to be constant.) For Brouwer (and Boltzmann) conditions we find results of the type (the index r labels the reaction)

$$c_j(T, P) = \alpha_j^{\beta_j} P^{N_j} \Pi_r K_r(T)^{\gamma_{rj}} \tag{33}$$

Table 1
Simple Defect Chemistry of $M_{1+\delta}X$

Reaction (r)	Mass Action Law
Internal	
Schottky (S)	$[V_X^\bullet][V_M'] = K_S$
Frenkel (F)	$[M_i^\bullet][V_M'] = K_F$
Anti-Frenkel ($\bar{F}$)	$[V_X^\bullet][X_i'] = K_{\bar{F}}$
Anti-Schottky ($\bar{S}$)	$[M_i^\bullet][X_i'] = K_{\bar{S}}$
Band-Band (B)	$[h^\bullet][e'] = K_B$

$$K_r(T) \propto \exp\left[+\frac{\Delta_r S_m^0}{R}\right] \exp\left[-\frac{\Delta_r H_m^0}{RT}\right]$$

External

Reaction with the gas phase (X)	$P_{X_2}^{-1/2}[V_X^\bullet]^{-1}[e']^{-1} = K_X$

Electroneutrality Condition

$$[V_X^\bullet] + [M_i^\bullet] + [h^\bullet] = [V_M'] + [X_i'] + [e'] (\pm C)$$

(N_j, γ_{rj}, α_j, β_j being simple rational numbers.) As the Brouwer conditions are only valid within certain parameter windows (belonging to the P_{O_2} -T-plane) and change from window to window, Eq. (33) is only a sectional solution and N_j, γ_{rj}, α_j, β_j change from window to window. Equation (33) defines van't Hoff-diagrams characterized by

$$-\frac{\partial \ln c_j}{\partial 1/RT} = \sum_r \gamma_r \Delta_r H^o \qquad (34)$$

For not too extended T-ranges $\Delta_r H^o$ is constant and straight lines are observed in the ln c vs. 1/T representation. Also straight lines are observed if we plot ln c_j vs. ln P defining Kröger-Vink diagrams with the characteristic slopes

$$\frac{\partial \ln c_j}{\partial \ln P} = N_j \qquad (35)$$

In most examples we will refer to the conductivity σ_j as a convenient measure of c_j. Since $\sigma_j \propto c_j$ with the proportionality factor containing the mobility $u_j(T)$, the temperature dependence (see Eq. 34) of σ_j will also include the migration enthalpy (cf. Section VI.3.*ii.*), while the P- (and later the C-) dependence (Eqs. 35 and 43) is the same.

Figure 5 displays the internal acid-base and redox chemistry within the phase width of MO. At low P_{O_2} vacant oxygen ions ($v_O^{\bullet\bullet}$) and
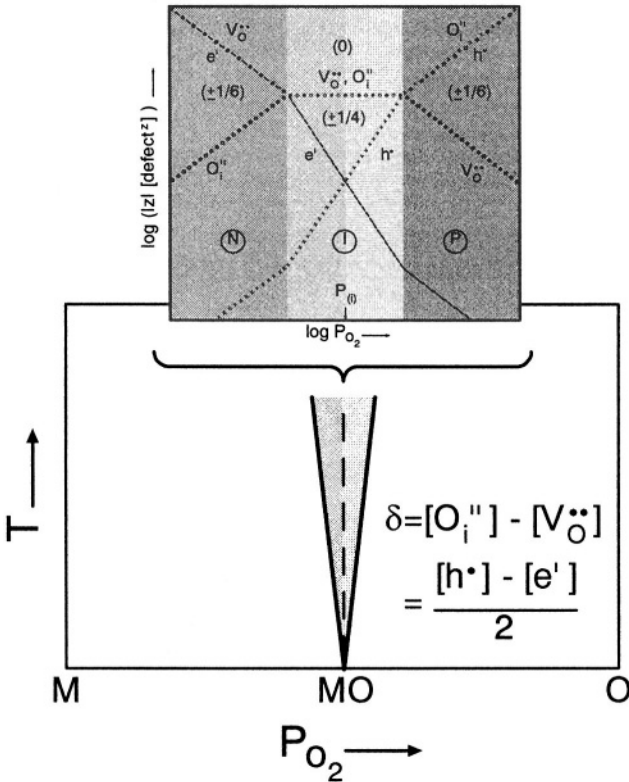
Figure 5. Internal redox and acid-base chemistry in a solid $MO_{1+\delta}$ within the phase width at a given temperature.

reduced   states (e') are   in   the   majority   according   to $2[v_O^{\bullet\bullet}] \approx [e'] >> \quad [O_i''], [h^\bullet]$ (N-regime); oxygen interstitials (O_i'') and   oxidized   states $(h^\bullet)$ dominate   for   very   high P_{O_2}: $2[O_i''] \approx [h^\bullet]$ $>> [e'], [v_O^{\bullet\bullet}]$ (P-regime). At intermediate P_{O_2} usually $[v_O^{\bullet\bullet}] \approx [O_i'']$ $>> [e'], [h^\bullet]$ (I-regime; the alternative $[e'] \approx [h^\bullet] >> [v_O^{\bullet\bullet}], [O_i'']$ is less usual). Exactly at the Dalton-composition, i.e., at $P_{O_2}^{(i)}$ where $2[O_i''] =$ $2[v_O^{\bullet\bullet}] = [e'] = [h^\bullet]$, the "non-stoichiometry" δ in $MO_{1+\delta}$ (i.e., $[O_i'']$ - $[v_O^{\bullet\bullet}] = (1/2)[h^\bullet] - (1/2)[e'])$ is precisely zero. For $\delta >> 0$ we meet a p-conductor (because the mobility of $h^\bullet$ is usually much greater than for O_i''), for $\delta << 0$ we meet (for analogous mobility reasons) an n-conductor, while at $\delta \simeq 0$ mixed conduction is expected (only if the ionic concentrations are much larger than the electronic ones, pure ion conduction is expected). Since there are limits of realizing extreme P_{O_2}–values and also limits with respect to the phase stability (formation of higher oxides, lower oxides or of the metal), usually not the entire diagram is observed.

 Figure 6 gives three examples. SnO_2 is an oxygen deficient material[43,44] and the solution of Eq. (22) with $2[v_O^{\bullet\bullet}] = [e']$ directly leads to

$$[e'] = 2[v_O^{\bullet\bullet}] \propto P_{O_2}^{-1/6} \tag{36}$$

(The slopes of -1/4 at lower T stem from doping effects, see below.) La_2CuO_4 is an example of a p-type conduction for which $[h^\bullet] = 2[O_i'']$; it follows that

$$[h^\bullet] = 2[O_i''] \propto P_{O_2}^{+1/6} \tag{37}$$

Figure 6. Three experimental examples of Kröger-Vink diagrams in a pure oxide MO with ideal defect chemistry: SnO_2 as n-type conductor, PbO as mixed conductor and La_2CuO_4 as p-type conductor.[45] (Reprinted from J. Maier, "Ionic and Mixed Conductors for Electrochemical Devices," *Radiat. Eff. Defects Solids,* **158,** 1-10. Copyright ©2003 with permission from Taylor & Francis.)
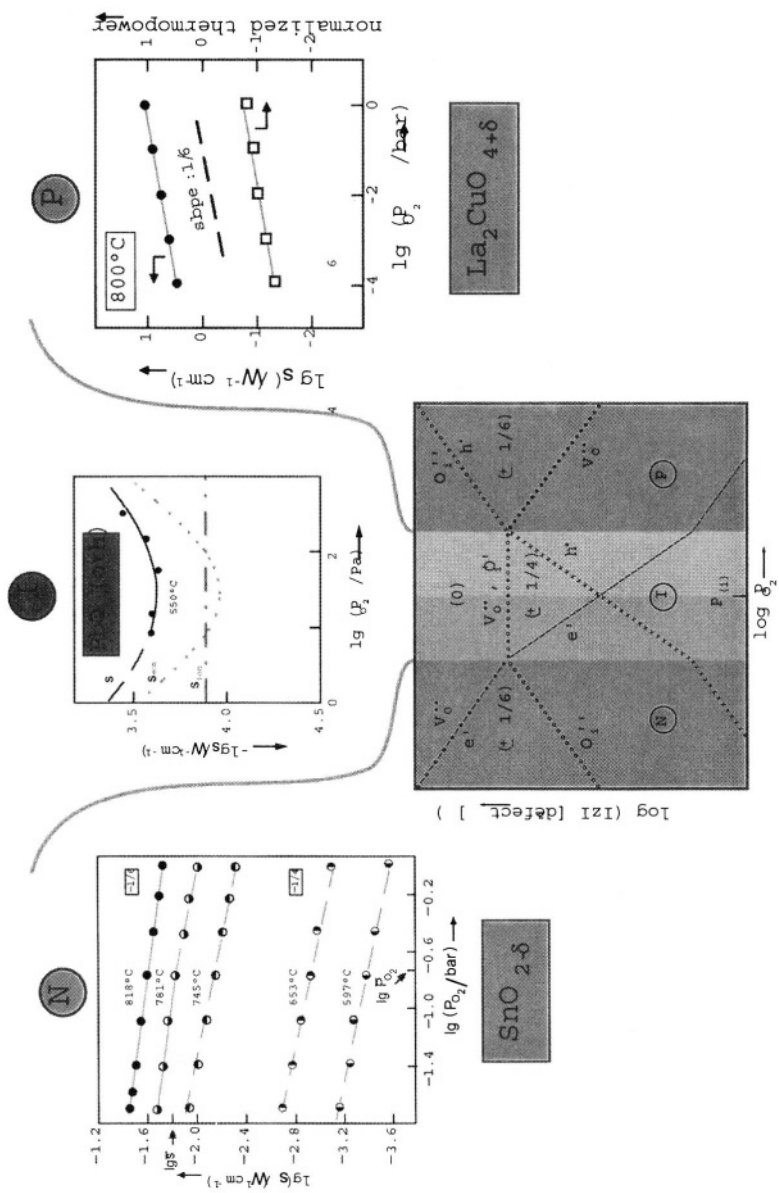
In this case the increased $[h^\bullet]$ at high P_{O_2} leads to superconductivity at very low temperatures.[46] (The fact that we are facing a ternary does not change the picture, as long as metal defects are negligible.)

PbO is an example of I-regime and exhibits mixed conduction,[47,48] σ_{ion} is constant since the decisive ionic defect concentration ($[O_i^{''}]$) is determined by the square of the mass action constant of the ionic disorder reaction. (In PbO very probably the counter-defect to $O_i^{''}$ is $Pb_i^{\bullet\bullet}$ rather than $\vee_O^{\bullet\bullet}$; the results, however, are not different then). Owing to Eq. (22), $[e'] \propto P_{O_2}^{-1/4}$, $[h^\bullet] \propto P_{O_2}^{+1/4}$.

A related example that also shows predominant ionic disorder, is AgCl.[49] Here the role of P_{O_2} is played by the chlorine partial pressure. Analogously $[\vee'_{Ag}] = [Ag_i^\bullet] = \sqrt{K_F}$, $[e'] \propto P_{Cl_2}^{-1/2}$, $[h^\bullet] \propto P_{Cl_2}^{+1/2}$ (where now the decisive disorder reaction is the Frenkel reaction of the Ag sublattice; the exponent 1/2 results since the effective charges are $\pm$ 1). Please note that in these examples with overwhelming ion disorder, e.g. $[Ag_i^\bullet] \approx [\vee'_{Ag}] \approx \sqrt{K_F}$, the equality sign refers to a *relative* constancy. Of course any Ag incorporated as Ag^+ involves equal *absolute* changes in the ionic and electronic budget. Thus, the more precise formulation would be $\ln [Ag_i^\bullet] \approx \ln [\vee'_{Ag}]$, i.e., approximate equality in terms of chemical potential.

3. Doping Effects

At low enough temperatures the defect concentration predicted by the above considerations fall below the impurity limit. In such an extrinsic regime impurity defects — if charged — have to be considered in the electroneutrality equation. In turn, purposeful introduction of impurities is a powerful means of tuning charge carrier chemistry. Since the impurities are considered to be immobile under measurement conditions, their concentration only appears in the electroneutrality equation. Such doping effects are quite characteristic for the solid state in that virtually only the foreign cation or anion is soluble, while usually both ions can be dissolved in a fluid phase and a net charge effect is not achieved. If AgCl contains Cd^{2+} impurities,[49] the electroneutrality equation reads
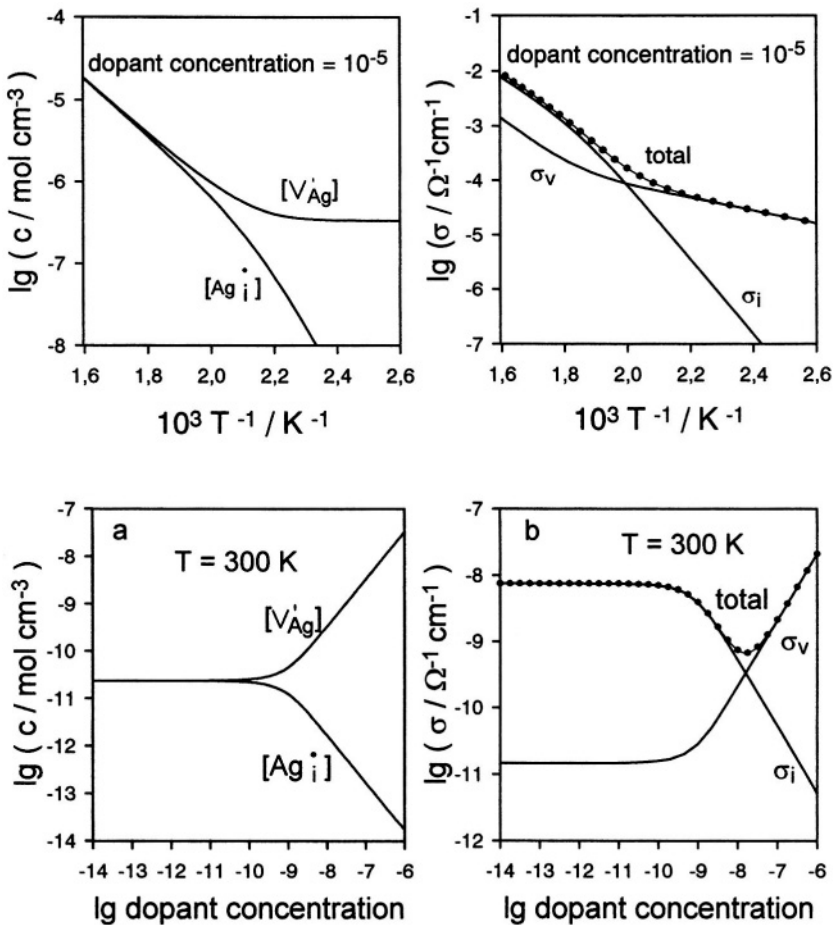
Figure 7. Defect concentrations (l.h.s.) and conductivities (r.h.s.) calculated according to Eq. (39) as a function of temperature for a fixed Cd-content (top row) and as a function of Cd-content for a fixed temperature (bottom row).[24]

$$[Ag_i^\bullet] + [Cd_{Ag}^\bullet] = [\vee_{Ag}'] \tag{38}$$

Coupling with the Frenkel equation, $[Ag_i^\bullet]\ [\vee_{Ag}'] = K_F$ leads to

$$[\vee_{Ag}'] = C/2 + \sqrt{C^2/4 + K_F} \tag{39a}$$

$$[Ag_i^\bullet] = -C/2 + \sqrt{C^2/4 + K_F} \tag{39b}$$

where C stands for $[Cd_{Ag}^\bullet]$. Let us again consider Brouwer conditions. For $C \ll \sqrt{K_F}$ the intrinsic result $[\vee_{Ag}^\bullet] = [Ag_i^\bullet] = \sqrt{K_F}$ is obtained. For $C \gg \sqrt{K_F}$ power laws are found that is immediately obvious by neglecting $[Ag_i^\bullet]$ already in the electroneutrality equation

$$[\vee_{Ag}^\bullet] = C \tag{40}$$

$$[Ag_i^\bullet] = K_F C^{-1} \tag{41}$$

Figure 7 shows the solutions obtained by the more accurate Eq. (39) for both concentrations and conductivities. As soon as the dopant content becomes appreciable, it correspondingly increases the concentration of the oppositely charged defect which depresses the active counter-defect via mass action. In AgCl the mobility of the silver interstitials exceeds that of the vacancies leading to a minimum in the overall ion conductivity approximately at $\sqrt{K_F u_i / u_v}$ as can be readily verified ($u_{i,v}$: mobility of $Ag_i^\bullet$, $\vee_{Ag}'$).

Figures 8 and 9 show the temperature dependence in pure samples and the doping dependence with regard to positive and negative doping. While the response to Cd^{2+} doping ($Cd_{Ag}^\bullet$) follows exactly the theory (Figs. 8 and 9), S^{2-}-doping (S_{Cl}') suffers from interaction effects (see below), but the absence of a minimum is in qualitative agreement with the fact that an increase of $[Ag_i^\bullet]$ is effected (Fig. 9, l.h.s.). Figures 7 and 8 display the succession of intrinsic ($C \ll \sqrt{K_F}$) and the extrinsic regimes on T decrease. The knee in the $\sigma(T)$ curve corresponds to the
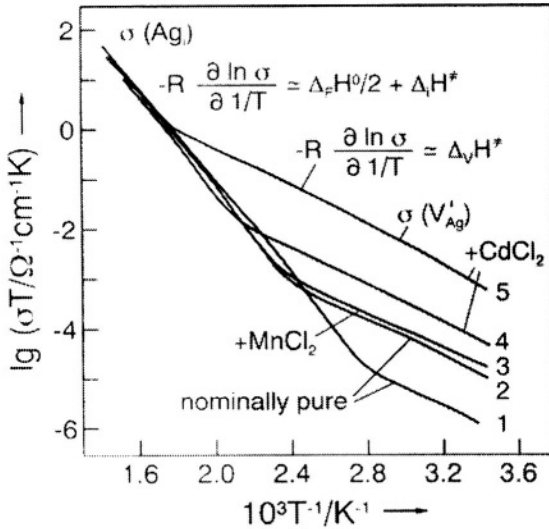
Figure 8. Experimental conductivity data for nominally pure and doped AgCl as a function of 1/T. Here $\lg (\sigma T)$ is plotted instead of $\lg \sigma$ to take account of the slight T-dependence of the pre-factor. However, this does not alter the slope noticeably.[50] (Reprinted from J. Corish, P. W. M. Jacobs, "Ionic conductivity of silver chloride single crystals." *J. Phys. Chem. Solids,* **33,** 1799-1818. Copyright © 1972 with permission from Elsevier.)

minimum in the $\sigma(C)$ curve; the low temperature branch reflects the dominance of the vacancy concentration which is now given by $\sigma \simeq \sigma_v = Fu_vC$. Since the concentration term is constant, the activation energy yields directly the migration energy of the vacancies.

It is clear that, in extension of Eq. (39), under Brouwer and Boltzmann conditions, the result for any carrier concentration must be (we also replace P^{N_j} by $\Pi_p P_p^{N_{pj}}$ in order to allow for multinary equilibria labeled by p)

$$c_j(T,P,C) = \alpha_j^{\beta_j} \Pi_p P_p^{N_{pj}} C^{M_j} \Pi_r K_r(T)^{\gamma_{rj}} \qquad (42)$$

which now also predicts sectionally constant slopes in diagrams of the type $\log c_j$ vs. $\log C$ according to

$$\frac{\partial \ln c_j}{\partial \ln C} = M_j \qquad (43)$$

Let us briefly discuss two further examples. If SnO_2 with the intrinsic electroneutrality equation $2[v_O^{\bullet\bullet}] = [e']$ is doped by Fe or In, the resulting Fe'_{Sn} or In'_{Sn} defects will increase $[v_O^{\bullet\bullet}]$ and depress $[e']$, resulting in a decrease of the electronic conductivity which will now be given by (K_O: mass action constant of reaction Eq. 22)

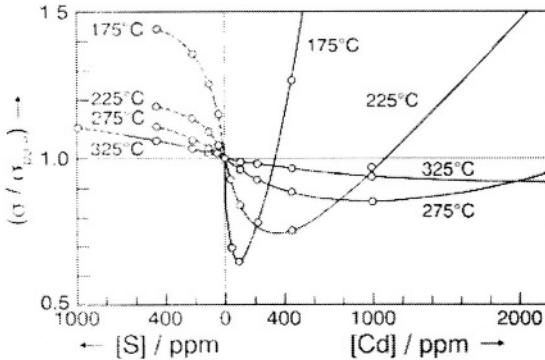$$\sigma \approx \sigma_n = u_n F P^{-1/4} C^{-1/2} K_O^{1/2} \qquad (44)$$

Figure 9. The dependence of the conductivity increase brought about by the impurities, on the S and Cd content of AgCl or AgBr. The solid curves (top) are calculated according to Eq. (39).[49] Reprinted from J. Teltow, Z. physik. Chem. 213-224, 195, Copyright © 1950 with permission from Oldenbourg Wissenschaftsverlag and from J. Teltow, Ann. Physik 63-70, 6, Copyright © 1949 with permission from WILEY-VCH.

This P_{O_2} behavior was seen in Fig. 6 (l.h.s., low T). Higher temperatures and low P_{O_2} favor the intrinsic situation with the slope -1/6. (Similarly also the T-dependence can be exploited.) If we positively dope SnO_2 via higher valent cations or lower valent anions ($Cl_O^{\bullet}$) we increase σ_n and make it P_{O_2} independent ($[e'] \simeq [Cl_O^{\bullet}]$) (Fig. 10).

On the contrary, the negative doping of La_2CuO_4 by Sr (Sr'_{La}) increases the hole conductivity (this "LSC" is a superconductor already below 40 K.)[52] According to $[Sr'_{La}] = [h^{\bullet}]$ the hole conductivity then becomes independent of P_{O_2} .

Figure 11 shows all relevant defect concentrations at high T as a function of Sr-content. It is visibly that all positively charged defects
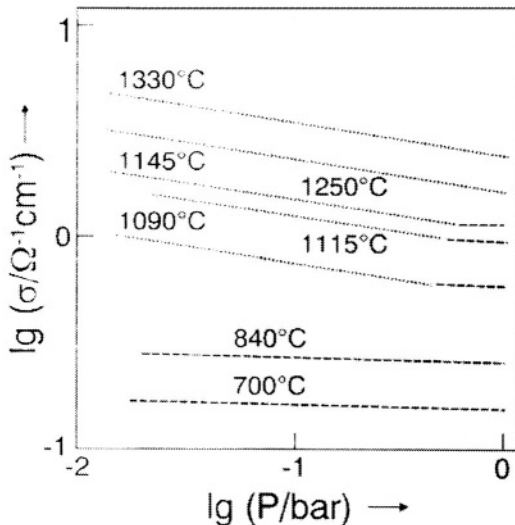

Figure 10. The P_{O_2} dependence of the conduc-tivity[44,45] for positively doped SnO_2 (doped with $SnCl_4$) exhibiting native and impurity-dominated regions.[44] (Reprinted from J. Maier and W. Göpel, *J. Solid St. Chem.* **72**, 293-302. Copy-right © 1988 with permission from Elsevier.)

are increased and all negatively charged defects are depressed in their number. The reason is not electroneutrality alone (this only would demand an overall increase of the positive counter-charge), but also the fact that two oppositely charged carriers appear in the individual disorder reactions.

Figure 11. The dependence of defect con-centrations on Sr doping of La_2CuO_4 for a given P_{O_2}. Interactions are not included. Only the formation of one associate $S_2V = (Sr'_{La})_2\,V_O^{\bullet\bullet}$ is taken into account (see following section). The figures in brackets give the M values (slopes). The parameter $|v|$ in the ordinate labeling gives the absolute value of the charge in the case of ionized defects; in the case of S_2V, however, the Sr content per formula unit ($|v| = 2$).[53]

Equation (42) highlights the basic parameters via which the defect chemistry can be tuned: these are T, P, C. Owing to their importance let us formulate the following qualitative T-, P-, C-rules which hold for simple defect chemistry:

1. Component activity rule (P-rule). If we increase the partial pressure of the electronegative (-positive) component we increase (decrease) the number of holes and decrease (increase) the number of excess electrons; we increase (decrease) the numbers of all defects which individually increase (decrease) the X to M stoichiometry and decrease (increase) the others. As the other rules, these statements—since compensation effects do not occur—are not trivial in that they would simply follow from conservation laws, but reflect also the individual mass action laws.

2. Temperature rule (T-rule). Temperature increase (decrease) favors endothermic (exothermic) reactions. Since the total T-dependence is determined by a combination of formation energies, the final result is not always obvious. However, usually, the defect concentrations rise with increasing temperature.

3. Rule of (homogeneous) doping (C-rule). If the effective charge of the dopant defect is positive (negative) we increase (decrease) the concentration of all negatively charged defects and decrease (increase) the concentration of all positively charged defects. Again compensation effects (that would be allowed within the electroneutrality equation) do not occur.

Since temperature and partial pressure are often fixed, as far as application is concerned, the most powerful means in modifying a given structure and compound is the homogeneous doping. (In the following we will also see that frozen-in higher dimensional defects as well as frozen-in native defects can act similarly).

Rule 3 can be expressed as

$$\frac{z_j \delta c_i}{z \delta C} < 0 \qquad (45)$$

or more concisely (see Eq. 42)

$$\frac{z_j}{z} M_j < 0 \qquad\qquad (46)$$

(z: charge number of the dopant.)

Let us briefly consider in this context two important classes of materials. The first are the oxides of fluorite type such as ZrO_2 or CeO_2. They can accommodate high concentrations of lower valent cations. Y_2O_3 doping of ZrO_2[10] leads to the very important YSZ electrolyte. According to

$$Y_2O_3 + 2Zr_{Zr} + O_O \rightarrow 2Y'_{Zr} + 2ZrO_2 + v_O^{\bullet\bullet} \qquad\qquad (47)$$
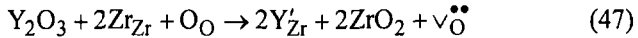
oxygen vacancies are introduced enabling the high oxygen ion conductivity at high T. The resulting conductivity is independent of P_{O_2} while the electronic minority species are following $\pm 1/4$ power laws (see Eq. 22). (In spite of the slope being $\pm\ 1/4$ quite accurately, these materials are far from being ideal, and their discussion belongs into Section IV.5.)

The same is true for negatively doped perovskites. However, here the conductivity is usually predominantly electronic. Iron doping produces primarily Fe'_{Ti} defects enhancing $[v_O^{\bullet\bullet}]$ and $[h^{\bullet}]$. The transition from n- to p-type is shown in Fig. 12. Further increase of the Fe-content increases $[v_O^{\bullet\bullet}]$ so much that the conductivity behavior around the minimum becomes very flat indicating ionic conductivity. It becomes also flat if we quench the high T situation down to much lower concentrations: the reason for this will be considered in the next section.

It is well known that in such negatively doped oxides H_2O[55-62] can be dissolved via the formation of two hydroxide groups. The "OH"-part occupies an oxygen vacancy while the "H"-part combines with a regular O^{2-} to form an OH^- (i.e., $OH^{\bullet}_O$):

$$H_2O(g) + v_O^{\bullet\bullet} + O_O^x \underset{\leftarrow}{\rightarrow} 2OH_O^{\bullet} \qquad\qquad (48)$$

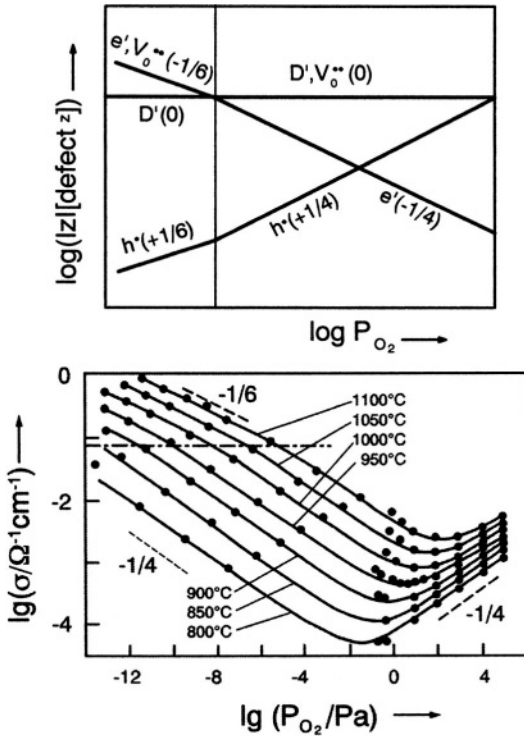The $OH^{\bullet}_O$ defect gives rise to proton conduction according to

Figure 12. The conductivity of negatively doped $SrTiO_3$ as a function of oxygen partial pressure. Top: model (D': negative doping), Bottom: experimental data from Ref.[54]. (Reprinted from G. M. Choi and H. L. Tuller, "Defect Structure and Electrical Properties of Single-Crystal $Ba_{0.03}Sr_{0.97}TiO_3$." *J. Am. Ceram. Soc.* **71**, 201-205. Copyright © 1988 with permission from the American Ceramic Society.)

$$OH_O^\bullet(x) + O_O^x(x') \underset{\leftarrow}{\rightarrow} O_O^x(x) + OH_O^\bullet(x') \qquad (49)$$
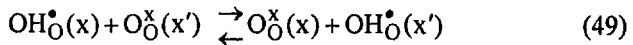
$(x, x'$ denoting two neighboring sites) as was studied in great detail by experimental and computational methods (see e.g. Refs.[59-61]). Equation

(48) has to be added to the above equations, and P_{H_2O} appears as a parameter in Eq. (42). (The detailed calculation is left to the reader as a useful exercise.) Figures 13a and 13b show the solution in forms of Brouwer diagrams. Hydroxide defects can also be formed by reaction with H_2. If this is the dominant reaction, a great amount of electrons is incorporated

$$\frac{1}{2} H_2(g) + O_O^x \underset{\leftarrow}{\overset{\rightarrow}{}} OH_O^\bullet + e' \qquad (50)$$
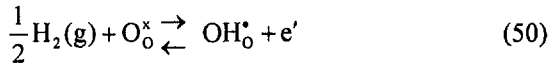
and the material will be primarily electronically conducting. (Note that reaction (48) is a pure acid-base reaction.) Thermodynamically speaking one of two incorporation reactions (Eqs. 48 and 50) is redundant in view of the oxygen-hydrogen equilibrium.

4. Frozen-In Defect Chemistry

At very high temperatures dopants such as Fe in $SrTiO_3$ can become mobile and then instead of having a fixed concentration, a reversible segregation reaction enters the game. Different defect kinetic regimes in terms of reversibility of defect concentrations have also to be considered in pure materials: The defect diagrams considered for the ternaries $SrTiO_3$ and La_2CuO_4 already assumed cation defects to be absent or immobile. If they are immobile such as Sr-vacancies in $SrTiO_3$ at temperatures below 1300 K, they enter the electroneutrality equation like an extrinsic dopant and may be called a native dopant.

The same happens with the oxygen sublattice when we typically go below 600 K, then also the oxygen vacancy concentration becomes invariant and only electronic transfer reactions are reversible. The ion defect concentration remains on a high level with unexpectedly high ion conduction at low temperatures (see Fig. 14).[63]

The regime that we just addressed is typically the regime of electronic applications. If one wants to understand how these low temperature concentrations depend on the control parameters that have to be tuned during fabrication or at least how to prepare these reproducibly, one has to look more carefully at the bridge between high and low temperature defect chemistry.[63-67] A very detailed analysis of this important subject is given in Refs.[65,66]. Here only a few points should be highlighted: In order to fix and calculate the low temperature
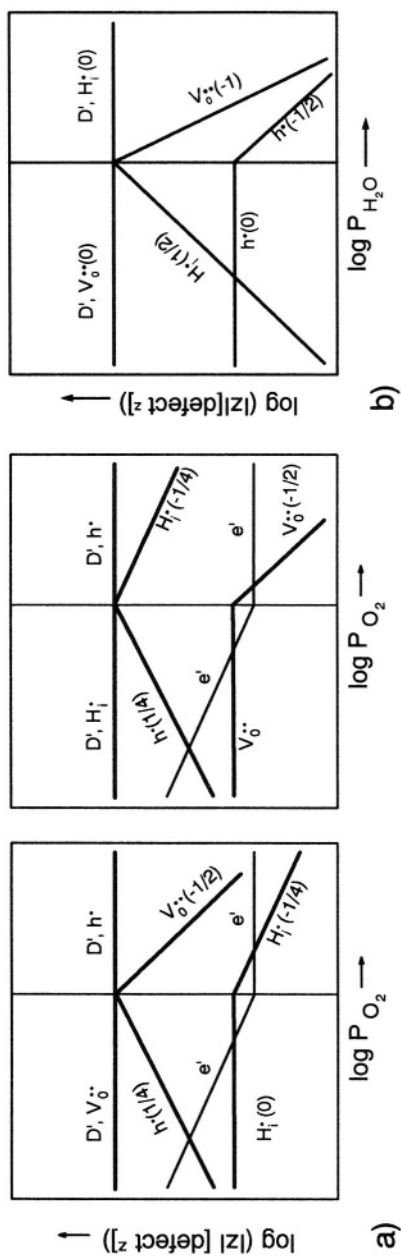
Figure 13: Defect chemistry of water containing perovskites ($D^{'}$: negative dopant) under reversible conditions. Dependence of the defect concentrations on oxygen partial pressure (for different water contents, l.h.s.) and on the partial pressure of water (r.h.s.).[24]
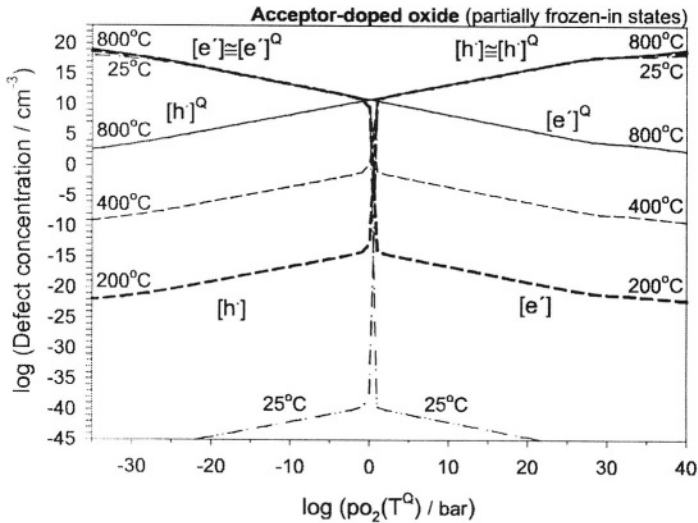
Figure 14. Defect concentrations in an acceptor-doped oxide (shallow acceptor: $c_A = 1 \times 10^{18}$ cm^{-3}), containing minor redox-active acceptor (deep acceptor: $c_M = 1 \times 10^{17}$ cm^{-3}) in partially frozen-in states. The P_{O_2} is the P_{O_2} at which the oxide has been equilibrated at $T^Q = 800°C$. According to Refs.[65,65]. (Reprinted from K. Sasaki and J. Maier, "Low-temperature defect chemistry of oxides. I. General aspects and numerical calculations." *J. Appl. Phys* **86,** 5422-5433. Copyright © 1999 with permission from the American Institute of Physics.)

defect concentration in a multinary material a multi-step quenching procedure is required.[67] The quenching temperature should be chosen such that the equilibration of the sublattice to be quenched takes as long as one can afford (e.g. a few days). Quenching from a higher T would cause kinetic problems during quenching. At a lower temperature partial equilibrium would not have been achieved. The reason that one cannot simply freeze in an equilibrium situation 1:1 is the occurrence of very different carrier mobilities. Hence if at about 300 K and lower the oxygen vacancy concentration is fixed (sluggish surface reaction), the electrons can still redistribute and react. When freezing one carrier concentration by reducing temperature, one loses a mass action law in
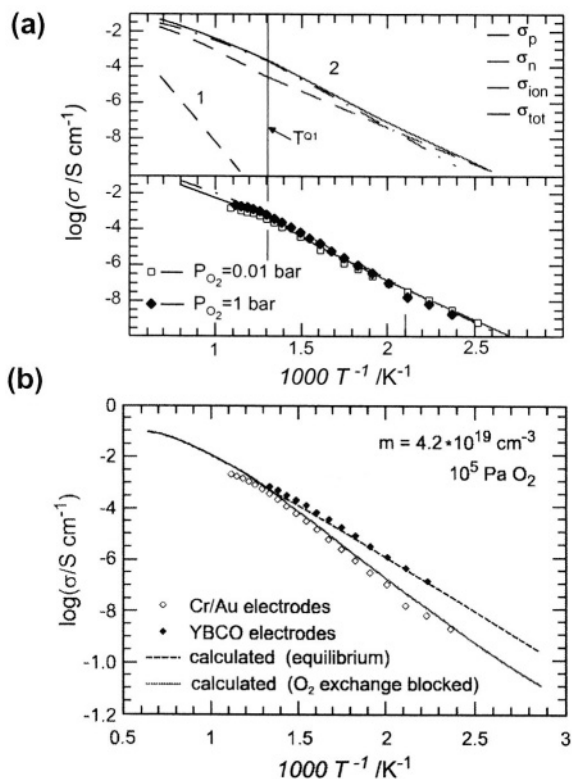
Figure 15. a) Partial (calculated, top) and total (calculated, top and measured, bottom) conductivity of Fe-doped $SrTiO_3$ in the reversible (regime 1) and in the quenched state (regime 2). At $T < T^{Ql}$ the surface reaction is frozen. b) Reversible and quenched path at lower temperatures. The reversible path is taken when the surface is covered by $YBa_2Cu_3O_{6+x}$ which acts as a catalyst of the surface reaction. According to Ref.[68].

the description and gains a conservation law, hence the number of control parameters remains constant. One parameter from the P-term in Eq. (42) (in-situ parameters) is re-shuffled to the C-term (ex-situ parameters). The number of "degrees of freedom" increases owing to the increased deviation from full equilibrium.[67]

Figure 15[68] shows how accurately the defect concentration can also be calculated even under such complicated conditions for the example of Fe-doped $SrTiO_3$, if the quenching procedure is carefully conducted.

5. Defect-Defect Interactions

Defect concentrations can be quite high in solids, and in fact the heavy admixture of a foreign component may lead to significant structural changes and even to new phases. Here we are considering situations in which the dilute limit is no longer fulfilled but severe perturbations are not yet met. Like in liquids we follow two approaches, one being the introduction of associates, which leads to a rescaling of the nature of the defects and allows treatment in terms of the new set in a dilute approximation.[7,69,70] The other is explicitly introducing corrections (activity coefficients) for each species. Of course both approaches can be combined as done in the Bjerrum-Debye-Hückel[71] approach.

(*i*) *Associates*

As already seen in Fig. 9, the Ag_2S-doping of AgCl leads to significant deviations from the dilute behavior. Unsurprisingly, the introduced S'_{Cl} and $Ag_i^\bullet$ defects, both being very polarizable, exert strong interactions that might be described by:

$$Ag_i^\bullet + S'_{Cl} \underset{\leftarrow}{\rightarrow} (Ag_iS_{Cl})^x \qquad (51)$$

The associate is formally neutral and drops out of the conduction process. The mass action law

$$K_{ass} = \frac{[(Ag_iS_{Cl})^x]}{[Ag_i^\bullet][S'_{Cl}]} \qquad (52)$$

introduces a new unknown. The mass conservation requires $C = [S'_{Cl}] + [(AgS_{Cl})^x]$, and combination with the electroneutrality equation and the Frenkel equation allows for the calculation of all the defect concentrations including the free silver defects which are responsible for the conductivity. Again it is helpful to consider the limiting cases (Brouwer approximations). For small K_{ass} the situation is as before, for great K_{ass} almost all sulphur is bound. Since for strong doping silver vacancies can be neglected, the electroneutrality equation reads $[Ag_i^\bullet] = [S'_{Cl}]$ leading to $K_{ass} = C/[Ag_i^\bullet]^2$, and hence to $[Ag_i^\bullet] = C^{1/2} K_{ass}^{-1/2}$. Unlike the situation in the non-associated cases where $[Ag_i^\bullet] = C$, the concentration is now thermally activated again. The situation is inverse for doping with $CdCl_2$ which enhances v'_{Ag} and reduces $Ag_i^\bullet$. On strong doping most of the v'_{Ag} defects are bound as $(Cd_{Ag} v_{Ag})^x$ while the free carriers are now thermally activated. Fig. 16 shows this for the case of positive doping $(CdCl_2)$.

Other prominent examples are associates such as $(v_O^{\bullet\bullet} Y'_{Zr})^\bullet$ or $(Y'_{Zr} v_O^{\bullet\bullet} Y'_{Zr})^x$ in heavily Y_2O_3 doped ZrO_2[10] or analogous centers in heavily Sr-doped La_2CuO_4 (Sr'_{La} instead of Y'_{Zr}) (cf. Fig. 11).[72] (If more and more neighbors have to be considered and/or ordering becomes more and more significant, we leave the comfortable point defect chemical treatment.[6])

Ion pairing is exceedingly the case in ion-conducting polymers. Polar functional groups enable a partial dissociation of the dissolved "salt molecules"[73] according to

$$M^+X^- \underset{\leftarrow}{\overset{\rightarrow}{\rightleftharpoons}} M^+ + X^- \tag{53}$$

Enhancement of the charge carrier density in such polymers is equivalent to shifting this reaction to the right by varying solvent, solute or adding additional particles (see Section VI.3.*ii.*).

Other variants of ionic defect pairs are vacancy pairs such as $(v_{Na} v_{Cl})^x$ in NaCl or $(Pb_i O_i)^x$ in PbO being precursors of pores or precipitates.

Very important are associations between ionic and electronic carriers. Examples are color centers formed in alkali halides.[18,74] If Na
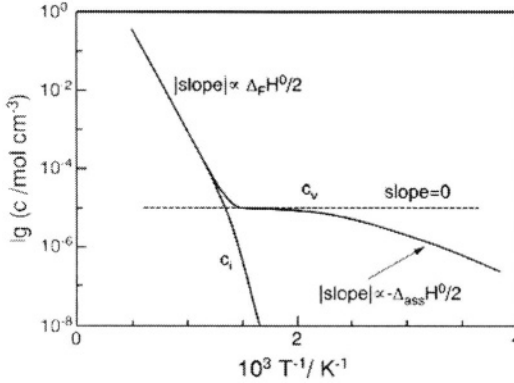
Figure 16. Concentrations of vacancies and interstitial particles in a positively doped Frenkel-disordered material taking account of association between cationic vacancies and dopant ions. The parameters used were $\Delta_{ass}S_m^o = 0, \Delta_F S_m^o = 10R, \Delta_{ass}H_m^o = -40kJ /$ mol and $\Delta_F H_m^o = 200\,kJ/mol$.[24]

is dissolved in NaCl, a Cl-deficiency is created and e' are introduced, which tend to strongly associate with the chlorine vacancy according to

$$V_{Cl}^{\bullet} + e' \underset{\leftarrow}{\overset{\rightarrow}{}} V_{Cl}^{x} \tag{54}$$

It is interesting that the electron cloud confined in the octahedron formed by the Na^+ neighbors can be approximately treated as a free electron in a box of such dimensions. The straightforward calculation directly explains the color "ab initio".[18] Trapping of electrons by $V_O^{\bullet\bullet}$ occurs in SnO_2 at lower temperatures and leads to $V_O^{\bullet}$ and V_O^{x}. Similarly a trapping of $h^{\bullet}$ and O_i'' is expected in the high temperature superconductors.[53] In fact trapping according to

$$O_i'' + 2h^{\bullet} \underset{\leftarrow}{\overset{\rightarrow}{}} O_i' + h^{\bullet} \underset{\leftarrow}{\overset{\rightarrow}{}} O_i^{x} \tag{55}$$
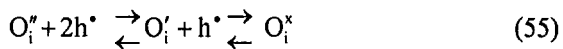
occurs in $YBa_2Cu_3O_{6+x}$ already at quite high temperatures owing to the high concentrations.

Valence changes of impurity defects such as

$$Fe_{Ti}^x + e' \underset{\leftarrow}{\rightarrow} Fe_{Ti}' \tag{56}$$

in $SrTiO_3$ or

$$P_{Si}^{\bullet} + e' \underset{\leftarrow}{\rightarrow} P_{Si}^x \tag{57}$$

in silicon also belong into this section.[75] While the equilibrium constant
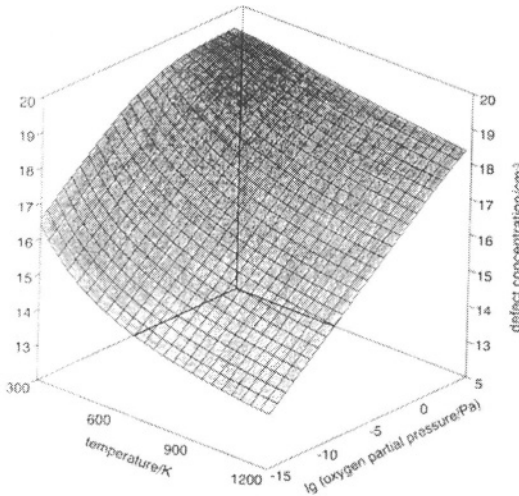
Figure 17. Fe^{4+} ("the color") concentration in Fe-doped $SrTiO_3$ as a function of T and P_{O_2}. The total iron concentration ($\sim 10^{19}/\ cm^3$) corresponds to the limiting case for $(T,\ P_{O_2}) \rightarrow (0,\ \infty)$.[76]

(Reprinted from T. Bieger, J. Maier and R. Waser, "An Optical In-Situ Method to Study Redox-Kinetics in $SrTiO_3$", *Ber. Bunsenges. Phys. Chem.,* **97** 1098-1104. Copyright © 1993 with permission from WILEY-VCH Verlag GmbH.)

of the first reaction is reasonably high, the one for the second equation is very small. In a band diagram we speak of a deep donor in the first case and a flat donor in the latter. Hence Fe^{4+} and Fe^{3+} both exist in $SrTiO_3$ (in Fig. 17) whilst phosphorus in silicium is almost exclusively tetravalent with the formal charge +1. This is visualized by defect levels in the band gap of the band diagram (see Fig. 18 r.h.s. bottom)
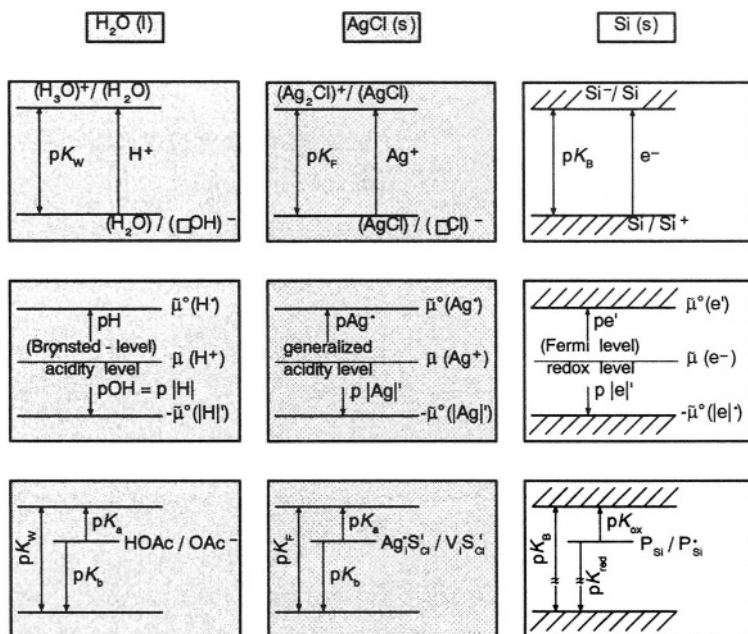

Figure 18. In the same way as the concentration of protonic charge carriers characterizes the acidity (basicity) of water and in the same way as the electronic charge carriers characterize the redox activity, the concentration of elementary ionic charge carriers, that is of point defects, measure the acidity (basicity) of ionic solids, while associates constitute internal acids and bases. The definition of acidity/basicity from the (electro-)chemical potential of the exchangeable ion, and, hence, of the defects leads to a generalized and thermodynamically firm acid-base concept that also allows to link acid-base scales of different solids.[77] (In order to match the decadic scale the levels are normalized by In 10.) (Reprinted from J. Maier, "Acid-Base Centers and Acid-Base Scales in Ionic Solids." *Chem. Eur. J.* **7**, 4762-4770. Copyright © 2001 with permission from WILEY-VCH Verlag GmbH.)
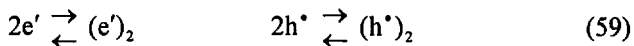
whose position is characterized as follows: The difference of the iron level to the conduction band is the reaction energy of Eq. (56) hence the difference of $\tilde{\mu}_{e'}^{\circ}$ and $\tilde{\mu}_{e^-(Fe)}^{\circ}$, the latter parameter being identical with $\tilde{\mu}_{Fe_{Ti}^{'}}^{\circ} - \tilde{\mu}_{Fe_{Ti}^{x}}^{\circ}$, while the distance to the valence band is given by $\tilde{\mu}_{Fe_{Ti}^{x}}^{\circ} - \tilde{\mu}_{Fe_{Ti}^{'}}^{\circ} - \tilde{\mu}_{h^{\bullet}}^{\circ}$ and is interrelated with the other value by the band gap $E_g = \tilde{\mu}_{e'}^{\circ} + \tilde{\mu}_{h^{\bullet}}^{\circ}$. Note that $\tilde{\mu}_{e'}^{\circ}$ and $-\tilde{\mu}_{h^{\bullet}}^{\circ}$ refer to the edges of conduction and valence band. (Strictly speaking the identification of the energy level with $\tilde{\mu}^{\circ}$ requires appropriate normalization, cf. Section IV.2.)

In the same way as the electron transfer is mapped by the band diagram, the ion transfer of the ion-ion associates can be represented by an "ionic" level diagram (see Fig. 18 center, bottom).[75,77] Figure 18 indicates that, in particular by comparison with the situation of water, the ionic associates play the role of internal acids and bases. It is even possible to transform the Brønsted-concept in its ionotropic generalization to solids by using the point defect concept. In the same way as the numbers of H^+ and OH^- reflect the acidity and basicity in water, the numbers of V_{Ag}' and $Ag_i^{\bullet}$ reflect the (ionotropic) acidity and basicity in AgCl. An acidity function based on $\tilde{\mu}_{Ag^+}$ which is identical with $\tilde{\mu}(Ag^{\bullet}) = -\tilde{\mu}(|Ag|')$ in equilibrium also includes the definition of surface acidity. For more details the reader is referred to Ref.[77].

Finally, there are also associates between electronic carriers such as

$$e' + h^{\bullet} \underset{\leftarrow}{\rightarrow} \left(e'h^{\bullet}\right) \tag{58}$$

or

$$2e' \underset{\leftarrow}{\rightarrow} (e')_2 \qquad\qquad 2h^{\bullet} \underset{\leftarrow}{\rightarrow} (h^{\bullet})_2 \tag{59}$$

that are worthy of mention. The first are excitons, the second Cooper pairs. While the first are separated by an activation threshold from the

ground state and play an important role in non-equilibrium situations, the second associates can be held together e.g. by phonon interactions and only exist at very low temperatures.[32,78]

(*ii*)   *Activity Coefficients*

According to our splitting the chemical potential in a non-configurational and a configurational term $\mu^{ex} = \mu^{ex(c)} + \mu^{ex(nc)}$, we can split the activity corrections in two parts. The activity coefficients defined by $\mu^{ex} \equiv RT \ln f$ then multiply $(f = f^{c} f^{nc})$. To a certain degree, the introduction of activity coefficients can circumvent the introduction of associates: if we do not distinguish between free and trapped vacancies in AgCl formed upon $CdCl_2$ doping, then the total cation content C would be identical with the (overall) vacancy concentration and we would have to introduce an activity coefficient given by $(K_{ass}C)^{1/2} < 1$ to satisfy the decreased activity. Of course if there are good reasons to introduce associates, it is much better to use these and to try to find activity coefficients for the detailed species. In this way both concepts can be combined (cf. the Bjerrum concept in liquids.[69])

The classical approach to correct charge carrier interactions in liquid systems is the Debye-Hückel theory which is extensively discussed in textbooks.[79] The decisive parameter is the screening length

$$\lambda = \sqrt{\frac{\varepsilon\, RT}{2z^2 F^2 c_{\infty}}} \tag{60}$$

c_{∞} being the defect concentration of the majority carriers for which we assumed the same charge number z.

The activity coefficient is approximately

$$RT \ln f_j^{nc} = -\frac{z_j^2 F^2}{8\pi\varepsilon N_m \lambda} \propto c_j^{1/2} \tag{61}$$

The Debye-Hückel concept fails very soon (see Fig. 19) and probably earlier than in liquid electrolytes (at latest for ~1). Also straightforward higher order corrections do not lead to reliable extensions into the defect range of practical interest where the coarse grained nature cannot be neglected. Accurate approaches that take into
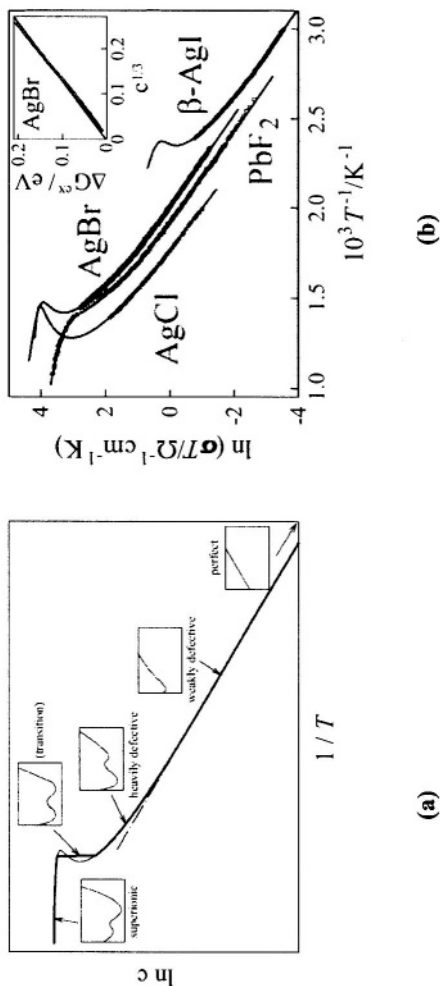
Figure 19. High temperature anomalies in the conductivity can be explained with the cube root law (see text). In the insert in (b) literature data[80] for the excess free enthalpy for AgBr are plotted against the cube root of the defect concentration. Even the phase transition temperatures themselves are well predicted.[81,82] (a): Behavior in terms of the energetic situation. (b): Experimental examples and curves fitted according to Eq. (62). (Reprinted from J. Maier and W. Münch, "Thermal Destiny of an Ionic Crystal" *Z. Anorg. Allg. Chem.* **626**, 264-269. Copyright © 2000 with permission from WILEY-VCH Verlag GmbH.)

account the structural feature become soon individual and non-manageable.[83]

In literature[81] an ad-hoc model has been used for the description of the conductivity properties of various binary halides that corrects the chemical potential according to

$$\mu^{ex} = -J_{\pm} x_{\pm}^{1/3} \tag{62}$$

($x_{\pm}$: defect mole fraction of the majority carriers).

It is worth noting that cube root corrections have also been used for liquid electrolytes,[84] however, there without real structural connection and without the possibility of testing that over a wide T-range. Supported by Monte Carlo calculations of molten salts[85] which show that their Coulomb energy can be approximated by a Madelung concept (with a somewhat smaller Madelung factor) in spite of the fluctuating distribution, it proposes the interaction energy to be similar to the Madelung energy of a defect superlattice superimposed on the perfect lattice. The calculation then readily gives Eq. (62) with $J_{\pm}$ being

$$J_{\pm} \simeq \frac{2}{3} \frac{\varphi_d}{\varphi} \frac{U}{\varepsilon_r} \tag{63}$$

(φ, φ_d: Madelung constants of perfect lattice and defect lattice, U, ε_r: lattice energy and dielectric number of the perfect lattice.) The concept was tested by conductivity (see Fig. 19) and specific heat experiments as well as by Monte Carlo and MD simulations and found to work surprisingly well.[86,87]

In contrast to the silver halides for which the use of the static dielectric constant in Eq. (57) yields good agreement, for PbF_2 with its high static dielectric constant a value more typical for this structure ($\varepsilon \approx \varepsilon_{CaF_2}$) had to be used. Since at the small distances involved the full static permittivity is not operative, the neglect of the high static polarizability of the lead ion makes sense. (Similarly the interaction between $V_O^{\bullet\bullet}$ and acceptor dopants in $SrTiO_3$ could be well described by a cube root law with an effective dielectric constant of ~10 instead of the static value which is one order of magnitude greater.[88])

There are a variety of important consequences of Eq. (62). First, the attractive defect interactions lower the effective formation energy according to the implicit function

$$x_\pm \equiv [Ag_i^\bullet] = [v'_{Ag}] = \exp-\frac{\Delta_F G_m^\circ - 2J_\pm x_\pm^{1/3}}{2RT} \qquad (64)$$

so that the conductivity rises over its values computed "according to Boltzmann". This is indeed found and called the pre-melting regime in ion conductors,[81] and is well described by Eq. (64) for AgCl, AgI and PbF$_2$. Moreover, since a higher defect concentration leads to ever higher values, this avalanche causes a phase transformation.[81,89] In contrast to Fig. 4, now the free enthalpy curve shows two minima (see inserts in Fig. 19, l.h.s.), the second of which becomes lower above the transition temperature (T_c) (see Fig. 19). Surprisingly the J-values given above suffice to even predict the phase transformations which are a first order transition from the low defective β-AgI to the completely disordered α-AgI (molten Ag$^+$ sublattice), a first order transition from the low defective AgCl to the totally molten state and a second order phase transition in the case of PbF$_2$ (Fig. 19). In the second case even the high T conductivity was described reasonably well. The precise criterion for the order of the phase transition is given in Ref.[81]. The fact that the T_c corresponds to reality even in the first order cases implies that the transition from the virtual sublattice molten crystal with the low temperature structure to the real structure of the partially or totally molten state does not exhibit great free energy changes. In principle only the upper limit of such a transition can be predicted in this way.

Interestingly also the electron-hole interaction can scale with such a distance law. The pre-melting corresponds then to what is called level narrowing,[90] and the transition to a superionic state (degenerate situation) corresponds to the insulator-metal transition expected in such a case.

These considerations should also be relevant for boundary effects and boundary phase transitions.

Figure 20 shows the "thermal destiny" of an ionic crystal which (given structure, bond strength and permeabilities) from the perfect state at T = 0 up to the superionic transitions.[81,82] Owing to the finite disorder energy (which depends on bond strength and permeabilities), there is a formation of point defects, the concentration of which first increases according to Boltzmann; with increasing concentrations the formation energy is successively lowered leading to an anomalous concentration increase (also determined by bond strength and permeabilities) and in a self-amplified way to the transition into a
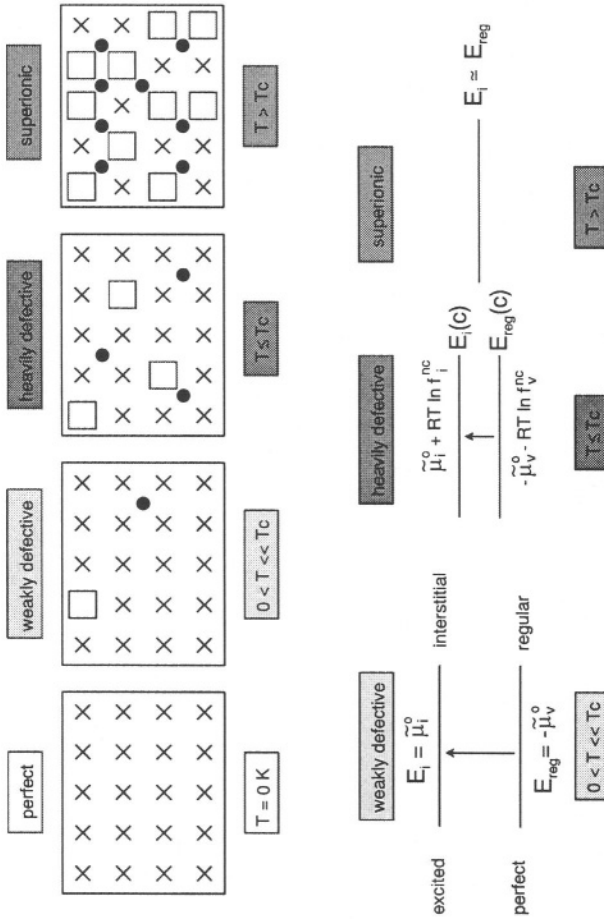
Figure 20. Sketch of the real structure of a Frenkel disordered crystal (only the affected sublattice is shown). The increase in temperature corresponds to an increase in defect concentration. Interaction leads to a narrowing of the spacing of the "energy levels" (electrochemical potentials minus configurational term) and eventually to a transition into the superionic state.[82] (Reprinted from J. Maier and W. Münch, *Z. Anorg. Allg. Chem.*, **626**, 264-269, Copyright © 2000 with permission from WILEY-VCH Verlag GmbH.)

totally disordered state (unless the system evades this by a structural transformation into another state). In master example AgCl the whole T-range also including the above discussed impurity effects can be described by the simple defect chemistry.

For high concentrations $x_\pm$ has to be replaced by $x_\pm/(1 - x_\pm)$ in order to account for the finite number of states. It was already mentioned that this stems from configurational corrections, more specifically from the Fermi-Dirac correction. The results are corrections of the type

$$f_\pm^c(x_\pm) = (1 - x_\pm)^{-1} \tag{65}$$

for ionic point defects or, in the case of electronic carriers, e.g. for the electrons in the conduction band[3,5] ($\mathfrak{F}_{1/2}$: Fermi-Dirac integral for parabolic state densities, Δ: distance from Fermi-level to band edge normalized with respect to kT)

$$f_{e'}^c = \frac{\pi^{1/2}\exp\Delta}{2\mathfrak{F}_{1/2}(\Delta)} \quad \text{with} \quad \mathfrak{F}_{1/2}(y) \equiv \int_0^\infty \frac{\tau^{1/2}d\tau}{\exp(\tau+y)+1} \tag{66}$$

which is obtained from Eq. (26).

It is noteworthy that these activity coefficients are larger than 1 and lead to an increased activity (cf. Fermi pressure) (see Fig. 21). The opposite is true for a Bose-Einstein statistics ($f_\pm^c = (1 + x_\pm)^{-1}$ instead of Eq. (65), cf. Bose condensation).

In realistic situations the interactions "act back" on the configuration, and the assumption of a random configuration for a situation with energetic interaction is not free from inconsistency. Nevertheless, experience shows that for weak interaction this may be a well-working assumption. Corrections in the configurational entropy are extremely complicated[83] and simple corrections are sought, even if very crude. Site exclusion is such a simple correction: Here it is, e.g. assumed that two positions may both be available with equal probability for the very first defect, but cannot be occupied both; then the binominal expression in Eq. (24) has to be simply multiplied by 2^{N_d}.[91] (In realistic situations the coordination number has to be considered rather than a factor of 2.)
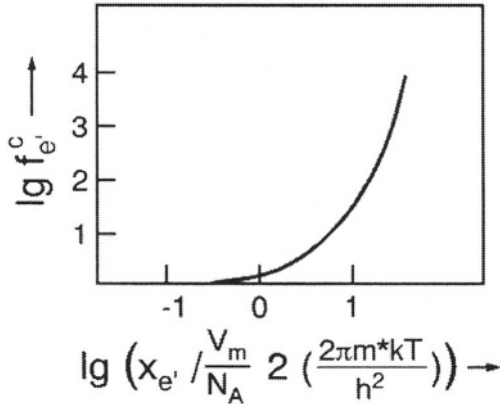
Figure 21. Fermi-Dirac activity coefficient of electronic charge carriers as a function of concentration.[4] (Reprinted from H. Schmalzried, *Solid State Reactions,* Verlag Chemie, Weinheim. Copyright © 1981 with permission from WILEY-VCH Verlag GmbH.)

V. DEFECT CHEMISTRY AT BOUNDARIES

1.   Space Charge Profiles and Capacitances

The treatment has to be changed if we are concerned with interfaces. The electroneutrality equation is only a limiting case valid for the homogeneous bulk (and valid there only on a coarse grained scale). When heterogeneities are introduced, the symmetry break results in space charges. Put differently, owing to the structural change at interfaces, the (free) formation energy and hence μ_d^o is different there; this not only leads to a changed point defect chemistry in this interfacial core but also to space charge zones in the region adjacent. In particular in materials of interest characterized by a low carrier density

but significant mobility in the bulk, the latter phenomenon is of prime importance. The situation is characterized by non-zero electrical potential gradients and electrochemical potentials. In order to describe the electrostatic information, the combination of the two relevant Maxwell-equations (magnetic fields will be neglected), namely $\nabla \bullet (\varepsilon\, \mathbf{E}) = \rho$ and $\nabla \times \mathbf{E} = \mathbf{0}$, i.e., $\mathbf{E} = -\nabla\phi$ ($\mathbf{E}$ being the electric field and $\rho = \Sigma_j z_j F c_j$ the charge density) leads to Poisson's equation (which for the bulk reduces to $\rho = 0$). The equilibrium condition (for random distribution)

$$\nabla \tilde{\mu}_j = \nabla \mu_j + z_j F \nabla \phi = RT \nabla c_j / c_j + \nabla \mu_j^{ex} + z_j F \nabla \phi = 0 \qquad (67)$$

offers the second information.[92] If we consider interaction-free solutions ($\mu^{ex} = 0$) and one-dimensional situations, the concentration profile in the boundary regions is determined by the electrical potential profile (space charge zone) according to

$$\left(\frac{c_j(x)}{c_{j\infty}} \right)^{1/z_j} \equiv \zeta_j^{1/z_j} = \exp - \frac{\phi(x) - \phi_\infty}{RT} F \qquad (68)$$

being independent of j. Combination with Poisson's equation leads to the well-known Poisson-Boltzmann equation[93]

$$\frac{d^2(\phi - \phi_\infty)}{dx^2} = -\frac{F}{\varepsilon} \Sigma_k c_{k\infty} z_k \exp - \left(z_k F \frac{\phi - \phi_\infty}{RT} \right) \qquad (69)$$

For two oppositely charged majority carriers with $z_+ = z_- \equiv z$ the Gouy-Chapman-profile (see textbooks on electrochemistry) results which we write ($\xi \equiv x/\lambda$) here as

$$\zeta_\pm = \left(\frac{1 + \vartheta_\pm \exp - \xi}{1 - \vartheta_\pm \exp - \xi} \right)^2 = \zeta_+^{-1} \qquad (70)$$

where

$$\vartheta_{\pm} = \frac{\zeta_{\pm0}^{1/2} - 1}{\zeta_{\pm0}^{1/2} + 1} = -\vartheta_{+} \tag{71}$$

The parameter ϑ varies between -1 and 0 for depletion and between 0 and +1 for accumulation, and plays the role of a degree of influence of the interface.[94]

Figure 22 (r.h.s.) illustrates the contact thermodynamics and its influence on ionic and electronic carrier concentrations. The level bending expresses the variation in the electrical potential, and the constancy of $\tilde{\mu}_{ion}$ and $\tilde{\mu}_{eon}$ the electronic and ionic contact equilibrium.[35] (Note that the electric potential term—as a non-configurational term—is to be included into the "energy levels".) The constancy of the chemical potential of the neutral component is automatically fulfilled (see Fig. 22 r.h.s.).

Two extreme cases are worth mentioning: the first if the concentration variation is small ($\vartheta \to 0$), then we end up with the exponential solution [$\zeta_{j0} \equiv \zeta_{j}(x = 0)$]

$$\zeta_{j} = 1 + (\zeta_{j0} - 1) \exp{-\xi} \tag{72}$$

and the other for large effects ($\vartheta_{1} \to 1$)

$$\zeta_{1} = \frac{\zeta_{10}}{(1 + \sqrt{\zeta_{10}} \xi / 2)^2} \tag{73}$$

where 1 denotes the accumulated carrier. The Gouy-Chapman solutions have been used in liquid electrochemistry for a long time when dealing with the metal/electrolyte contact.[95,96] There space charge zones occur, the charge of which is compensated by adsorbed carriers at the very interface and also by an excess electronic charge at the metal side of the contact.[96] In materials with low carrier concentrations, such as dilute electrolytes (ions) or weakly doped semi-conductors (electrons) this
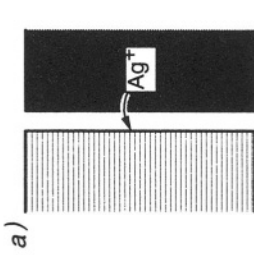

Figure 22. L.h.s.: Four basic space charge situations involving ionic conductors (here silver ion conductor): a) contact with an isolator, b) contact with a second ion conductor, c) grain boundary, d) contact with a fluid phase. R.h.s.: Bending of "energy levels" and concentration profiles in space charge zones ($\xi = 0$ refers to the interfacial edge).
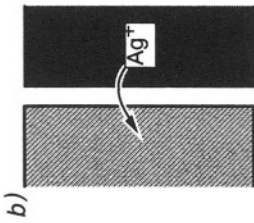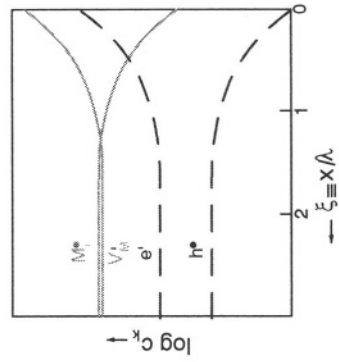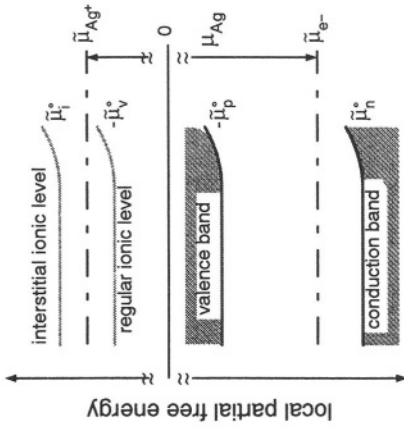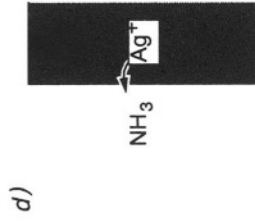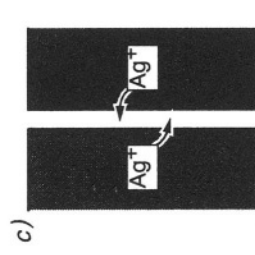
charge distribution is diffuse.[33] In our more general case we have to consider electronic and ionic profiles in both phases as well as in the core of the boundary. Later we will mainly work[24] with Eq. (73), which in essence ignores the counter defect in the charge density. For the same reason this approximation is—given that large effects are indeed met—quite general in terms of defect chemistry and independent of whether or not the counter-defect is immobile or whether or not its charge coincides with the majority defect. A completely different situation is only met if an immobile dopant forms the majority carrier and the counter defect (2) is depleted. Then a constant dopant profile means a constant charge density, and a Mott-Schottky-profile is obtained[97,98] for the majority counter carrier:

$$\zeta_2 = \exp-\left|\frac{z_2}{z_1}\right|\left(\frac{x-\lambda^*}{2\lambda}\right)^2 = \exp-\left|\frac{z_2}{z_1}\right|\left(\frac{\xi-\xi^*}{2}\right)^2 \tag{74}$$

Unlike the Debye length the effective width λ^* depends on the space charge potential:

$$\lambda^* \equiv \sqrt{\frac{2\varepsilon}{z_1 F c_{1\infty}}(\phi_\infty - \phi_0)} \tag{75}$$

From Eqs. (73) and (74) which describe accumulation and depletion for strong effects, the concentrations of the other mobile species are simply accessible through Eq. (68). In liquid electrochemistry these profiles have been used to evaluate electrode/liquid electrolyte capacitances.[79]

In the Gouy-Chapman case the differential capacitance (a: area) follows as

$$C_{sc}/a = \frac{\varepsilon}{\lambda}\cosh\frac{|z|F(\phi_0 - \phi_\infty)}{2RT} \tag{76}$$

which (for small space charge potentials) reduces to $(C_{sc}/a) = \varepsilon / \lambda$, a result that can be generalized[101] to

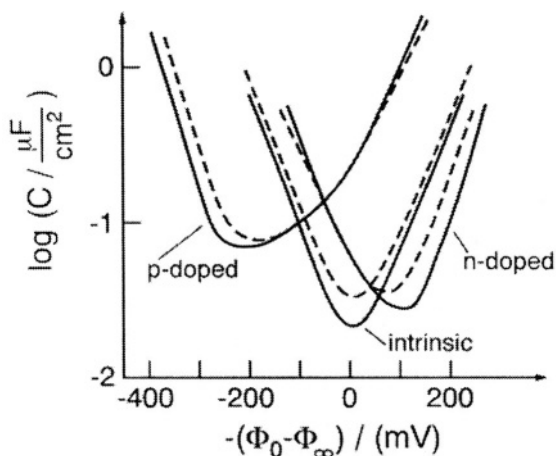$$C_{sc}/a = \varepsilon / l_0 \tag{77}$$

Figure 23.   Theoretical space charge capacitance according to Bohnenkamp and Engell as a function of the voltage drop over the boundary $-(\phi_0 - \phi_\infty)$ for intrinsic and doped semiconductors (donor concentration N_D/V $3.5\times10^{14}cm^{-3}$, acceptor concentration $N_A/V =$ $7.5\cdot10^{15}cm^{-3}$) at room temperature (dashed line: 45°C).[99]
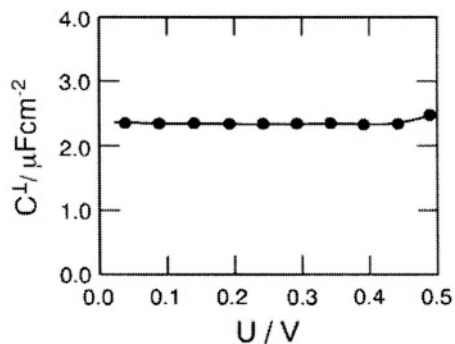

Figure 24. Voltage dependence of the boundary layer capacitance for $C|\alpha$-AgI at 175 °C. From Ref.[102]. (Reprinted from R. D. Armstrong and R. Mason, "Double Layer Capacity Measurements involving Solid Electrolytes." *J. Electroanal. Chem.* **41,** 231-241. Copyright © 1973 with permission from Elsevier.)

where l_0 is the centroid of the charge perturbation. The space charge capacitance in the Mott-Schottky case is given by:

$$C_{sc}/a = \sqrt{\frac{|z|Fm\varepsilon}{2|\phi_0 - \phi_\infty|}} = \frac{\varepsilon}{\lambda^*} \tag{78}$$

Equation (78) has been widely used in semiconductor physics and semiconductor electrochemistry, in particular with respect to the evaluation of important parameters such as the potential of zero-charge (flat-band potential).[71] Equation (76) predicts a minimum in the capacitance vs. potential curve. (The generalization to a doped situation[99] (see Fig. 23) shows that this minimum is sensitive to the dopant concentration.) A minimum has never clearly been observed for solid ionic conductors, what was attributed to interfacial states, saturation and finite size effects.[103,104] The total capacitance also includes contributions from the core layer itself.[71] Figure 24 shows the double layer capacitance of α-AgI for which the Debye-length is negligible. Figure 25 refers to a depletion layer in the mixed conductor $SrTiO_3$. According to Eq. (78) the boundary capacitance changes only weakly with P_{O_2}.

In mixed conductors the "chemical capacitance" plays an important role. This will be extensively considered in Part II[1] (see also Section VI, in particular VI.7.).

2. Space Charge Conductance

The space charge regions naturally lead to severe conductance effects. In solid state electrochemistry such effects can be well measured by using thin films, dispersions, polycrystalline materials and/or by taking advantage of special configurations.[1,23,94] Table 2 compiles conductance effects, parallel and perpendicular to the interface, calculated on the basis of Eqs. (68), (73) and (74) for a variety of situations. Let us first refer to accumulation effects and study the conduction effects along the interfaces. Four basic space charge situations in ionically conducting systems displayed in Fig. 22 (l.h.s.) will be discussed in more detail in the following text.
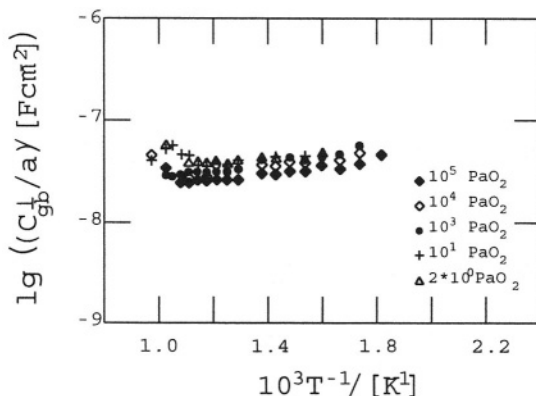
Figure 25. Grain boundary capacitance of a Fe-doped $SrTiO_3$ polycrystal ($m_{Fe} = 6.5 \times 10^{19} cm^{-3}$), normalized to the electrode surface and measured at various oxygen partial pressures as a function of reciprocal temperature.[100] Typical space charge potentials vary between 300 and 800 mV. (Reprinted from I. Denk, J. Claus and J. Maier, "Electrochemical Investigations of $SrTiO_3$ Boundaries." *J. Electrochem. Soc.* **144**, 3526-3536. (Copyright © 1997 with permission from The Electrochemical Society, Inc.)

Before we do so, let us mention a particular difference between solid and liquid systems which is very important in this context, namely the occurrence of a network of internal boundaries in multiphase or polycrystalline materials. The proportion of boundary regions can be so high that the overall conductivity can be interfacially dominated.

As far as solid state ion conductors are concerned, the interest in boundary effects started with the surprising finding that the overall conductivity in two-phase systems can exceed the conductivities of the bulk phases by several orders of magnitude.[106-109] If e.g. fine Al_2O_3 particles are dispersed in matrices of moderate cation or anion conductors such as LiI, AgCl, AgBr, β-AgI, CuCl, $TlCl^{94}$ or CaF_2, PbF_2,[110] the ion conductivity—at not too high temperatures—drastically increases with an activation energy close to the migration energy of the mobile ion (see Fig. 26). The more acidic oxides (e.g. SiO_2) are less active in the case of the cation conductors but more active in the case of

Table 2

Possible space charge situations and the respective conductance effects parallel ($\parallel$) or perpendicular ($\perp$) to the interface.[105] (Reprinted from S. Kim, J. Fleig and J. Maier, "Space charge conduction: Simple analytical solutions for ionic and mixed conductors and application to nanocrystalline ceria.", Phys. Chem. Chem. Phys. 2268-2273, 5, Copyright © 2003 with permission from the PCCP Owner Societies.)
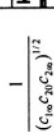
Table 2
Continuation

	m	n	o	p
Mott-Schottky	$(\sigma_m^{\parallel})_1 \propto \dfrac{c_{10}}{c_{2\infty}^{1/2}\,[\ln(c_{10}/c_{1\infty})]^{1/2}}$ $(\rho_m^{\perp})_2 \propto \dfrac{1}{c_{2\infty}^{1/2}\,c_{20l}\,[\ln(c_{2\infty}/c_{20l})]^{1/2}}$		$(\sigma_m^{\parallel})_1 \propto c_{10}^{1/2}$ $(\rho_m^{\perp})_2 \propto \dfrac{1}{c_{1\infty}^{1/2}(c_{20}^{3/4}c_{2\infty}^{1/4})}$	$(\sigma_m^{\parallel})_1 \propto c_{10}^{1/2}$ $(\rho_m^{\perp})_2 \propto \dfrac{1}{c_{1\infty}^{1/2}\,c_{2\infty}}\ln\!\left(\dfrac{c_{2\infty}}{c_{20}}\right)$
Combined	$(\sigma_m^{\parallel})_1 \propto c_{10}^{1/2}$ $(\rho_m^{\perp})_2 \propto \dfrac{1}{(c_{1\infty}c_{20}\bar{c}_{2\infty})^{1/2}}$			

Figure 26. Experimental results (symbols) and theoretical calculations (solid lines) for $AgBr:Al_2O_3$ and $AgCl:Al_2O_3$ two-phase mixtures. The labels give the volume fraction of Al_2O_3 as a percentage and refer to an Al_2O_3 grain size of $0.06\mu m$ (if not in brackets) or $0.15\mu m$ (if in brackets). The line marked with dashes for AgCl refers to the nominally pure single crystal, the dotted line to the polycrystal and the broken line to a positively doped single crystal (with respect to the knee, cf. Fig 27).[94,109] (Reprinted from J. Maier, "Ionic Conduction in Space Charge Regions." *Prog. Solid St. Chem.* **23**, 171-263. Copyright © 1995 with permission from Elsevier.)

the fluoride ion conductors. $\gamma\text{-}Al_2O_3$ proved to be more active than $\alpha\text{-}Al_2O_3$ which was attributed to the OH-groups on the surface. Making the surface non-polar (using $(CH_3)_3SiCl$) nullifies the effect. All these phenomena can be explained by a strong adsorption of the mobile ion towards the surface leaving behind vacant sites and hence refer to case

a in Fig. 22a, which in the case of a cation conductor, is described by[108,109]

$$\vee_A + M_M \underset{\leftarrow}{\overset{\rightarrow}{\rightleftharpoons}} M_A^\bullet + \vee_{M^\bullet}' \tag{79}$$

A denotes a site at the oxide/halide interface. In principle the superposition of the individual pathways to the overall response can be very complicated. Standard percolation theory starts from two phases of extremely different conductivities, assumes a random distribution and equal particle sizes. In this case the simplest situation is to assume a highly conducting interface between two insulating phases. Then two percolation thresholds have to be considered: the first on the Al_2O_3 poor side where the first interface pathway is formed, and the second on the Al_2O_3 rich side where the last interface pathway is blocked.[111] Even though this is intelligible, the agreement is only qualitative. The assumption of a homogeneous interface conductivity and the neglect of the conductivity of the base material is, however, not the most serious shortcoming: (i) The very small size of the Al_2O_3 particles depresses the first percolation threshold to very small values. (ii) The assumption of random distribution is inconsistent owing to the necessary interfacial interaction and not independent of this. (iii) The grain size of the matrix changes upon increasing the volume fraction of Al_2O_3. As expected from the local energetics, the Al_2O_3 particles populate the grain boundaries and very soon form percolating pathways. On increasing the volume fraction of alumina the grain size of the AgCl particles is reduced and the monolayer situation maintained. Hence, the excess conductivity is approximately proportional to both the specific area (Ω_A) and to the volume fraction of the oxide particles. The measured conductivity (see Table 2, case a) is then given by[94,108,109]

$$\sigma_m = (1 - \varphi_A)\sigma_\infty + \beta_L \Omega_A \varphi_A (2\varepsilon RT)^{1/2} u_1 \sqrt{c_{10}} \tag{80}$$

(For the mechanism proposed by Eq. (79), carrier 1 is the metal vacancy. The parameter β_L is explained in Section V.4., Eq. 90.) Figure 26 shows that Eq. (80) describes the conductivity effects excellently. Since $\sqrt{c_{10}}$ is only weakly activated, the T-dependence of the heterogeneously doped samples is similar to the positively (homogeneously) doped samples (e.g. $CdCl_2$).

Like the homogeneous $CdCl_2$ doping, the heterogeneous Al_2O_3 doping leads to a change in the conduction mechanism in pure silver halides in which the interstitial defects dominate the conductivity. Unlike there, however, we do not only meet a transition in the overall conductivity from v- to i-type, the type of the conductivity changes also locally from the bulk towards the boundary. Similarly TlCl which is an anion conductor intrinsically and exhibits Schottky disorder, can be made cation-conducting if heterogeneously doped by Al_2O_3.[112]

Figure 27 compares the heterogeneous and homogeneous doping situations. In both cases the excess charge introduced generates an enhancement (depression) of the concentration of the oppositely (equally) charged intrinsic defects; the distribution of charge and counter charge, however, is different in both situations. The similarity is also expressed by the rule of heterogeneous doping (Σ-rule)[20] (adding to the three defect chemical rules given in Section IV.3., c.f. Eq. 45.)

$$\frac{z_j \delta c_j}{\delta \Sigma} < 0 \qquad (81)$$

or in words:

(4) If one introduces higher dimensional defects into a system, which attract a positive (negative) charge, the concentrations of all mobile negatively (positively) charged defects will be increased (decreased) in the space charge zone and vice versa. Compensation effects do not occur (Σ: charge density at the interfacial core).

One consequence of the modified defect chemistry being restricted to the boundary is readily seen in Fig. 27. Unlike in the case of homogeneous doping, in heterogeneous doping the transition from interstitial to vacancy type does not show up as a knee in the conductivity curves, since, as soon as the boundary zone becomes less conductive, the bulk which is in parallel, dominates.[113]

The depletion in the silver interstitial concentration has been investigated at the contact $RuO_2/AgCl$, in which the role of RuO_2 corresponds to that of Al_2O_3; however, due to its high electronic conductivity, it can also serve as an electrode and the effect across the space charge zone including the space charge capacitance can be measured.[114]
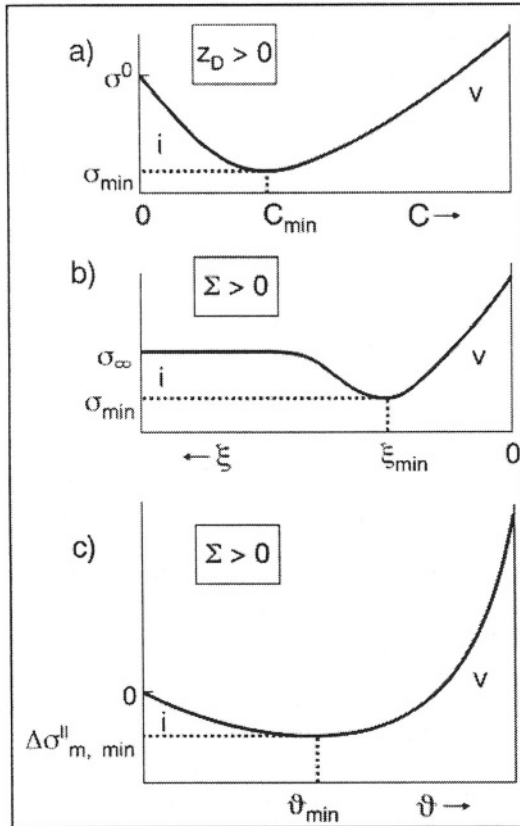
Figure 27. I: a) Comparison of homogeneously (a) and heterogeneously (b,c) doped material (example: AgCl): (a) conductivity as a function of the concentration of a homogeneous positive dopant $(z_D > 0)$ of concentration C, (b) local conductivity as a function of the spatial coordinate at positive charge density of the interface core $(\Sigma > 0)$ in the case of heterogeneous doping $(\xi \equiv x/\lambda)$; $\xi = 0$ denotes the layer adjacent to the interfacial core, (c) integral conductivity increase $(\Delta\sigma_m!)$ as a function of the strength of the interfacial interaction in heterogeneous doping. II.: The dependence of the conductivity on temperature for positively homogeneously and heterogeneously doped material (example: AgCl[94]). The "knee" which is characteristic for the homogeneous case, is by-passed in the heterogeneous case.[24] Reprinted from J. Maier, "Ionic Conduction in Space Charge Regions." *Prog. Solid St. Chem.* **23**, 171-263. Copyright © 1995 with permission from Elsevier.)
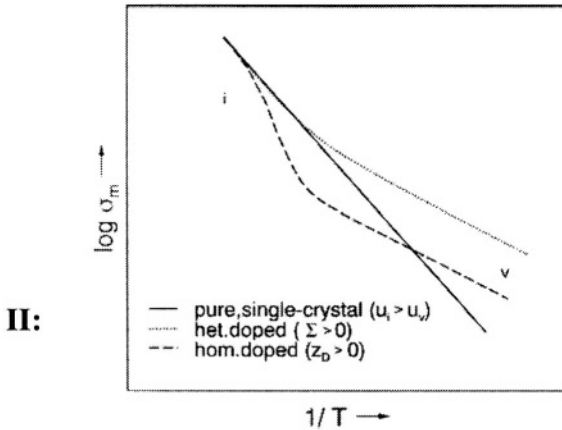
Figure 27. Continuation

A revealing experiment consists in blocking the ionic conduction in $AgCl/Al_2O_3$ composites by pure electron conductors. This addresses the extension of the Wagner-Hebb method to inhomogeneous systems[115] (see Part II[1]) and leads to the detection of minority species therein. The results are completely in agreement with the space charge picture (cf. Eq. 68) which predicts by an increased $[e']$ and a decreased $[h^\bullet]$ in the space charge zones. The total information can be comprised by Kröger-Vink diagrams of boundary regions which exhibit the distance from the boundary as a different parameter (see Section V.3., Fig. 35). One point is worthy of note at this stage: If these carriers are also the minority carriers in the core of the boundary, they are—unlike the majority carriers—not important for the establishment of the space charge field, do, however, react on it equally. In this respect it is pertinent to speak of a "fellow traveler effect".[94] As far as electron conductors are concerned, much more attention should be paid to such a foreign control, since the space charge effects of the electrons often control the conductivity, whereas, however, the origin of the space

charge potential may be solely due to ionic carrier effects (see e.g. the $SrTiO_3$ below).

Oxide admixtures also proved beneficial (see, e.g. reference[116]) in the case of ion conducting polymers. Even though mobility effects occur, too, the separation of an ion pair in the rather covalent matrix by adsorbing one partner is possible, an effect that can be subsumed under the phenomenon of heterogeneous doping.[37]

The second contact problem of significance is the contact of two ionic (or more generally two mixed) conductors (see Fig. 22, case b).[94,107,117,118] Here a redistribution affects two boundary layers (charge storage in the proper interface is now neglected). Let us consider the contact MX/MX' of two M^+ conducting materials in which also electronic carriers (but not X^-) may be mobile. The full thermodynamic equilibrium demands the invariance of $\tilde{\mu}_{M^+}(=\tilde{\mu}_{M_i^\bullet}=-\tilde{\mu}_{V_{M'}})$, $\tilde{\mu}_{X^-}$ and $\tilde{\mu}_{e^-}(=\tilde{\mu}_{e'}=-\tilde{\mu}_{h^\bullet})$. The global bulk thermodynamics characterized by $\nabla\mu_M = 0$, $\nabla\mu_X = 0$, is then automatically fulfilled ($\mu_M = \tilde{\mu}_{M^+} + \tilde{\mu}_{e^-}$; $\mu_X = \tilde{\mu}_{X^-} - \tilde{\mu}_{e^-}$; $\mu_{MX} = \mu_M + \mu_X$) and hence also $\nabla\mu_{MX} = 0 = \nabla\mu_{MX'}$. At the temperatures of interest only the sufficiently mobile ions can redistribute $\nabla\mu_M = 0 \neq \nabla\mu_X$, $\nabla\mu_{M^+} = 0 \neq \nabla\mu_{X^-}$ (i.e., $\nabla\mu_{MX} \neq 0$). Figure. 28 plots the decisive potentials and functions for the contact together with the profiles for the ionic carriers. The behavior of the electronic carriers is not shown. Here we refer to Fig. 22 (r.h.s.) which applies for one side of the contact. The construction of the total energy level diagram for ions and electrons (analogously to Fig. 22 (r.h.s., top)) is left to the reader as useful exercise.[35] Relevant cases in which we assume or observe ion redistribution are the contacts AgI/AgCl and BaF_2/CaF_2[118,119]

$$Ag_{Ag}^x(\beta-AgI)+v_i(AgCl) \underset{\leftarrow}{\overset{\rightarrow}{\rightleftarrows}} Ag_i^\bullet(AgCl)+v_{Ag}'(\beta-AgI) \qquad (82)$$

$$F_F^x(BaF_2)+v_i(CaF_2) \underset{\leftarrow}{\overset{\rightarrow}{\rightleftarrows}} F_i'(CaF_2)+v_F^\bullet(BaF_2) \qquad (83)$$

(Of course the thermodynamics can also be described in terms of transfer reactions of the individual defects given the coupling of the

Figure 28. a) Ion redistribution process at the contact MX/MX′: concentration effects. [117] b) Variation of the potentials, charge densities, and dielectric displacements at the contact of two Frenkel defect ionic conductors. [94] (Reprinted from J. Maier, "Ionic Conduction in Space Charge Regions." Prog. Solid St. Chem. 171-263, 23, Copyright © 1995 with permission from Elsevier.)
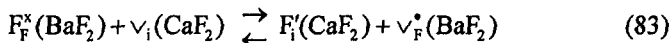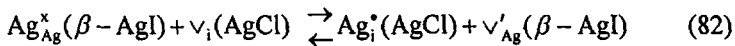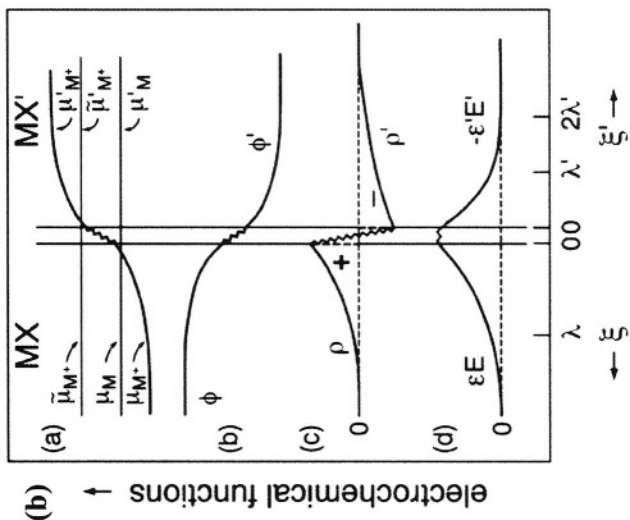
bulk disorder equations.[117]) In this way we can produce v-i transitions which correspond to "ionic p-n transitions". The two boundary concentrations that appear as parameters in the conductance in MX and MX' are simply linked via the ratio of the dielectric constants if we assume large space charge potentials and ignore charge storage between x = 0 and $x' = 0$. Equation (82) explains the large conductivity anomalies in the two-phase system AgI/AgCl which is shown in Fig. 29 (l.h.s.). (Here the preparation is made from quenching a high temperature homogeneous mixture into the solubility gap such that we can assume a coexistence of AgI(AgCl) with AgCl(AgI).)

A more elegant example which does not involve the complicated percolation effects[117] of these two phase mixtures, refers to MBE grown heterolayers of BaF_2 and CaF_2.[119] Here owing to the comparatively low preparation temperature almost no cation mixing occurs. The anion redistribution gives rise to a strong excess conductivity due to interfaces, which increases progressively if the interfacial density is increased. In both examples the space charge calculations are in very good agreement with the results.

The third contact is the contact of two chemically identical but differently oriented grains, i.e., a grain boundary (cf. Fig. 30).[94,120] A grain boundary can also separate two similarly oriented but "badly contacted" grains which may imply insufficient sintering (e.g. inclusion of pores) or inclusion of impurities (e.g. OH-groups or glassy phases). In all cases, however, the symmetry break introduced by the grain boundary will change the ion distribution at the expense of an excess charge (see Fig. 30a). Examples are highly conducting grain boundaries in AgCl that can be even locally investigated in Fig. 30b.[121,122] The effect is very related to the above heterogeneous doping in the case of which small second phase particles within the grain boundaries caused similar but enhanced boundary potentials. The conductivity can also be tuned by treatment with Lewis acids and bases. One example is the effect of contamination with NH_3 on the conductivity of AgCl.[94] While the cation adsorption is enhanced by bases, the inverse effect occurs in the case of the anti-Frenkel disordered earth alkaline fluorides. An increased internal adsorption of F^- is achieved here by treatment with Lewis-acids. (Analogously, SiO_2 particles in the grain boundary are more active than the more basic Al_2O_3.) In the case of SbF_5 contaminated CaF_2 grain boundaries[123] the F^- segregation which already occurs in the clean boundaries according to
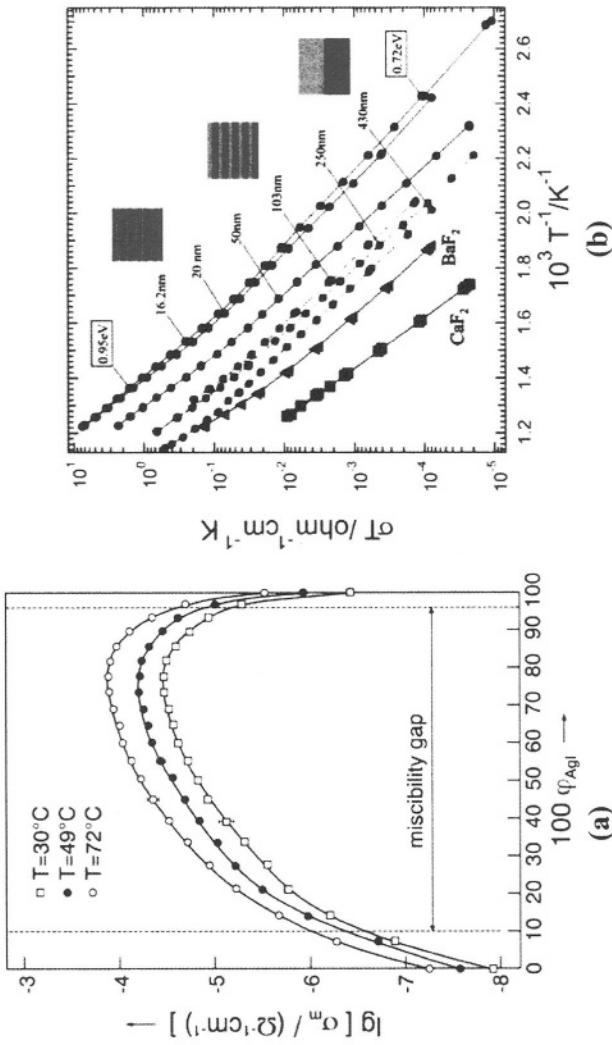
Figure 29. a) Conductivity variation in the system β-AgI-AgCl (φ: volume fraction) for different temperatures.[118] b) Conductivity variation in CaF$_2$-BaF$_2$ heterolayers as a function of temperature for different periods (spacings).[119] (Reprinted from N. Sata, K. Eberman, K. Eberl and J. Maier, "Mesoscopic fast ion conduction in nanometre-scale planar heterostructures." *Nature*, 408, 946-949. Copyright © 2000 with permission from Macmillan Magazines Ltd.)

(a)

(b)
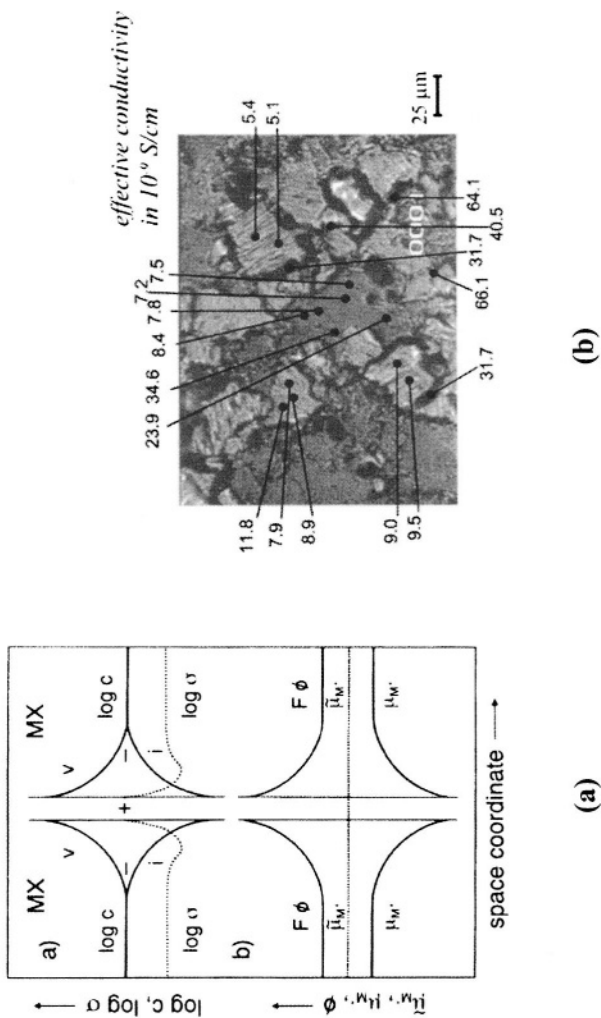
Figure 30. Ionic space charge effects at grain boundaries in Frenkel disordered materials. (a) Theoretical profiles if $u_i > u_v$.[120] (b) The enhanced grain boundary conductivity can be verified by point electrode impedance spectroscopy.[121] The number given are in units of nS / cm and refer to room temperature.

$$F_F + \vee_{gb} \;\overset{\rightarrow}{\underset{\leftarrow}{\rightleftharpoons}}\; F'_{gb} + \vee_F^\bullet \tag{84}$$

is additionally increased most probably according to

$$F_F^x + SbF_5(gb) \;\overset{\rightarrow}{\underset{\leftarrow}{\rightleftharpoons}}\; SbF_6'(gb) + \vee_F^\bullet \tag{85}$$
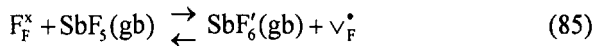
These acid-base effects can be directly studied by exposing surfaces of the ion conductors to acid-base active gases, such as CaF_2 to BF_3, or AgCl to NH_3 according to

$$NH_3(ad) + Ag_{Ag} \;\overset{\rightarrow}{\underset{\leftarrow}{\rightleftharpoons}}\; NH_3...Ag^\bullet(ad) + \vee'_{Ag^\bullet} \tag{86}$$
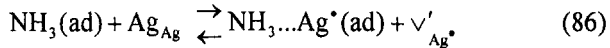
In the latter case, the increased vacancy conductivity can be used to sense ammonia quite selectively.[124,125] This is obviously the analogue to the Taguchi sensor[126] where an electron conductor senses redox active gases, e.g. O_2 by trapping electrons according to

$$O_2(ad) + e' \;\overset{\rightarrow}{\underset{\leftarrow}{\rightleftharpoons}}\; O_2...e^-(ad) \tag{87}$$
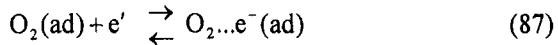
The correspondence between ions and electrons is displayed by Fig. 31. Besides its importance for conductivity sensors, surface defect chemistry should be paid much more attention to in terms of heterogeneous catalysis. While in homogeneous catalysis acid-base effects are overwhelmingly studied, the role of the point defects as elementary acid-base centers are not really acknowledged. Examples are the dehydrohalogenation of t-BuCl by homogeneously or heterogeneously doped AgCl[127,128] (see also Refs.[129,130])

Depletion layers with respect to ionic conductors are no less interesting. In acceptor doped $SrTiO_3$,[131-134] CeO_2[135,136] and presumably also in ZrO_2,[137-141] space charge layers have been found to exhibit a positive space charge potential. As a consequence the oxygen vacancies, the relevant ionic carriers, are depleted as well as holes, while e' should be enriched.
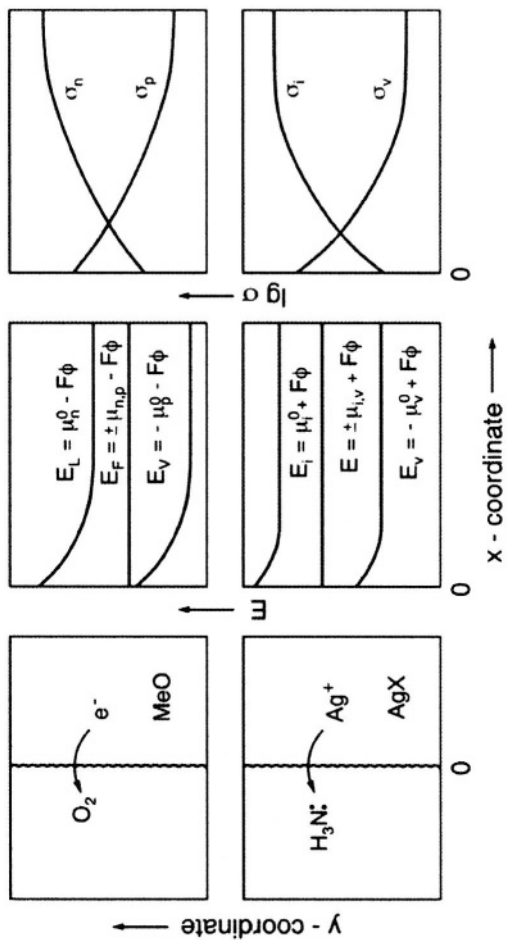
Figure 31. The change in the ionic surface conductivity upon a variation in the partial pressure of the acidbase active gas (bottom) is analogous to the Taguchi sensor which works for redox-active gases.[20]

In the case of the Fe-doped $SrTiO_3$ bicrystal referred to in Fig. 32a (grain boundary parallel to the electrodes), the impedance response shows a clear interfacial response whose capacitance (cf.Mott-Schottky length λ^* (Eq. 75) as well as resistance parameters provide evidence of a hole-depletion zone. Evaluating these parameters as a function of partial pressure, doping content, temperature and bias (see, e.g. Fig. 32a) gives a clear picture of the defect chemistry. The space charge potentials for the boundary under investigation (here $\Sigma$5-tilt) obtained are typically of the order of several 100 mV (here 500 mV) almost independent of P_{O_2} and weakly dependent on temperature in agreement with the defect chemical modeling (see Fig. 32b).[100,131]

According to Eq. (68) we now also expect an oxygen vacancy depletion, and in fact a much more severe one according to the double positive charge. The separation of electronic and ionic conductivity by a blocking technique confirmed the predictions in detail (Fig. 33[134]).

The simultaneous depletion of both the relevant ionic and the relevant electronic carriers leads to two further consequences. One is a severe chemical resistance with respect to the kinetics of stoichiometry[142] changes which we will consider later in more detail in Section VI.4.*iii*. Figure 32b shows the good agreement between electrical and chemical experiments in terms of the space charge potential. The second is the finding that a changed $\sigma_{ion}/\sigma_{eon}$ ratio at the boundaries compared to the bulk leads to a bulk polarization if an electrical field is applied,[143] similar to the electrochemical polarization induced by selectively blocking electrodes which will be considered in Part II.[1]

The last consequence to be discussed is the fact that a positive space charge potential does not only lead to a hole depletion but also to an accumulation of excess electrons. Their influence may be observed in $SrTiO_3$ only at very high space charge potentials,[144] but has been clearly seen in nanocrystalline CeO_2[136,159] (space charge potential $\simeq 300$ mV) and will be considered again in Section V.4.

3. Interfacial Defect Thermodynamics

The parameter c_0 measuring the concentration in the first layer adjacent to the core, i.e., in the first layer of the assumed bulk structure, is a convenient parameter for the mathematical description but not a
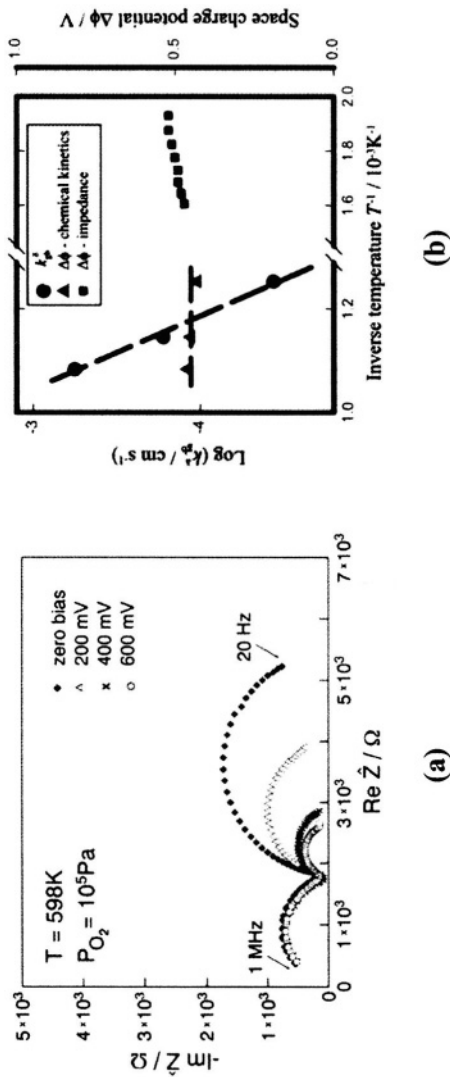
Figure 32. a) Impedance measurements on the O_2, $Pt|SrTiO_3|SrTiO_3|Pt$, O_2 as function of the superimposed d. c. bias. Electrodes are parallel to the bicrystal boundary ($\Sigma 5$ tilt grain boundary, iron content: $2 \times 10^{18} cm^{-3}$). Both bulk and boundary resistances are predominatly electronic resistances.[100] b) Measurements of oxygen diffusion into a $SrTiO_3$ bicrystal (interface perpendicular to transport), effective rate constants, K_{gb}^{δ}, and space charge potentials, $\Delta\phi$, determined by impedance spectroscopy at low temperatures and by the diffusion experiment at high temperatures.[142] (Reprinted from M. Leonhardt, J. Jannik and J. Maier, "In situ Monitoring and Quantitative Analysis of Oxygen Diffusion through Schottky-Barriers in $SrTiO_3$ Bicrystal." *Electrochem. Solid-St. Lett.* **2**, 333-335. Copyright © 1999 with permission from The Electrochemical Society, Inc.)
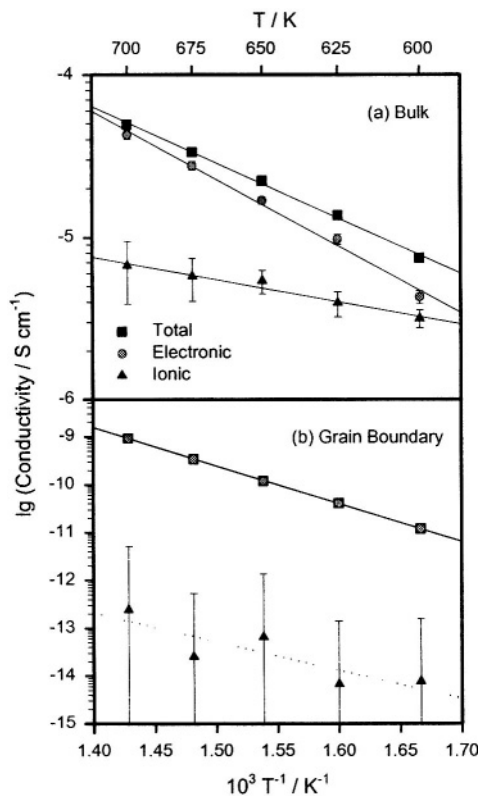
Figure 33. Temperature dependence of total and partial conductivities (a) in bulk and (b) at the grain boundary. Note that the values of the ionic conductivity at the grain boundary are approximate.[134] (Reprinted from X. Guo, J. Fleig and J. Maier, "Sepa-ration of Electronic and Ionic Contributions to the Grain Boundary Conductivity in Acceptor-Doped SrTiO₃." *J. Electrochem. Soc.,* **148,** J50-J53. Copyright © 2001 with permission from The Electrochemical Society, Inc.)

fundamental interfacial materials parameter; the same is true for the surface charge or the space charge potential. A pertinent parameter is the local standard chemical potential of a particle or defect (i.e., its "energy level") in the boundary zone. This leads to the (rigid) core-space charge picture described in Refs.[23,24,108,145] and is illustrated by Fig. 34 for the charging of the boundary core (e.g. a grain boundary).

In the simplest case the perfect structure changes at the boundary in an abrupt way, and the standard chemical potential of the carriers can
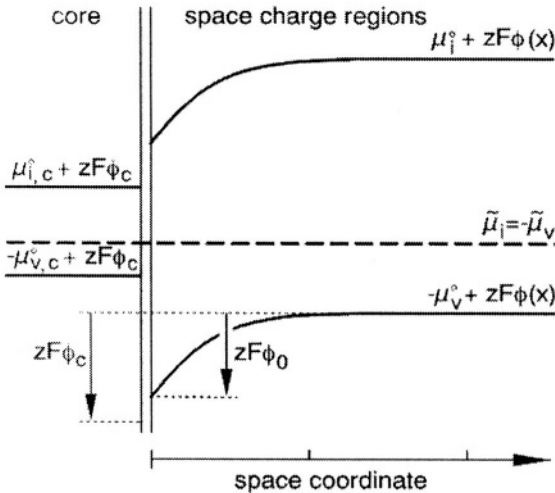
Figure 34. Boundary equilibrium in the level diagram for Frenkel defects (i, v: e.g. $Ag_i^\bullet$, v'_{Ag}, $z = 1$) or anti-Frenkel defects (i,v: e.g. O_i'', $v_O^{\bullet\bullet}$, $z = -2$). The electrical potentials cause the levels ($\tilde{\mu}^\circ$) to bend in the space charge zone and to shift in the core in order to satisfy that $\tilde{\mu} = \text{const}$. For the sake of simplicity the electrical bulk potential (ϕ_∞) is set to zero. The index c designates the core region.[145] (Reprinted from J. Jamnik, J. Maier, S. Pejovnik, "Interfaces in solid ionic conductors: Equilibrium and small signal picture." *Solid State Ionics, **75**, 51-58. Copyright © 1995 with permission from Elsevier.)
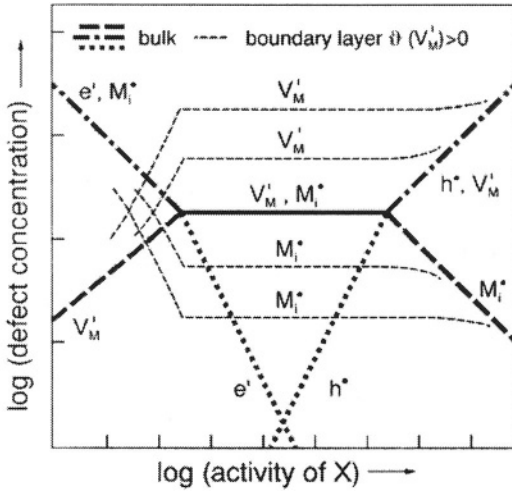
Figure 35. Kröger-Vink diagram of boundary layers for our model substance MX when $\vartheta(V_M') > 0$. The broken lines refer to the ionic defect concentrations at (two) different distances from the interface. The behavior of the electrons in boundary regions is not shown. The approach to the bulk values (printed boldface) for extreme abscissa values is attributable to the disappearing Debye length. The mirror symmetry on compa-rison of V_M' with $M_i^\bullet$ follows from Eq. (68).[94] (Reprinted from J. Maier, "Ionic Conduction in Space Charge Regions." *Prog. Solid St. Chem.* **23**, 171-263. Copyright © 1995 with permission from Elsevier.)

be described by a step function. Without great loss of generality, let us consider the case of a grain boundary (Fig. 34). The boundary core may be approximately conceived as a region of special structure of the width of one or a few atomic layers, which again for simplicity's sake is considered to be homogeneous. As experiments and capacitances show, this picture is not only simple but in many cases also quite realistic.[146]

The different structure is energetically reflected by a non-zero interfacial tension γ. The terms γa (a: interfacial area) and $\sum \mu_k n_k^\Sigma$ add to the bulk value of the free energy (μ_k describes the chemical potential

of the neutral component, n_k^Σ the interfacial excess mole number). This knowledge is not sufficient for the defect chemical treatment. For this purpose we need to know the standard chemical potentials (or at least the relevant differences) of the defects also in the core regions. The defect concentrations then follow by a lattice-gas statistical model as indicated in Fig. 34. In more detail this is described for an oxide surface in Refs.[23,24]. There also the P_{O_2} and T dependencies are discussed, which are particularly simple if a power law form (analogous to Eq. 42) is valid for c_0. This then leads to the Kröger-Vink diagram of boundary regions (see Fig. 35). Calculation of the partial free energies ("energy levels") of the point defects for the interfacial layers as well as the elucidation of more advanced core-space charge models is of pronounced significance in this context. The latter point includes questions of structural flexibility of the interfacial core (i.e., variance of $\tilde{\mu}_j^\circ$ in the core layer) as well as more realistic profiles of $\tilde{\mu}_j^\circ$ within the core layer. The situation is more complicated if the interface is curved. For more details see Refs.[23,24,28,147].

4. Non-Trivial and Trivial Size Effects: Nanoionics

So far we essentially discussed the behavior under semi-infinite boundary conditions, i.e., situations that are locally not affected by the presence of neighboring interfaces. This is different if the spacing is very narrow and of the order of the characteristic decay length at semi-infinite interfaces (i.e., the above discussed Debye length).[94,148,149] If the latter is fulfilled or the interface structure itself is changed by the presence of a neighboring interface, the properties change locally and are different from the properties at isolated interfaces. In this case we speak of true size effects.[36,37,150,151] Also in the other cases the overall response may perceptibly depend on the spacing of interfaces simply due to the increased interface-to-volume proportion. This we name trivial size effects. The distinction is precise as long as the interfaces are planar and edges and corners are neglected, as it is the case for thin films, or for polycrystalline materials that can be described by the bricklayer model (cf. reference[152]) which will be explained in more detail below.
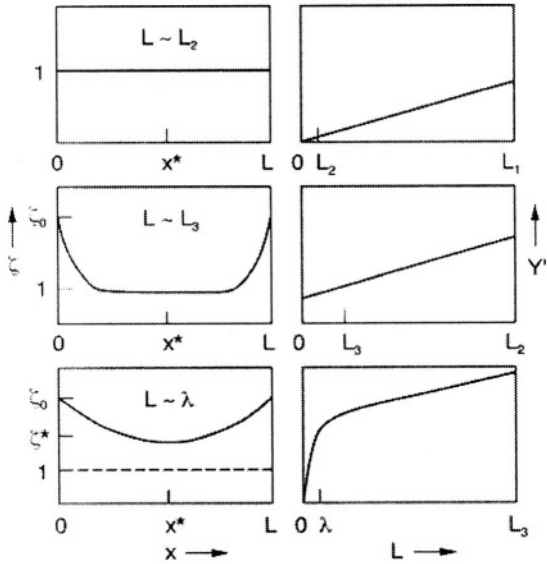
Figure 36. Defect concentration and conductance effects for three different thicknesses $L_1 \gg L_2 \gg L_3$. The mesoscale effect on defect concentration (l.h.s.) discussed in the text, when $L < 4\lambda$, is also mirrored in the dependence of the conductance on thickness (r.h.s.). If the boundary layers "overlap", the interfacial effect previously hidden in the intercept is now resolved. It is presupposed that surface concentration and Debye length do not depend on L. (Both can be violated, c_∞, at sufficiently small L because of interaction effects and exhaustibility of bulk concentrations.)[36,94] (Reprinted from J. Maier, "Defect chemistry and ion transport in nanostructured materials. Part II. Aspects of nano-ionics." *Solid State Ionics,* **157**, 327-334. Copyright © 2003 with permission from Elsevier.)

Before dealing with the superposition in polycrystalline materials, let us first consider the conductance of a thin film with an accumulation[148] effect at the interface to the (identical) neighboring phases for different thicknesses and consider Fig. 36. In the top figure the film is so thick that the interfacial effect is not seen; the carrier

profile is horizontal and the (parallel) conductance increases linearly with increasing thickness with a zero intercept. At distinctly smaller thicknesses the boundary effects appear and manifest themselves as a non-zero intercept in the conductance behavior; however, the interfaces are still separated. Only if the thickness is of the order of the space charge width or below, the conductance varies in a more sophisticated way according to

$$\Delta\sigma_m^\parallel \cdot L \equiv \Delta Y^\parallel \simeq 2u_1[2RT\varepsilon(c_{10} - c_1^*)]^{1/2} \qquad (88)$$

(1 denotes the accumulated majority carrier, c^* is the concentration value in the center and can be calculated from L and c_{10} via elliptical integrals of the first kind.) The detailed calculation is given in Ref.[148]. References[94,148,149] give experimental examples for the above situations. Figure 37 shows the same phenomenon in alternative presentations. The l.h.s. figure plots the mean excess film conductivity (i.e., the excess conductance normalized to the film thickness) as a function of the inverse thickness. Now the film thickness decreases from the left to the right. As long as $L > 4\lambda$, the boundary parts approach but are still separated leading to a linear increase of the mean conductivity as non-contributing bulk parts drop out. When L becomes smaller than 4λ, the mean specific value does not remain constant, rather the defect concentration is now locally enhanced (see Fig. 38, l.h.s. bottom). This enhancement can be described by the nano-size factor

$$g(L)- \approx \frac{4\lambda}{L}\left[\frac{c_{10} - c_1^*}{c_{10}}\right]^{1/2} \qquad (89)$$

In the r.h.s. part of the figure the excess conductance is normalized with respect to the space charge width (2λ if $L > 4\lambda$ and L if $L < 4\lambda$) being a measure of the mean conductivity of the space charge zone. This value remains constant in the regime of trivial size effects but increases according to g(L) in the regime of true size effects.

Analogously we have to proceed if we are measuring in the orthogonal direction; the results will be completely different (space charge profile, core effects). Even though the overall effect can be obtained more precisely by a superposition of bulk values and interfacial excess contributions, it is more convenient for large space
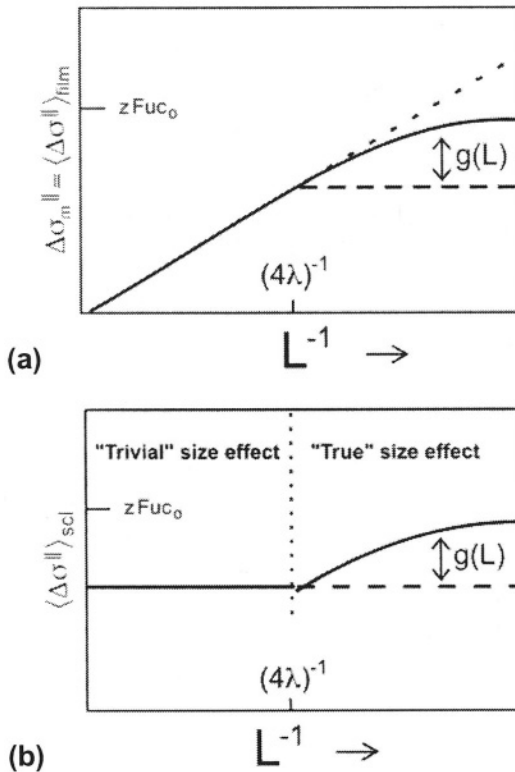
Figure 37. (a) Area related space charge conductance per film thickness representing the measured excess space charge conductivity, as a function of inverse spacing. (b) Area related space charge conductance per boundary thickness representing the mean specific excess space charge conductivity, as a function of inverse spacing.[37] (Space charge width is 4λ for $L \geq 4\lambda$, and L otherwise.) (Reprinted from J. Maier, "Nano-Ionics: Trivial and Non-Trivial Size Effects on Ion Conduction in Solids." *Z. Physik. Chem.* **217**, 415-436. Copyright © 2003 with permission from Oldenbourg Wissenschaftsverlag.)
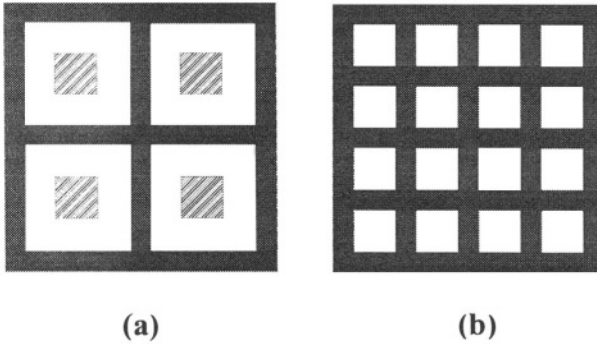
Figure 38. Section of a polycrystal (bricklayer-model), (a) Grain size large compared to 4λ. (b) Grain size smaller than 4λ. The white area refers to the space charge zones, the hatched to the electroneutral bulk and the dark to the interfacial core.[151] (Reprinted from J. Maier, "Thermodynamic aspects and morphology of nano-structured ion conductors. Aspects of nano-ionics. Part I." *Solid State Ionics* **154-155,** 291-301. Copyright © 2002 with permission from Elsevier.)

charge potentials to describe it approximately by a superposition of spatially separated regions of different transport parameters.

Now let us proceed to the description of a polycrystalline material and the superposition of bulk and both perpendicular ($\perp$) and parallel ($\parallel$) boundary effects in a bricklayer model (Fig. 38). The bricklayer model replaces the complex microstructure[153] by a primitive periodic arrangement of cubes. The superposition of bulk conductivity (σ_∞) and boundary conductivities ($\sigma_{gb}^{\parallel}, \sigma_{gb}^{\perp}$) within such a model can be approximately described by[120]

$$\sigma_m = [\sigma_\infty \sigma_{gb} + \beta_{gb}^{\parallel} \varphi_{gb} \sigma_{gb}^{\parallel} \sigma_{gb}^{\perp}] / [\sigma_{gb}^{\perp} + \beta_{gb}^{\perp} \varphi_{gb} \sigma_\infty] \qquad (90)$$

(φ_{gb} being the volume fraction of the boundary; $\beta_{gb}^{\parallel}, \beta_{gb}^{\perp}$ measuring the fraction of pathways that percolate, ideally 2/3 and 1/3). These transport parameters can also be conceived as complex quantities

allowing the interpretation of impedance spectra. The deconvolution into core (co) and space charge layers (sc) can be approximated by

$$\varphi_{gb} / \sigma_{gb}^{\perp} = \varphi_{sc} / \sigma_{sc}^{\perp} + \varphi_{co} / \sigma_{co}^{\perp} \qquad (91a)$$

$$\varphi_{gb} \sigma_{gb}^{\parallel} = \varphi_{sc} \sigma_{sc}^{\parallel} + \varphi_{co} \sigma_{co}^{\parallel} \qquad (91b)$$

The space charge values $\sigma_{sc}^{\parallel}$ and $\sigma_{sc}^{\perp}$ in Eq. (91) are mean values and calculated by integration of $c(x)$ or $1/c(x)$ (and normalization to the thickness of the space charge zone), respectively.

On this level we can state: Trivial size effects are size effects in which σ_m but not $\sigma_{\infty}, \sigma_{gb}^{\perp}, \sigma_{gb}^{\parallel}$ depend on φ, whereas the latter vary with φ in the case of the true size effects. (If edges and corners have to be considered, this distinction can be successively refined for different levels of resolutions.[152])

As the previous section showed, in a variety of examples severe enhancements of the ionic conductivity has been found and successfully attributed to space charge effects. Typical examples are silver halides or alkaline earth fluorides (see Section V.2.). How significantly these effects can be augmented by a particle size reduction, is demonstrated by the example of nano-crystalline CaF_2.[154] Epitaxial fluoride heterolayers prepared by molecular beam epitaxy not only show the thermodynamically demanded redistribution effect postulated above (see Section V.2.), they also highlight the mesoscopic situation in extremely thin films in which the electroneutral bulk has disappeared and an artificial ion conductor has been achieved (see Fig. 39).[119, 155-157]

As already stated in Section V.2., materials such as acceptor doped ZrO_2, CeO_2 and $SrTiO_3$ show a space charge behavior that is characterized by a depletion of oxygen vacancies leading to a depression of the ionic conductivity.[158]

The positive space charge potential leads to peculiar effects in nano-crystalline CeO_2.[136,159] In weakly positively doped material in which the electronic concentration is quite high but still low enough for it to remain an ion conductor in the bulk, the space charge effect (depletion of positive carriers such as holes and oxygen vacancies but accumulation of negative carriers such as excess electrons) makes its overall conductivity change to n-type. The enhanced electron transport
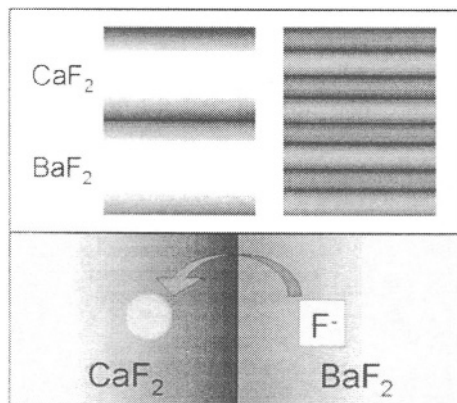
Figure 39. Ionic heterostructures composed of CaF_2 and BaF_2 leading to mesoscopic ion conduction.[36,119] (Reprinted from J. Maier, "Defect chemistry and ion transport in nanostructured materials. Part II. Aspects of nano-ionics." *Solid State Ionics,* **157,** 327-334. Copyright © 2003 with permission from Elsevier.)

along the boundaries as well as the depressed vacancy transport across them (which limits the bulk-to-bulk path) could be concluded from detailed electrochemical experiments (impedance spectroscopy, dc experiments using reversible and blocking electrodes).[136]

In the case of depletion layers the space charge overlap leads to extremely resistive situations. A relevant example are low angle grain boundaries in Fe-doped $SrTiO_3$. Such low angle grain boundaries consist of regularly arranged dislocations. Here the dislocations are positively charged, and the spacing between them is definitely smaller than the space charge width resulting in a severe and homogeneous blocking with respect to hole as well as ionic and atomic oxygen transport.[160]

Naturally, the space charge overlap is not the only possible true size effect.[37,161,162]

Others are structural effects that come into play when the effective size of a charge carrier (radius of influence) is of the order on the
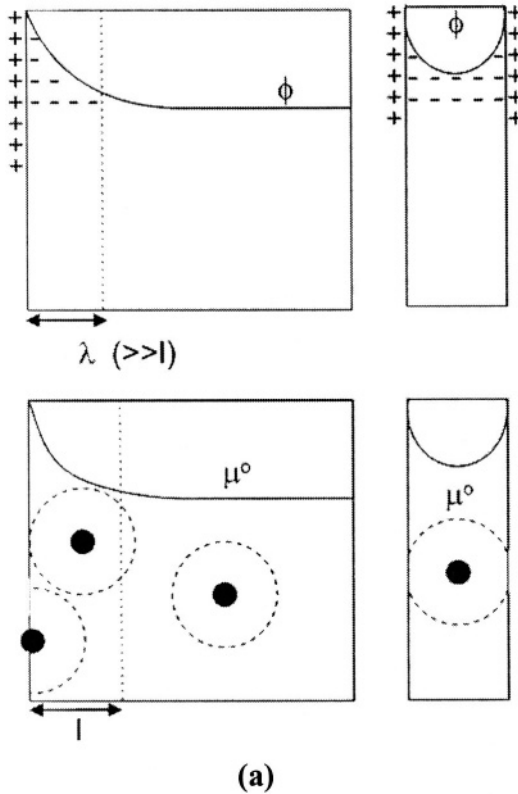
Figure 40. (a) Top: Space charge effects decaying with λ. Bottom: Structural effects that decay rapidly in the bulk. Within the indicated distance (ℓ) the structurally per-turbed core (not shown, extension s) is per-ceived by the defects as far as μ^o is concerning.[37] (b) Delocalized electrons perceive the boundaries much earlier ($\Delta\mu^o \propto L^{-2}$). (Reprinted from J. Maier, "Nano-Ionics: Trivial and Non-Trivial Size Effects on Ion Conduction in Solids." *Z. Physik. Chem.,* **217**, 415-436. Copyright © 2003 with permission from Oldenbourg Wissenschaftsverlag.)
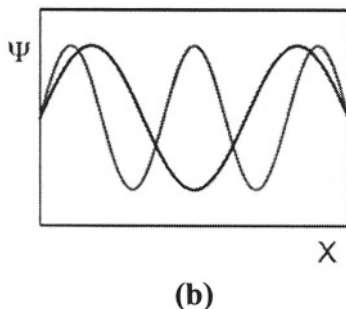
Figure 40. Continuation

interfacial spacing (or even earlier when e.g. elastic effects penetrate quite deeply). Then the standard chemical potential is affected (see Fig. 40). It is often found that the structure of crystals is well-maintained down to the range of a few nm. In NaCl, e.g. below 1 nm cluster forms represent the equilibrium structure, that are completely different from the rock-salt structure adopted at larger sizes.[163] Above 1 nm bulk and surface energies rapidly approach the values of the massive crystals.[164] In a very hand-waving way a parameter ℓ may be defined which is of such an order of magnitude. Since 1 nm is also typically the order of magnitude of interfacial core regions as well as typically the extension of the relaxation sphere around defects, it sets roughly the limit for the above core-space layer model.[36,37] Figure 40 refers to this point. Attention has to be paid to the fact that these two mesoscales are not necessarily de-convoluted, i.e., ℓ need not be small against λ nor need both parameters be constant concerning L. In the case of delocalised electrons (Fig. 40, bottom) this confinement (which affects μ^0) is already relevant for moderately small sizes and leads to the spectacular effects in the field of nano-electronics.[165] In reference[37] a variety of further geometrical and structural size effects are discussed. Only three shall be mentioned here: (i) One is the fact that the curvature introduces a Gibbs-Kelvin term into the chemical potential of two chemically different particles. This predicts a charging at the contact of two particles that are only different in terms of curvature. (Such a charging

is even expected in the case of zero curvature, i.e., in the core of thin films, if we refer to the sub-Debye regime.[166]) (ii) In small crystallites defect pairs (excitons, Frenkel-pairs) may not be separated sufficiently resulting in severe interaction effects. The reader is referred to it for more details.[167] (iii) Of special importance are interfacial phase transformations.[168] One example are highly disordered stacking faults occurring at special interfaces of AgI (e.g. $AgI:Al_2O_3$). They can be conceived as heterolayers of $\gamma/\beta/\gamma...$-AgI being highly disordered (note the similarity to the above fluoride heterolayers).[169] The field of nanoionics is not only of fundamental interest but also of technological significance. Li-batteries may serve as an example. While in the rocking-chair secondary cells must reversibly insert Li into the homogeneous phase, heterogenous storage is possible in the nanocrystalline state.[170,171] Not only are the lengths of the transport paths (see following chapter) drastically diminished, but also the differences between double layer capacitance and insertion capacitance are getting blurred.[150,161] Already these few examples show that nanostructured matter, given sufficient stability, can combine advantages from both the solid and the fluid state and constitutes an exciting future area of solid state chemistry.

VI. KINETICS OF CHARGE TRANSFER AND TRANSPORT

1. Three Experimental Situations

Charge transport in the bulk has to obey electroneutrality. Figure 41 shows three simple experiments that comply with this restriction. For brevity let us call them the electrical (a), the tracer (b) and the chemical experiment (c); and, to be specific, let us consider an oxide. In the electrical experiment an electrical potential difference is applied, the electrons flowing in the outer circuit compensate the charge flow within the sample (Figure 41a shows this for the case of a pure ion conductor). If we apply reversible electrodes, in the steady state there is no compositional change involved. (At this point we are not interested in (electro-)chemical effects caused by non-reversible electrodes. This is considered in detail in Part II.[1]) The tracer transport (b) caused by the application of a chemical potential difference of the isotopes consists of a counter motion of the two isotope ions. Finally, experiment (c) presupposes a mixed conduction; her the outer wire is, as it were,
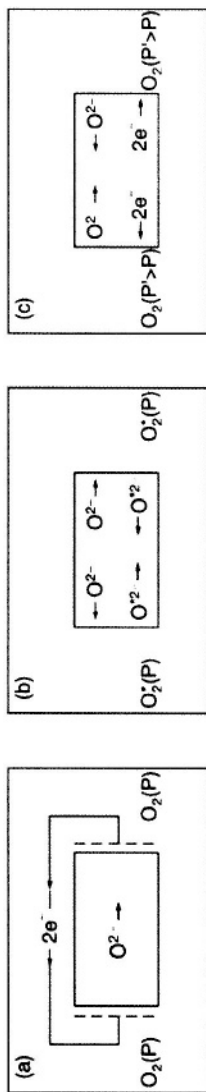
Figure 41. The three basic experiments discussed in the text: (a) electrical, (b) tracer, (c) chemical.[172] (Reprinted from J. Maier, "On the correlation of macroscopic and microscopic rate constants in solid state chemistry." *Solid State Ionics* **112**, 197-228. Copyright © 1998 with permission from Elsevier.)

internalized. The chemical transport is a consequence of different the chemical potentials of neutral oxygen and consists of an ambipolar motion of ions and electrons corresponding to a motion of "O". Unlike in the previous experiments now a compositional change occurs. Unlike experiment a, the experiments b and c represent true diffusion experiments. We will see that it is possible to decompose the diffusive transport coefficients into a resistive part and a chemical capacitance part. In the tracer case the chemical capacitance is simply given by the total ion concentration and hence a constant. The stationary electrical experiment only involves a resistance part (nevertheless diffusive transport coefficients, later labeled with upper index Q, are defined that allow a direct comparison); the transient behavior of the electrical experiment involves electrical capacitances.

If the bulk process is dominating, in the electrical experiment the total conductivity (ionic and electronic) is measured, the second gives information on the tracer diffusion coefficient (D^*) which is directly related to the ionic conductivity (or D^Q). In the third experiment one measures the chemical diffusion coefficient (D^δ), which is a measure of the propagation rate of stoichiometric changes (at given chemical gradient); it is evidently a combination of ionic and electronic conductivities and concentrations.[3,4,173-175]

In all three cases also surfaces or internal interfaces may be dominating which can be described in terms of effective rate constants $\bar{k}^Q, \bar{k}^*, \bar{k}^\delta$. As for the bulk processes $\bar{k}^Q$ is only formally obtained from the steady state parameters. The elucidation of $\bar{k}^Q$ is the basic problem of electrode kinetics extensively dealt with in liquid electrochemistry.

The three experiments do not only introduce decisive mass and charge transport parameters, they also permit their determination. Some points relevant in this context will be investigated in the following. (Note that electrochemical measurement techniques are covered by Part II.[1]) At the end of this section we will have seen that—close to equilibrium—not only all the D's and the $\bar{k}$'s can be expressed as the inverse of a product of generalized resistances and capacitances, but that these elements can be implemented into a generalized equivalent circuit with the help of which one can study the response of a material on electrical and/or chemical driving forces.

2. Rates, Fluxes and Driving Forces

(*i*) *Transport, Transfer and Reaction*

In spite of the complexity of real processes most cases of interest may be effectively described by a heterogeneous pseudo-monomolecular reaction of the type

$$A(x) \underset{\leftarrow}{\overset{\rightarrow}{\rule{1.5em}{0pt}}} B(x') \tag{92}$$

i.e., the transport of A from x to $x' \equiv x + \Delta x$ while it simultaneously transforms into B. The special cases of $x = x'$ and A = B correspond to a homogeneous chemical reaction

$$A \underset{\leftarrow}{\overset{\rightarrow}{\rule{1.5em}{0pt}}} B \tag{93}$$

and a pure transport $(A' \equiv A(x'))$

$$A \underset{\leftarrow}{\overset{\rightarrow}{\rule{1.5em}{0pt}}} A' \tag{94}$$

In both cases we are not specifically dealing with reorganization processes which are more complicated than in the case of liquids and specifically related with the crystal structure.[176,177] More precisely the first special case is met, if, for reactions, the difference in the space coordinate does not matter (i.e., if $z_A \phi(x) = z_B \phi(x')$). Hence pure gas phase reactions or neutral surface reactions can be described by Eq. (93), while Eq. (94) refers to pure transport steps (transport within the same structure). The description of typical electrochemical reactions such as charge transfer reactions require the analysis of Eq. (92). (We will see later that mechanistic equations are typically bimolecular, however, owing to the constancy of regular constituents, the consideration of Eq. (92) suffices in most cases of interest.)

Two approaches will be considered: one is to apply linear irreversible thermodynamics according to which the generalized rate $\widetilde{\mathfrak{R}}$ depends linearly on the generalized driving force $\widetilde{A}$ (corresponding

to the first approximation of a Taylor expansion of $\widetilde{\mathfrak{R}}$ in $\widetilde{A}$, since $\widetilde{\mathfrak{R}}$ ($\widetilde{A} = 0$) disappears):

$$\widetilde{\mathfrak{R}} = L\widetilde{A} + (L'\widetilde{A}^2 + L''\widetilde{A}^3 + ...) \tag{95}$$

In a better approximation $\widetilde{\mathfrak{R}}$ (of process k) can also depend on secondary driving forces such that

$$\widetilde{\mathfrak{R}}_i = \Sigma_{i'}L_{ii'}\widetilde{A}_{i'} \tag{96}$$

where $L_{ii'} = L_{i'i}$ owing to microscopic reversibility.[178] This approach obviously holds only for small driving forces but is general otherwise.

An alternative approach that applies irrespective of the deviation from equilibrium but presupposes small concentrations, is chemical kinetics, according to which the rate of the elementary reaction is determined by

$$\widetilde{\mathfrak{R}} = \overset{\sim}{\vec{k}}[A(x)] - \overset{\sim}{\overleftarrow{k}}[B(x')] \tag{97}$$

(For the limits of Eq. 97 see e.g. Ref.[6]) The rate constants for forward and backward reaction contain a purely chemical part that is determined by the free activation energies $\Delta\vec{G}^{\neq}, \Delta\overleftarrow{G}^{\neq}$ and a factor that is determined by the portion of the electrical potential drop that adds to activation energy, i.e., $\overset{\sim}{\vec{\alpha}}\Delta\phi$, $\overset{\sim}{\overleftarrow{\alpha}}\Delta\phi$.[179] Hence $\Delta\overset{\sim}{\vec{G}}^{\neq} = \Delta\vec{G}^{\neq} + \vec{\alpha}zF\Delta\phi$, $\Delta\overset{\sim}{\overleftarrow{G}}^{\neq} = \Delta\overleftarrow{G}^{\neq} + \overleftarrow{\alpha}zF\Delta\phi$, and

$$\overset{\sim}{\vec{k}} = k_0 \exp-\frac{\Delta\vec{G} + \vec{\alpha}zF\Delta\phi}{RT} \tag{98}$$

$$\overset{\sim}{\overleftarrow{k}} = k_0 \exp-\frac{\Delta\overleftarrow{G} + \overleftarrow{\alpha}zF\Delta\phi}{RT} \tag{99}$$

$\overrightarrow{\alpha}$ and $\overleftarrow{\alpha}$ being symmetry factors.[180] The pre-factor k_0 is a measure of the transition attempts. Field corrections in Eqs. (98) and (99) are of equal magnitude if the activation threshold is halfway the reaction coordinate.

While the reaction rate is usually defined by the (normalized) concentration increase of species k, i.e., by $\partial c_k/\partial t$, the flux density j_k (concentration times velocity) can be introduced by the continuity equation

$$\partial c_k /\partial t = -\text{div } \mathbf{j}_k \tag{100}$$

For a simple elementary reaction like Eq. (94) div j_k corresponds to $(\overset{\cdot}{j}_A - \overset{\cdot}{j}_A)/\Delta x$, and we can consider rates and fluxes almost synonymously in this case for pure transport. (Note that, unlike fluxes, usually rates are differently normalized with respect to stoichiometric number (ν_k) and geometry.) In many cases, in particular on a coarse grain-level it is meaningful to distinguish between transport effects (fluxes, transport rates) and generation/annihilation effects (local reaction rates). Then the continuity equation for k reads

$$\partial c_k /\partial t = -\text{div } \mathbf{j}_k + \nu_k \mathfrak{R}^{(k)} \tag{101}$$

where $\mathfrak{R}^{(k)}$ is the rate which produces (annihilates) the species k. In the steady state of pure transport the constancy of $\mathbf{j}_k$ follows, while a stationary conversion of $\mathfrak{R}^{(k)}$ into a flux $\mathbf{j}_k$ (consider e.g., electrode reaction at the electrode/electrolyte contact) implies $\mathfrak{R}^{(k)} \propto j_k$.

(ii) ***Transport in Terms of Linear Irreversible Thermodynamics and Chemical Kinetics***

For Eq. (92) the driving force $\widetilde{A}$ is obviously the difference in the electrochemical potentials

$$\widetilde{A} = -[\widetilde{\mu}_B(x') - \widetilde{\mu}_A(x)] \tag{102}$$

Table 3
Diagram for the non-equilibrium behavior in solids close to equilibrium. Conventional chemical reaction (x $\equiv$ x′) and particle transport (A $\equiv$ B) are described in a general manner. Particle transport also includes the limiting cases of pure diffusion (zF$\Delta\phi$ = 0) and pure electrical conduction ($\Delta\mu$ = 0).[21] Note slight deviations to the notation in the text (e.g. β as pro-portionality factor between flux and driving force).

linear irreversible thermodynamics
particle transport or reaction

$$\boxed{A(x) \rightleftharpoons B(x')}$$

$$\boxed{\begin{array}{c} \tilde{\mu}_A(x) \neq \tilde{\mu}_B(x') \\ J \propto -[\tilde{\mu}_B(x) - \tilde{\mu}_A(x)] \end{array}}$$

$zF\phi(x') = zF\phi(x)$ $A \equiv B$

conventional   particle transport
chemical reaction

$$\boxed{A \rightleftharpoons B} \qquad\qquad \boxed{A(x) \rightleftharpoons A(x')}$$

$$\boxed{\begin{array}{c} \mu_B - \mu_A = \Delta_R G \neq 0 \\ J_R \propto -\Delta_R G \end{array}}$$
für $\Delta_R G \ll RT$
$J_R = \Re$ = reaction rate

$$\boxed{\begin{array}{c} \tilde{\mu}(x') - \tilde{\mu}(x) \neq 0 \\ J_T = -\beta(\delta/\delta x)\tilde{\mu} \end{array}}$$

$(\delta/\delta x)zF\phi = 0$ $(\delta/\delta x)\mu = 0$
diffusion   conduction

$$\boxed{\begin{array}{c} \mu(x') - \mu(x) \neq 0 \\ J_T = -\beta(\delta/\delta x)\mu \\ j = -\dfrac{RT}{c}(\beta(\delta/\delta x)c) \end{array}} \quad \boxed{\begin{array}{c} \phi(x') - \phi(x) \neq 0 \\ J_T = -\beta zF(\delta/\delta x)\phi \\ i = -\beta z^2 F^2(\delta/\delta x)\phi \end{array}}$$

j = flux density   i = current density

$$D \equiv \dfrac{RT}{c}\beta \qquad\qquad \sigma = z^2 F^2 \beta$$

$$\frac{D}{RT} = \frac{\sigma}{cz^2 F^2} = \frac{u}{zF}$$

Nernst-Einstein-relation

which reduces to $-(\mu_B - \mu_A) = -\Delta_R G$ for a pure chemical reaction, and to $-[\tilde{\mu}_A(x') - \tilde{\mu}_A(x)] \propto -(\partial/\partial x)\tilde{\mu}_A$ for pure transport. If the electrical potential gradient is of no influence, e.g., in the case of neutral particles, the driving force is—according to $(\partial/\partial x)\mu_k = RT(w_k/c_k)(\partial/\partial x)c_k$ where w_k denotes the thermodynamic factor d ln a_k/d ln c_k and a_k the activity—finally determined by the concentration gradient.[*] If, however, the chemical potential is virtually constant, as it is the case for systems with a high carrier concentration (metals, superionic conductors), $z_k F(\partial/\partial x)\phi$ remains as driving force. For the linear approximation to be valid $\tilde{A}$ must be sufficiently small. Experimental experience confirms the validity of Fick's and Ohm's law (that immediately follow from Table 3 for diffusion[*] and electrical transport) in usual cases, but questions the validity of the linear relationship Eq. (96) in the case of chemical reactions. For a generalized transport we will use in the following the relation:[173,178,181]

$$j_k = -\frac{\sigma_k}{z^2 F^2} \nabla \tilde{\mu}_k \qquad (103)$$

The interpretation of the pre-factor as a conductivity as well as the correlation between defect diffusion coefficient D_k and mobility u_k known as Nernst-Einstein equation follow directly from Table 3.

The chemical kinetics approach provides us with more insight with respect to the range of validity. We see from Table 4 that Fick's law indeed results without approximations (l.h.s.). For the pure electrical conduction (r.h.s.) we have to linearize the exponentials (Eqs. 98 and 99), i.e., to assume $|F\Delta\phi| \ll RT$ which is definitely a good approximation for transport in usual samples; it fails at boundaries or for ultrathin samples. Hence the application of Eq. (103) has to presuppose sufficiently thick samples and not too high fields. Table 4 also reveals the connection between D_k, u_k and the transport rate constant k_k and hence their microscopic meaning:

$$D_k \propto u_k \propto k_k \qquad (104)$$

---

[*] Close to equilibrium the pre-factors, even though containing concentrations terms, can be considered to be constant, yet the range of validity changes. The chemical kinetics treatment (Table 4) shows that for dilute conditions $j \propto -\nabla c$ is valid at much larger derivations from equilibrium than $j \propto -\nabla \mu$.

Table 4
Diagram of the kinetic treatment of the non-equilibrium behavior in the dilute states.[21] Reaction, diffusion and electrical conduction appear as special cases ($\hat{c}$: equilibrium concentration) of the electrochemical reaction $A(x) \underset{\leftarrow}{\overset{\rightarrow}{\rightleftarrows}} B(x')$.
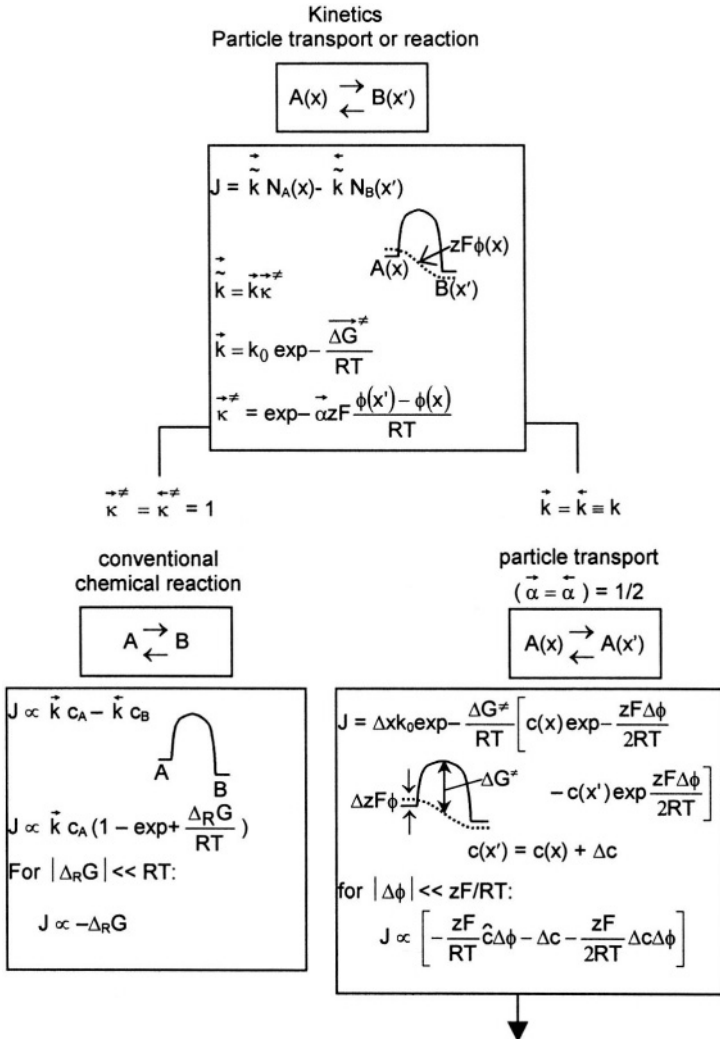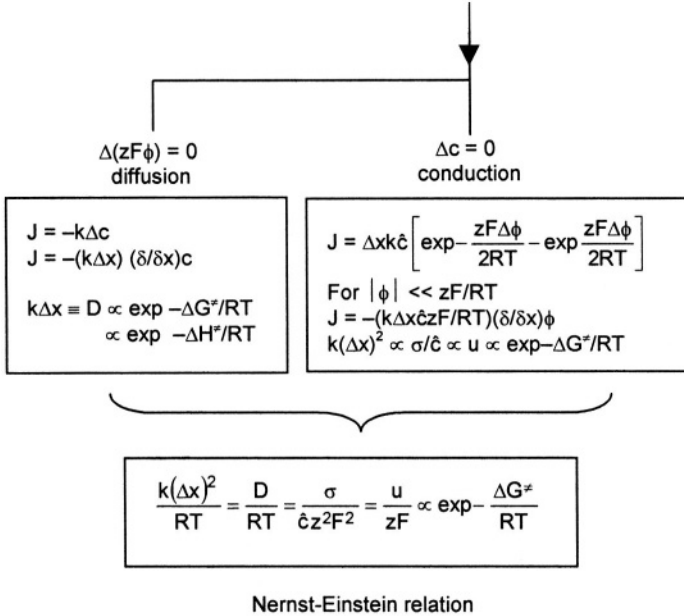

Kinetics
Particle transport or reaction

$$A(x) \underset{\leftarrow}{\overset{\rightarrow}{\rightleftarrows}} B(x')$$

$$J = \overset{\rightarrow}{\tilde{k}}\, N_A(x) - \overset{\leftarrow}{\tilde{k}}\, N_B(x')$$

$$\overset{\rightarrow}{\tilde{k}} = \vec{k}\,\overset{\rightarrow\neq}{\kappa}$$

$$\vec{k} = k_0 \exp-\frac{\overrightarrow{\Delta G}^{\neq}}{RT}$$

$$\overset{\rightarrow\neq}{\kappa} = \exp-\overset{\rightarrow}{\alpha}zF\frac{\phi(x')-\phi(x)}{RT}$$

$$\overset{\rightarrow\neq}{\kappa} = \overset{\leftarrow\neq}{\kappa} = 1$$

conventional
chemical reaction

$$A \underset{\leftarrow}{\overset{\rightarrow}{\rightleftarrows}} B$$

$$J \propto \vec{k}\, c_A - \overset{\leftarrow}{k}\, c_B$$

$$J \propto \vec{k}\, c_A \left(1 - \exp+\frac{\Delta_R G}{RT}\right)$$

For $|\Delta_R G| \ll RT$:

$$J \propto -\Delta_R G$$

$$\vec{k} = \overset{\leftarrow}{k} \equiv k$$

particle transport
$(\overset{\rightarrow}{\alpha} = \overset{\leftarrow}{\alpha}) = 1/2$

$$A(x) \underset{\leftarrow}{\overset{\rightarrow}{\rightleftarrows}} A(x')$$

$$J = \Delta x k_0 \exp-\frac{\Delta G^{\neq}}{RT}\left[c(x)\exp-\frac{zF\Delta\phi}{2RT} - c(x')\exp\frac{zF\Delta\phi}{2RT}\right]$$

$$c(x') = c(x) + \Delta c$$

for $|\Delta\phi| \ll zF/RT$:

$$J \propto \left[-\frac{zF}{RT}\hat{c}\Delta\phi - \Delta c - \frac{zF}{2RT}\Delta c\Delta\phi\right]$$

**Table 4
Continuation.**

The diagram shows a branching flowchart:

Left branch:

$\Delta(zF\phi) = 0$
diffusion

$$J = -k\Delta c$$
$$J = -(k\Delta x)(\delta/\delta x)c$$

$$k\Delta x \equiv D \propto exp\,-\Delta G^*/RT$$
$$\propto exp\,-\Delta H^\neq/RT$$

Right branch:

$\Delta c = 0$
conduction

$$J = \Delta x k\hat{c}\left[exp-\frac{zF\Delta\phi}{2RT} - exp\frac{zF\Delta\phi}{2RT}\right]$$

For $|\phi| \ll zF/RT$
$$J = -(k\Delta x\hat{c}zF/RT)(\delta/\delta x)\phi$$
$$k(\Delta x)^2 \propto \sigma/\hat{c} \propto u \propto exp-\Delta G^*/RT$$

Combined:

$$\frac{k(\Delta x)^2}{RT} = \frac{D}{RT} = \frac{\sigma}{\hat{c}z^2F^2} = \frac{u}{zF} \propto exp-\frac{\Delta G^\neq}{RT}$$

Nernst-Einstein relation

(Eq. 104 ignores weak T-dependencies in the pre-factors.)

In the case of chemical processes, one also has to linearize exponentials, i.e., to assume $|\Delta_R G/RT \ll 1|$. This is, however, now a very severe approximation owing to the large values of reaction free energies (difference in μ^o-**values** now important), unless we slightly perturb an already existing equilibrium. Thus, for a pure chemical process but also for the general electrochemical reaction we are advised to use the full description.

This is of course also true if we need to consider the general electrochemical reaction Eq. (92). If the applied driving force (cf. electrical experiment) is an electrical potential gradient, Eq. (97) leads to the well-known non-linear Butler-Volmer equation.[79] We will become acquainted with equally important kinetic equations for the cases of the tracer and the chemical experiment.[172]

Let us briefly consider two further formulations of Eq. (97) that will prove helpful when dealing with reaction kinetics. The first is

$$\widetilde{\mathfrak{R}} = \vec{\widetilde{\mathfrak{R}}}\left(1 - \frac{\overleftarrow{\widetilde{\mathfrak{R}}}}{\vec{\widetilde{\mathfrak{R}}}}\right) = \vec{\widetilde{\mathfrak{R}}}\left(1 - \exp-\frac{\widetilde{A}}{RT}\right) \tag{105}$$

For $\widetilde{A} \to 0$ (i.e., $\vec{\widetilde{\mathfrak{R}}} \to \widehat{\widetilde{\mathfrak{R}}} \equiv \mathfrak{R}^\circ$) the result

$$\widetilde{\mathfrak{R}} = \widetilde{\mathfrak{R}}^\circ \widetilde{A} \tag{106}$$

complies with linear irreversible thermodynamics. The comparison with Eq. (95) shows that the exchange rate $\widetilde{\mathfrak{R}}^\circ$ plays the role of the decisive equilibrium permeability. (Note that in the case of transport $\widetilde{A} \propto (\partial/\partial x)\widetilde{\mu}$, and $\widetilde{\mathfrak{R}}^\circ \propto \sigma$.)

Equation (97) can also be rewritten as

$$\widetilde{\mathfrak{R}} = \widetilde{\mathfrak{R}}^\circ\left[\frac{\delta\vec{\widetilde{\mathfrak{R}}}}{\widetilde{\mathfrak{R}}^\circ} - \frac{\delta\overleftarrow{\widetilde{\mathfrak{R}}}}{\widetilde{\mathfrak{R}}^\circ}\right] = \widetilde{\mathfrak{R}}^\circ\left[\frac{\delta\left(\vec{\widetilde{k}}[A]\right)}{\vec{\widehat{k}}[\widehat{A}]} - \frac{\delta\left(\overleftarrow{\widetilde{k}}[B]\right)}{\overleftarrow{\widehat{k}}[\widehat{B}]}\right] \tag{107}$$

where δ refers to the perturbation from the equilibrium value (denoted by an arc). We will exploit this formulation in Section VI.5.

It is well-known from thermodynamics that the entropy production or better the related quantity, the dissipation, $\Pi = T\delta S/\delta t$ is a positive-definite function being related with the rates and forces via[182,183]

$$\Pi \equiv \Sigma_i \widetilde{\mathfrak{R}}_i \widetilde{A}_i \geq 0 \tag{108}$$

If the linear relations are valid (Eq. 96), Π is a bilinear function in the $\widetilde{A}$'s. One implication of the positive definiteness of Π is that all the pure transport terms L_{ii} cannot be negative. It can be shown that in

steady states Π is at minimum for linear processes.[183] Moreover, processes near the steady state are characterized by a decrease of Π meaning that in the linear regime steady states are automatically stable, which is no longer the case for non-linear processes (see Section VI.9.).

3. Bulk Processes

(*i*) *Electrical Conduction: Mobility, Conductivity and Random Walk*

In the pure electrical experiment we measure the conductivity which can be broken down into contributions of ions and electrons and finally into the defect contributions (k: conduction electron, hole; vacancy, interstitial)

$$\sigma = \sigma_{ion} + \sigma_{eon} = \Sigma_k \sigma_k \qquad (109)$$

In Part II[1] we will become acquainted with methods to de-convolute ionic and electron conductivity. According to Table 4 σ_k can be broken down into charge number, concentration and mobility according to

$$\sigma_k = z_k F u_k c_k \qquad (110)$$

the mobility being proportional to the defect diffusion coefficient D_k according to the Nernst-Einstein relation. Let us consider the case where the ion conductivity is dominated by a single defect k. Had we no idea about the defect concentration, then it would be reasonable to define an average ion mobility (corresponding to a self-diffusion coefficient D_{ion}) which could the be recast into an ionic diffusion D^Q coefficient:

$$D^Q = D_{ion} = D_k c_k / c_{ion} \qquad (111)$$

Equation (111) follows from the fact that the potential gradients and flux densities in Eq. (103) are invariant against the substitution ion $\leftrightarrow$ defect. Hence σ is invariant ($\sigma_k = \sigma_{ion}$) and so is the product DC. (The generalization is given by Eqs. 150 and 151.)

Let us discuss in the following some fundamental aspects of the mobility of ions and electrons and consider specific conductors.

(ii) Mobility

   The previous paragraphs (see Table 4) showed that the mobility of the defect is proportional to its (self-) diffusion coefficient. A realistic self-diffusion process involves jumps in different directions as well as a sequence of jumps leading to a long range transport. It is easy to show that Eq. (104) still applies in essence as long as the jump situation is isotropic and homogeneous and the long range transport follows a random walk process.[184,185] If the jump i refers to a spatial variation $\mathbf{r_i}$, after n jumps the particle is displaced from the origin by $\sum_{i=0}^{n} \mathbf{r_i}$
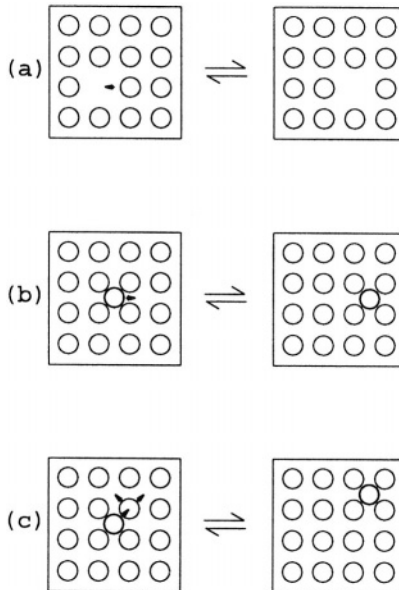
Figure 42. Elementary jump mechanisms in crystals: a) vacancy mechanism, b) direct interstitial mechanism, c) (collinear or non-collinear), indirect interstitial mechanism (interstitialcy mechanism).

corresponding to a square displacement $nr^2 + 2\sum\limits_{i=j+1}^{n}\sum\limits_{j=1}^{n-1} r^2 \cos_{ij}$ after n

steps. The mean square displacement for a random walk ($\overline{\cos\alpha_{ij}} = 0$) is then nr^2. On the other hand the probability function of reaching a given distance at n jumps is determined by a Gauss-function provided n is large enough. This yields the value 6Dt for the mean square displacement.[6] The combination of the two expressions leads to $n/t = 6D/r^2$ (where $r = \Delta x$ in the one-dimensional treatment). The quantity $\Gamma \equiv n/t$ is the jump frequency which is proportional to the rate constant k used for the simplistic elementary reaction in Eq. (94). Hence, D and thus the mobility (more precisely the product uT) of the defect is proportional to the jump frequency, the latter being activated via the migration threshold (Γ_o: attempt frequency)

$$uT = const\ \Gamma_o(\Delta x)^2 \exp\frac{\Delta S^{\neq}}{R} \exp-\frac{\Delta H^{\neq}}{RT} \qquad (112)$$
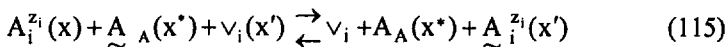
Figure 42 shows the basic elementary ion migration processes in a low defective isotropic ion conductor with a mobility in the A-sublattice. The vacancy mechanism (Fig. 42 top) can be described by a transport process (z_v = effective charge of the A-vacancy) such as

$$A_A(x) + v_A^{z_v}(x') \underset{\leftarrow}{\overset{\rightarrow}{}} v_A^{z_v}(x) + A_A(x') \qquad (113)$$
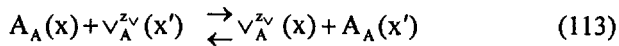
Interstitial ions ($z_i = -z_v$) are either transported directly (see Fig. 42 center) according to

$$A_i^{z_i}(x) + v_i(x') \underset{\leftarrow}{\overset{\rightarrow}{}} v_i(x) + A_i^{z_i}(x') \qquad (114)$$
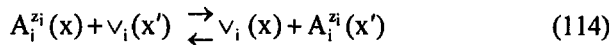
or more frequently indirectly (see Fig. 42 bottom) by pushing a regular neighbor at $x^{\bullet}$ into the free interstitial site while occupying its position:

$$A_i^{z_i}(x) + \underset{\sim}{A}_A(x^{\bullet}) + v_i(x') \underset{\leftarrow}{\overset{\rightarrow}{}} v_i + A_A(x^{\bullet}) + \underset{\sim}{A}_i^{z_i}(x') \qquad (115)$$
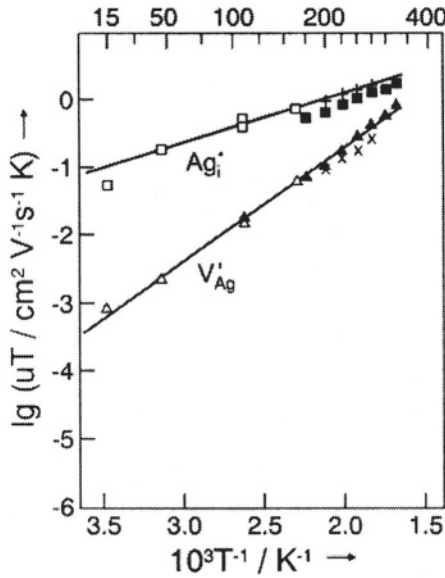
Figure 43. The mobility of the Frenkel defects in AgBr as a function of the temperature (according to Eq. 113). From Ref.[186]. (Reprinted from P. Müller, "Ionenleitfähig-keit von reinen und dotierten AgBr- und AgCl-Einkristallen." *Phys. Stat. Sol.* **12**, 775-794. Copyright © 1965 with permission from WILEY-VCH Verlag GmbH.)

It is clear that at high carrier concentrations Eq. (112) has to be modified and at least a term that takes account of the (then varying) concentrations of the regular partners have to be introduced ($u \propto 1\text{-}x$). Figure 43 shows mobilities for vacancies and interstitials in AgBr and Fig. 44 conductivities of Ag ion conductors.
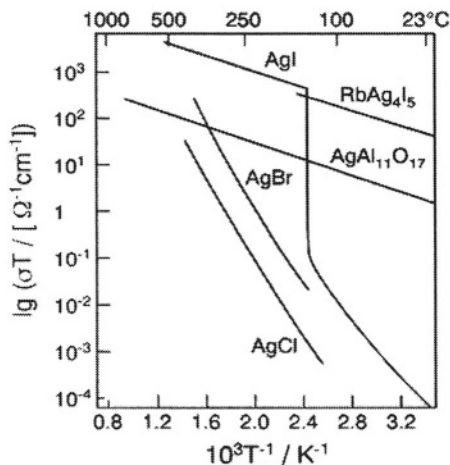
Figure 44. The temperature dependence of the specific conductivity for a series of selected silver ion conductors. ($AgAl_{11}O_{17}$ reads more correctly $Ag_{1+x}Al_{11}O_{17+x/2}$). The "superionic conductors" are characterized by flat slopes and high absolute values.[23]

In the so-called superionic conductors (see Fig. 44) virtually all constituents are carriers and usually the migration thresholds are very small (~ 0.1 eV in α-AgI) leading to very high ion conductivities (cf. Section IV.5.*ii*). The most popular example is α-AgI the crystal structure of which is displayed in Fig. 45.[187] Another example is β-**alumina** in which there is a ^{2}D superconduction in so-called conduction planes.[198] A detailed discussion of individual crystal structures would lead us too far from the scope of this contribution (see, e.g., reference[10]).

Figure 46 gives a selection of anion conductors in a **log** σ vs. 1/T representation. Proton transport deserves special treatment owing to the extremely polarizing nature of this elementary particle. Figure 47 shows a transition configuration of proton transport in $BaCeO_3$ (cf. Section IV.3.) according to molecular dynamics simulation.[192] The
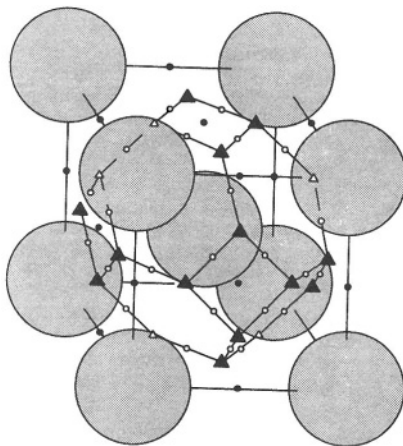
Figure 45. Crystal structure of α-AgI. The iodide ions are represented by large spheres. The multiplicity of (not precisely) energetically identical sites for Ag^+ ions and the low activation energy compared with the thermal energy when T > 146 °C lead to a "melting" of the Ag^+ partial lattice. According to Ref.[187].

transport is best described as a dynamic breaking and forming of hydrogen bonds in interaction with the lattice dynamics. The transport is liquid-like in ion exchange membranes in which protons of internal sulfonic acid groups are dissolved by water molecules and migrating within water channels in the polymer matrix. Heterocycles with proton-donor and acceptor function can replace water in this respect.[199]

For a discussion of conductivity aspects in disordered systems cf. Ref.[200] Polar groups of covalent polymers can also solvate ions (see Fig. 48) and lead to high conductivities, as PEO does with respect to LiX dissociation.[193,201]

Interesting in this context is the finding that oxides such as Al_2O_3, TiO_2 etc. can be used as fillers that enhance the ion conductivity.[116] Even though effects such as impact on crystallinity or on segmental motion are expected to have a great influence, the picture developed in Section V.2. should also be relevant: In a covalent matrix most of
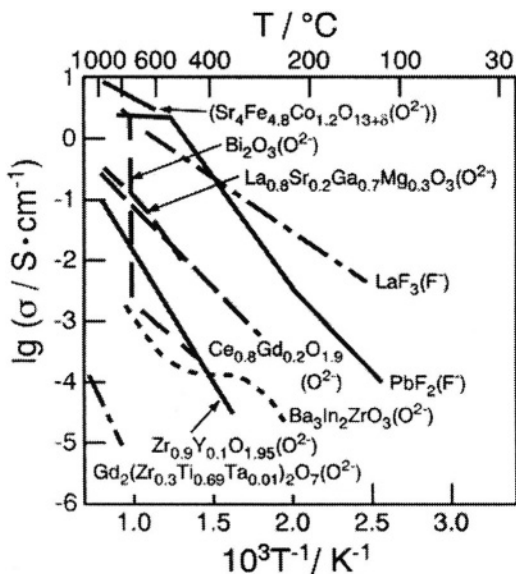
Figure 46. Specific conductivity of a few selected anion conductors as a function of the temperature (O^{2-}, F^-).[23] Very high O^{2-} conductivities are met in some perovskites, typically in doped ferrates.[188] These materials (cf. $Sr_4Fe_{4.8}Co_{1.2}O_{13+\delta}(O^{2-})$) are however mixed conductors and hence excellent materials for permeation membranes (cf. also Part II[1]). For more detailed data collections see Ref.[188-191].

the salt constituents should be associated (ion pairs). An acidic (basic) second phase should partly break these ion pairs by adsorbing the anion (cation) and releasing the counter ion. The experimental observation that in many cases acidic oxides enhance the Li^+ conductivity substantially, may be explained by this effect.[202]

The mobility of electrons will only be briefly touched upon as there is extensive solid physics literature on this (see e.g., Ref.[203]). In many cases electrons or holes behave as polarons, i.e., similar as the ionic defects. Then, they substantially polarize their environment,
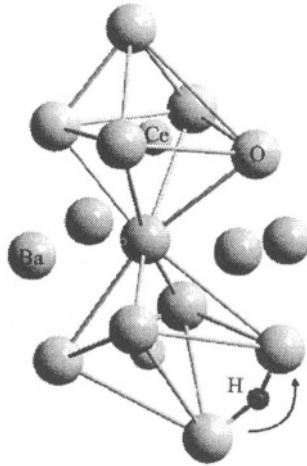
Figure 47. As oxygen ions move towards each other on account of lattice vibrations, the activation energy for proton jump is lowered, and the proton changes partner. According to Ref..[192]. (Reprinted from K. D. Kreuer, W. Münch, U. Traub and J. Maier, "On Proton Transport in Perovskite-Type Oxides and Plastic Hydroxides", *Ber. Bunsenges. Phys Chem.* **102,** 552-559. Copyright © 1998 with permission from WILEY-VCH Verlag GmbH.)

leading to perceptible migration thresholds on the order of 0.1 eV or more (small polarons). Large polarons can be approximately described by the band model. Whereas in the first case the T-dependence of the pre-factor may be neglected, in the second case it is the decisive contribution. For acoustic phonon scattering typically a $T^{3/2}$ law is obtained (Fig. 49), and the mobility decreases with increasing temperature (as assumed hi Fig. 49 for high temperatures). Even though the phenomenon of nearly free electrons in metals is comparable with the superionic situation in terms of degree of disorder, the mobility is
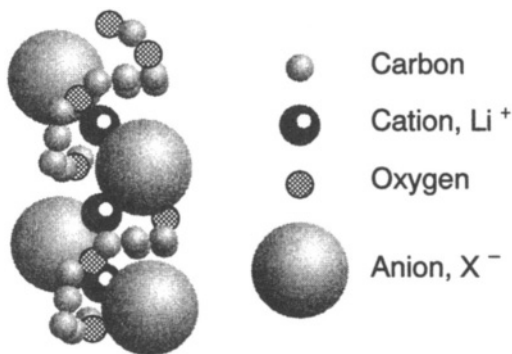
Figure 48. Schematic illustration of the structure of a PEO-LiX complex (Li^+X^- dissolved in poly ethylene oxide[193]). (The relative magnitudes are not representative.) From Ref.[194]. (Reprinted from B. Scrosati, "Lithium Ion Plastic Batteries." in: *Lithium Ion Batteries* (M. Wakihara and O. Yamamoto eds.), VCH, Weinheim Copyright © 1998 with permission from WILEY–VCH, Verlag GmbH.)

very different and of course much higher owing to quantum mechanics. In superconductors[197] the mobility is formally infinite. Figure 50 shows the disappearance of resistivity in the high temperature superconductor "LSC" at $T \approx 40$ K. Much literature is also concerned with organic metals based on conjugated polymers. Since one-dimensional delocalization cannot be very extended due to the Peierls-distortion,[204] an appropriate doping (redox effect) is necessary (shown in Fig. 51) to achieve high conductivities.

(iii)   *Tracer Diffusion*

As already mentioned the tracer experiment (which can also be conceived as a counter motion of the isotopes) delivers the tracer diffusion coefficient. In the case of oxides ideally the natural oxygen gas phase is instantaneously replaced by a gas phase with the same oxygen partial pressure but exhibiting a different isotope ratio (or an oxide is contacted with the same oxide in which a cation isotope is
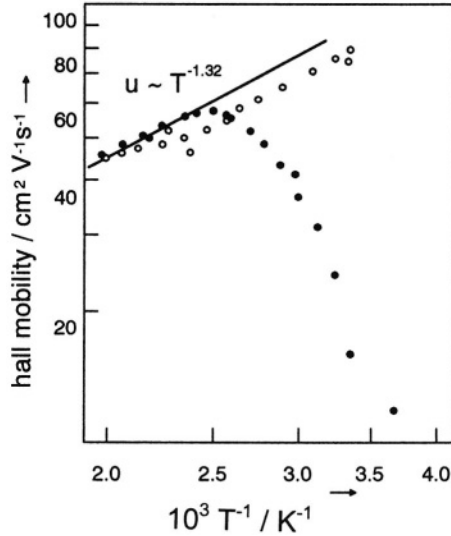
Figure 49. The mobility of the excess electrons in various SnO_2 samples determined by means of the Hall effect and conductivity. The high temperature behavior points to acoustic phonon scattering. Both samples differ in purity. According to Ref..[195]. (Reprinted from H. J. van Daal, "Polar Optical-Mode Scattering of Electrons in SnO_2.", *Solid State Commun.* **6,** 5-9. Copyright © 1968 with permission from Elsevier.)

enriched), then the diffusion is detected in-situ, e.g.,, by weight increase, or quenched non-equilibrium profiles are investigated, e.g., by SIMS (secondary ion mass spectroscopy). Owing to the ideality of the situation (asterisk denotes tracer)

$$j^* \propto \sigma^* \nabla \tilde{\mu}^* = \sigma^* \nabla \mu^* \propto \frac{\sigma^*}{c^*} \nabla c^* = \frac{\sigma}{c} \nabla c^* \qquad (116)$$

(The transport quantities refer to the ions.) In this approximation $D^* = D^Q$. A closer inspection shows that correction factors f^* have to be introduced, that will be considered in Section VI.4.[205]

Figure 50. The resistivity of SrO-doped La_2CuO_4 disappears at temperatures less than $T_C \simeq 40$ K. The $(h^\bullet)_2$ "associates" (Cooper pairs) are responsible for this. The two curves are based on samples, that are annealed at differing partial pressures of oxygen.[196,197] Compare here Section IV..3. (Reprinted from J. C. Philips (ed.), *Physics of High Temperature Superconductors*, Academie Press, New York, Copyright © 1989 with permission from Elsevier.)

Figure 51. The doping of poly-acethylene with iodine leads to the formation of a hole. Iodide (or poly-iodide) is the counterion.

Irrespective of the relevance of tracer diffusion for the systematic discussion, it is a very important technique to detect the nature of conductive species and to identify transport mechanisms.[206,207]

(*iv*)   *Chemical Diffusion*

The most important transport parameter for chemical processes is the chemical diffusion coefficient D^δ.[4,173-175,181] The relevance for electrochemistry is twofold. (*i*) Chemical diffusion is typically established by a counter flow of two charge carriers. (*ii*) It is the central bulk process occurring in response to an electrical polarization using non-reversible or selectively blocking electrodes (cf. Part II). Together with the geometry D^δ describes the time constant of the propagation of the chemical signal "stoichiometry" into the bulk. In the case that oxygen stoichiometry is concerned according to

$$MO_{1+\delta} + \frac{1}{2}\Delta O_2 \underset{\leftarrow}{\rightarrow} MO_{1+\delta+\Delta} \tag{117}$$
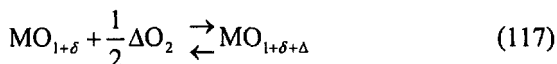
the underlying process is an ambipolar motion of O^{2-} and $2e^-$.

If we consider O_i'' and $h^\bullet$ as carriers, we refer, e.g., to chemical diffusion of oxygen in La_2CuO_4. Writing down the one-dimensional transport equations (Eq. 103) for ionic and electronic carriers and considering flux coupling and electroneutrality, we immediately obtain for this case (see, e.g., Ref.[173])

$$j_{O_i'} = j_{O^{2-}} = j_O = D_O^\delta \frac{\partial c_O}{\partial x} = D_O^\delta \frac{\partial c_{O_i'}}{\partial x} = \frac{1}{2}D_O^\delta \frac{\partial c_{h^\bullet}}{\partial x} = \frac{1}{2}j_{h^\bullet}. \tag{118}$$

where

$$D_O^\delta = \frac{1}{4F^2}\sigma_O^\delta \frac{\partial \mu_O}{\partial c_O} = \frac{RT}{4F^2}\frac{\sigma_O^\delta}{c_O}\frac{\partial \ln a_O}{\partial \ln c_O} \equiv \frac{RT}{4F^2}\frac{\sigma_O^\delta}{c_O}w_O \equiv \frac{RT}{4F^2}\frac{\sigma_O^\delta}{c_O^\delta} \tag{119}$$

The ambipolar conductivity σ^δ represents the harmonic mean of $\sigma_{h^\bullet}$ and $\sigma_{O_i''}$ (i.e., $\sigma_{h^\bullet}\sigma_{O_i'}/\sigma$). The term $\partial\mu_O/\partial c_O$ can also be referred to as an inverse chemical capacitance (by analogy to the electrical capacitance $\partial charge/\partial\phi$) and is given by RTw_O/c_O, w_O being the

thermodynamic factor.[15] The latter quantity can be expressed by the relevant parameters of the ionic and electronic constituent ($\partial\mu_O = \partial\mu_{O^{2-}} - 2\partial\mu_{e^-}$; $\partial c_O = \partial c_{O^{2-}} = -\frac{1}{2}\partial c_{e^-}$)

$$D_O^\delta = \frac{RT}{4F^2}\frac{\sigma_{O^{2-}}\sigma_{e^-}}{\sigma_{O^{2-}}+\sigma_{e^-}}\left(\frac{1}{c_{O^{2-}}}\frac{\partial\ln a_{O^{2-}}}{\partial\ln c_{O^{2-}}}+4\frac{1}{c_{e^-}}\frac{\partial\ln a_{e^-}}{\partial\ln c_{e^-}}\right) \tag{120a}$$

A further discussion requires the translation into defect parameters ($\partial\mu_{O_i'} = \partial\mu_{O^{2-}}$, $\partial\mu_{e^-} = -\partial\mu_{h^\bullet}$; $\partial c_{e^-} = -\partial c_{h^\bullet}$, $\partial c_{O^{2-}} = \partial c_{O_i'}$)

$$D_O^\delta = \frac{RT}{4F^2}\frac{\sigma_{O_i'}\sigma_{h^\bullet}}{\sigma_{O_i'}+\sigma_{h^\bullet}}\left(\frac{1}{c_{O_i'}}\frac{\partial\ln a_{O_i'}}{\partial\ln c_{O_i'}}+4\frac{1}{c_{h^\bullet}}\frac{\partial\ln a_{h^\bullet}}{\partial\ln c_{h^\bullet}}\right) \tag{120b}$$

Since (unlike $w_O, w_{O^{2-}}, w_{e^-}$) now $w_{O_i'}, w_{h^\bullet}$ are unity for a low defective material, it follows that

$$D^\delta = \frac{(D_{h^\bullet}c_{h^\bullet})(D_{O_i'}c_{O_i'})}{(D_{h^\bullet}c_{h^\bullet})+4(D_{O_i'}c_{O_i'})}\left(\frac{1}{c_{O_i'}}+\frac{4}{c_{h^\bullet}}\right) = t_{h^\bullet}D_{O_i'} + t_{O_i'}D_{h^\bullet} \tag{120c}$$

(t: transference number).

This equation shows how defect concentrations and mobilities constitute D^δ and how D^δ depends on materials and control (P, T, C) parameters. D_O^δ obviously lies between $D_{O_i'}$ and $D_{h^\bullet}$, and is hence

much larger than $D_{O^{2-}} = D_O^Q \approx D_O^*$. Since the mobility of the electronic carriers is usually much larger than that of the ionic carriers, a predominantly ionically conducting solid implies $c_{O_i'} >> c_{h^\bullet}$ and hence $D_O^\delta \approx D_{h^\bullet}$; in the case of an electronic conductor, $c_{h^\bullet}$ may still be smaller than $c_{O_i'}$, if this is the case, then $D_O^\delta = 4(c_{O_i'}/c_{h^\bullet})D_{O_i'}$; only in the case of the electron-rich electronic conductor the other limiting case $D_O^\delta \approx D_{O_i'}$ is arrived at.
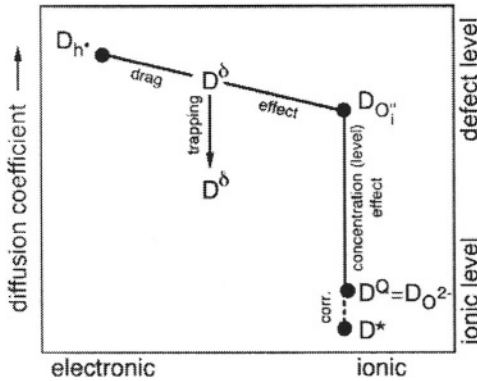
Figure 52. The relationships between the different diffusion coefficients discussed in the text. Holes and interstitial oxygen ions ars assumed as mobile defects.

Table 5

Comparison of ion conductivity tracer diffusion and chemical diffusion for electron-rich electron conductors, using

$$j \propto \Re = \vec{k} c_{O^{2-}}(x) c_{V_O^{\bullet\bullet}}(x') - \overleftarrow{k} c_{O^{2-}}(x') c_{V_O^{\bullet\bullet}}(x)$$

(Δk refers to the difference of the electrochemical rate constants $\vec{\tilde{k}}$ and $\overleftarrow{\tilde{k}}$. The tilde has been suppressed for simplicity.)

Experiment	Simplification ($\Re$)
Ionic conductivity	$-(\Delta k)\, c_{O^{2-}} c_{V_O^{\bullet\bullet}}$
Tracer exchange	$-k\,(\Delta c_{O^{2-}})\, c_{V_O^{\bullet\bullet}}$
Chemical diffusion	$-k c_{O^{2-}}\,(\Delta c_{V_O^{\bullet\bullet}})$

Figure 52 illustrates the situation. The more general case in which different defects contribute will be tackled below in the framework of Conservative Ensembles (Section VI.4.*ii*.) which also explains the displayed depression of D^{δ} by trapping effects (see Fig. 52).

It is instructive to compare the three transport processes (conduction, tracer diffusion and chemical diffusion) by using chemical kinetics and for simplicity concentrating on the electron-rich electron conductor, i.e., referring to the r.h.s. of Fig. 52. The results of applying Eq. (97) are summarized in Table 5 and directly verify the conclusions. Unlike in Section VI.2.*i*., we now refer more precisely to bimolecular rate equations (according to Eqs. 113-115); nonetheless the pseudo-monomolecular description is still a good approximation, since only one parameter is actually varied. This is also the reason why we can use concentrations for the regular constituents in the case of chemical diffusion. In the case of tracer diffusion this is allowed because of the ideality of distribution.

The kinetic procedures also work in more general cases and also reproduce the detailed thermodynamic factor.[208] This approach is generally helpful when dealing with large driving forces.

There are cases in which compositional changes are only caused by ionic fluxes, e.g., by counter diffusion of cations during spinel formation (cf. Section VI.8) or diffusion of H_2O into perovskites. In such cases we do not deal with redox reactions. As regards the H_2O diffusion into oxides, the process is described by counter diffusion of H^+ (via $OH_O^{\bullet}$) and O^{2-} (via $v_O^{\bullet\bullet}$). The relations are completely analogous: A convenient representation of $D_{H_2O}^{\delta}$ is then[57,60]

$$D_{H_2O}^{\delta} = t_{OH_O^{\bullet}} D_{v_O^{\bullet\bullet}} + t_{v_O^{\bullet\bullet}} D_{OH_O^{\bullet}} \qquad (121)$$

D^{δ} can be measured by recording the time changes of a signal that is unambiguously correlated with stoichiometry or by spatial detection of diffusion profiles at a given time. While in Part II[1] we will encounter powerful electrochemical polarization methods, here we will just refer to chemical diffusion processes that are caused by changes in the chemical driving force. To be specific, we consider an oxide subject to a sudden change in the partial pressure of oxygen and follow an appropriate signal. Usually the signal integrates over the stoichiometry profile. If the stoichiometry change is substantial,[209] one may use

weight as a measure. A sensitive and convenient measure is usually the electrical conductance which—according to Eq. (33)—depends in a power law on P_{O_2}. If the characteristic exponent N is appreciably large, this is a very recommended method (Fig. 53) (see, e.g.., Ref.[210]). In the case of solid electrolytes (e.g., Y_2O_3-doped ZrO_2) $N \equiv 0$ and the method fails (unless one uses a blocking technique). In these cases spectroscopic methods relying on changes in EPR, NMR or optical absorption signals are appropriate.[211] A method that allows for spatial resolution, yet, only in the quenched state, is SIMS already mentioned in the context of tracer diffusion experiments;[207] in terms of chemical diffusion it is not sensitive enough to detect small relative changes in composition (like weight) but may be a good method to determine, e.g., H_2O incorporation in oxides.

In Ref.[212] an optical absorption technique was developed in order to follow chemical diffusion in Fe-doped $SrTiO_3$, which enables a spatially resolved in-situ detection, i.e., makes it possible to follow the stoichiometry as a function of space and time at high temperatures.

The solution to the diffusion equation are modulated Fourier series of the form[213]

$$\frac{S(x,t) - S_1}{S_2 - S_1} = \frac{c_O(x,t) - c_{O1}}{c_{O2} - c_{O1}} \tag{122}$$

$$= 1 - \sum_0^\infty \frac{4(-1)^i}{\pi(2i+1)} \cos\left[\pi(2i+1)\frac{x}{L}\right] \exp\left[-\pi^2(2i+1)^2 \frac{D^\delta t}{L^2}\right]$$

S can be any detection signal that is linearly correlated with the oxygen concentration c_O (here the absorption coefficient). The indices 1 and 2 denote the homogeneous equilibrium situations corresponding to P_1 and P_2. Switching from P_1 to P_2 occurs at $t = 0$.

Figure 54 displays the normalized profiles as a function of the normalized position coordinate for a sample half. The parameter at the curves is the normalized time $t/(L/2\sqrt{D^\delta})^2$. If this parameter reaches the value 1 (then $t \equiv \tau_{eq}$) the sample value equals the mean square displacement,
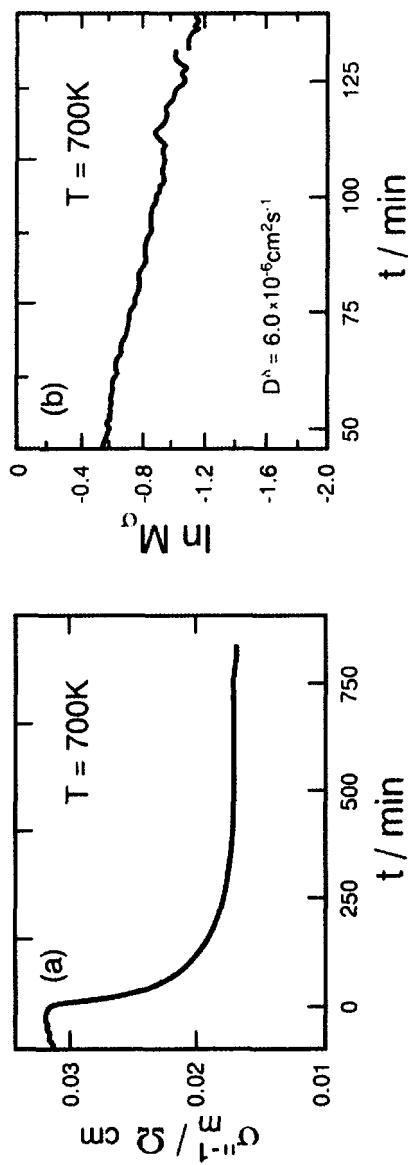
$$L^2 \approx 2Dt_{eq} \tag{123}$$

Figure 53. In the logarithmic plot (b) the measurement curve of the specific resistance of $YBa_2Cu_3O_{6+x}$ as a function of time (a) linearizes if the time is not too short; the slope is determined by D^δ and L.[215]
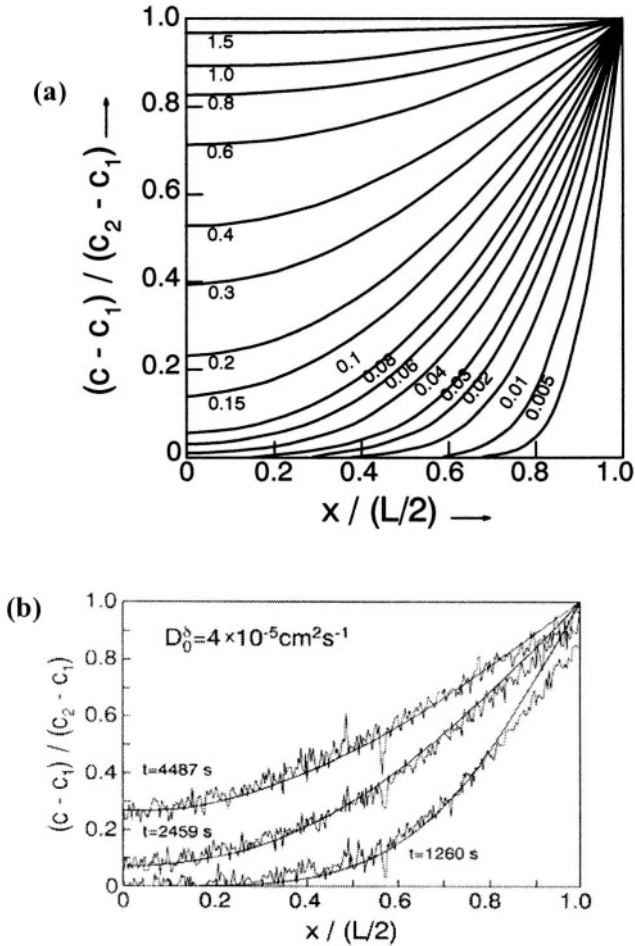
Figure 54. (a) Profiles for half the sample on rapid exchange of the surface concentration on both sides by x = ±L/2. The value x = 0 refers to the center of the sample. The parameter on the curves is $D^\delta t/(L/2)^2$. (b) Concentration profiles during oxygen diffusion into $SrTiO_3$ (848 K), as a function of space and time. The smooth curves are obtained by fitting with a constant D^δ. The introduction of a concentration dependence only alters the result slightly.[214]

and the relative signal changes are less than 1% of the overall change (see Eq. 122). Figure 54 shows in-situ profiles for oxygen diffusion in the case of Fe-doped $SrTiO_3$. The absorption signal detects $[Fe^{4+}]$, which is linearly correlated with the oxygen content. The optical signal is followed by a CCD-camera.

If we follow the integrated signal $\overline{S}$ (conductance parallel or absorbance perpendicular to the interface), the position dependence disappears resulting in

$$\frac{\overline{S}(t) - S_1}{S_2 - S_1} = 1 - \frac{8}{\pi^2} \sum_0^\infty \frac{1}{(2i+1)^2} \exp\left(-\frac{t}{\tau^\delta}(2i+1)^2\right) \qquad (124)$$

with the time constant $\tau^\delta = L^2/\pi^2 D_0^\delta$. (It is worthy of note that τ^δ can be written as $R^\delta \cdot C^\delta$ with the chemical resistance $R^\delta \propto 1/\sigma^\delta$, and C^δ being the already mentioned chemical capacitance.) For long times an exponential law results (Fig. 53), which reads for the conductance experiment ($\sigma_m^\parallel$ being proportional to the parallel conductance)

$$M_\sigma \cong \frac{\sigma_m^\parallel(t) - \sigma_2}{\sigma_1 - \sigma_2} = \frac{8}{\pi^2} \exp - t/\tau^\delta \qquad (125)$$

while for shorter times a $\sqrt{t}$ law is fulfilled.

Table 6 shows equilibration times (τ_{eq}^δ, see above) for one-dimensional diffusion into 1 mm thick samples for various diffusion coefficients, indicating the tremendous span of the rate of diffusion controlled reactions even for the same driving force. High diffusion coefficients are rather the exception in the solid state and, if they occur, they typically occur for one ion sort. This highlights the significance of transport steps in solid state science in general and the significance of frozen situations in particular.

Table 6
Equilibration times for one-dimensional diffusion in a 1 mm thick sample after a jump in external chemical component potential.

D^δ /cm^{2}s^{-1}	τ^δ_{eq} (L = 1 mm)	
10^{-20}	5×10^{17} s	~ 4 x Earth's age
10^{-10}	5×10^{7} s	~ duration of PhD work
10^{-8}	5×10^{5} s	~ 1 w
10^{-6}	5×10^{3} s	~ 1 h
10^{-5}	5×10^{2} s	~ 10 min
10^{-4}	50 s	~ 1 min
10^{-3}	5 s	$\left.\rule{0pt}{14pt}\right\}$ (fluid phases)
10^{-2}	0.5 s	

4. Correlations and Complications

(i) Conductivity: Static and Dynamic Correlation Factors

The above considerations relied on a site exchange describable by simple chemical kinetics and a random walk behavior over large distances in a homogeneous medium subject to a small driving force. In the following we will briefly consider some of the most important complications to this picture.

In general in each experiment individual deviations from random walk can occur. Noteworthy is the tracer correlation factor (f^*) (cf. Section VI.3. *iii.*) which is caused by the non-ubiquity of the jump partner (defect). If an ion has just changed its site from x to x' via hopping into a vacancy and so releasing a vacancy at x, a further vacancy is not immediately available and the dance of a particle between x and x' leads to a backward correlation ($\overline{\cos \alpha_{ij}} \neq 0$, cf. Section VI.3.*i.* and Ref.[205]); this is not the case for a vacancy migrating in an electrical experiment, nor for an isotope in a tracer experiment moving according to an interstitial mechanism (Fig. 42 bottom). The relation between D^* and D^Q then reads

$$D^* = f^* D^Q \tag{126}$$

Whereas such correlation factors are typically between 0.5 and 1, severe discrepancies between D^* and D^Q can occur if the mechanisms differ. This happens in the case that defect contribute in different valence states, in particular if neutral transport is involved (see below). More generally then Eq. (126) has to be replaced by[3,4]

$$D^* = HD^Q \qquad (127)$$

In alkali hydroxides extended ring mechanism for proton motion can occur leading to a tracer propagation but not to any charge transport. The Haven ratio (H) amounts to several thousand in such cases.[216]

Dynamic correlation effects can occur in conductivity experiments if defect-defect interactions have to be considered. Then the relaxation
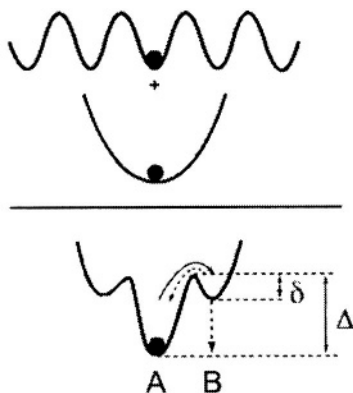

Figure 55. A jump within the true potential (lattice potential (top) plus defect potential (center)) requires the surmounting of a relatively high activation energy and a subsequent relaxation of the environment, before the site B takes on the original potential surroundings of A (see text). From Ref.[217]. (Reprinted from K. Funke, "Ion transport in fast ion conductors—spectra and models", *Solid State Ionics*. **94**, 27-33. Copyright © 1997 with permission from Elsevier.)

of the surrounding is not very rapid compared to an ion hop such that backward jumps are favored as the environment at x' is not yet equilibrated, leading to a frequency dependent conductivity.

Figure 55 sketches the situation. The realistic potential includes lattice potential and interaction potential. Two functions are crucial in the description of the jump relaxation model, developed and refined by Funke et al.[217-219]: (i) the probability W(t) that no correlated backward jump has occurred at time t (-W being the backward jump rate); and (ii) g(t) describing the positional mismatch (-g measuring the stabilization rate). The basic assumption of the jump relaxation model is

$$\dot{W}(t) \propto W(t) \cdot \dot{g}(t) \tag{128}$$

implying that the tendency for backward hops and the tendency of rearrangement are proportional to each other. In Ref.[219] it was proposed by theoretical and empirical arguments that W(t) and g(t) can be obtained by combining Eq. (128) with the second differential equation

$$-\dot{g}(t) \propto g^k(t)W(t) \tag{129}$$

where k = 2 describes well the situation for high charge carrier concentrations. This conception which is based on dynamic inhomogeneities caused by the carrier transport, reproduces a manifold of experimental situations and particularly the frequency dependence of the complex conductivity. It is evident that the rigidity of the solid makes a general description more difficult than in fluids (cf. Debye-Hückel-Onsager theory[71]). It remains to be clarified in how far a quasi-Madelung approach for the dynamic relaxation can be helpful.[81,84]

In many cases—in particular in disordered media—static inhomogeneities (accompanied by a broad distribution of jump probabilities) have to be taken into account which obviously also result in a non-Debye relaxation and comparable frequency dependencies (see e.g., a recent review on this topic).[220]

Significant non-idealities can occur in the solids with two kinds of mobile cations (or anions). The so-called mixed alkali effect refers to the partly extremely strong depression of the alkali ion conductivity in crystals or glasses if substituted by another alkali ion. This is explained by the individually preferred environments and their interactions.[221-228]

Interestingly in the opposite case in which the counter ions are mixed, at least frequently, a conductivity enhancement has been observed (e.g., Ag(I, Br) or $(Ca, Ba)F_2$). [107,118,229]

Also in the case of chemical diffusion it may be questionable whether local equilibrium is always fulfilled. This is particularly the case at interfaces or in situations in which a very high electronic mobility enhances D^δ strongly compared with the ionic defect diffusivity.[177]

In the following we will study in more detail chemical diffusion and in particular the situation with various charge carriers. Let us concentrate on the case that, besides electrons and holes, oxygen ions in different valence states are mobile via interstitial and/or vacancy defects.

(ii) Chemical Diffusion and Conservative Ensembles

The chemical diffusion coefficient includes, as we know from the formal treatment in Section VI..3.*iv*., both an effective ambipolar conductivity and an effective ambipolar concentration. The latter parameter is determined by the thermodynamic factor which is large for the components but close to unity for the defects.

If defects are not randomly distributed, in a better approximation $c^{1/2}$ or $c^{1/3}$ dependencies (see Section IV.5.*ii*.) may be introduced in the thermodynamic factors of the defects (Eq. 120b).

Formally, it will be even necessary to make corrections already in the starting flux equations. The detailed formulation of linear irreversible thermodynamics also includes coupling terms (cross terms) obeying the Onsager reciprocity relation. They take into account that the flux of a defect k may also depend on the gradient of the electrochemical potential of other defects. This concept has been worked out, in particular, for the case of the ambipolar transport of ions and electrons.[230]

A more explicit procedure is to introduce chemical interactions directly: There is a certain analogy with the equilibrium situation where it is possible to avoid the use of activity corrections over wide ranges by considering associates to correct for the interactions (see Section IV.5.*i*.). The relevance of this method of treatment is particularly evident if such associates can also be detected experimentally, e.g., by spectroscopic techniques in the case of ionic defects with differing charge states. This leads to a rescaling of defect concentrations and

defect fluxes, which can now be taken to be ideal again to a good approximation (i.e., with negligible activity corrections and negligible coupling terms in the Onsager relationships). However, it is necessary to include source and sink terms from the start on account of the internal dissociation and association reactions (see Fig. 56). This leads us, in the case of local equilibrium, to the concept of "conservative ensembles",[231,232] which will now be described.

Figure 56 uses the example of associate formation between the ionic defect O_i'' and the electronic defect $h^\bullet$ to emphasize that the strict treatment requires the solution of coupled diffusion-reaction relationships, describing the general (electro-)chemical reaction scheme with individual diffusion or rate constants as parameters (cf. Section VI.2). Source terms (q) must be taken into account in the relevant continuity equations, e.g., for defect B that can be created by

$$\nu_A A \underset{\leftarrow}{\overset{\rightarrow}{\rightleftarrows}} \nu_B B \qquad (130)$$
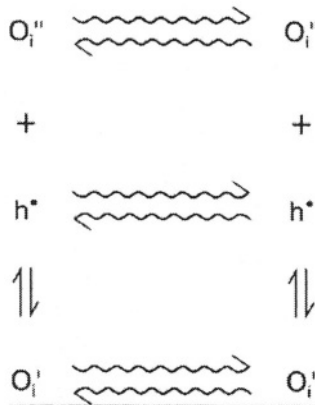

Figure 56. The internal mass and charge transport as a reaction-diffusion problem.

In the case that Eq. (130) describes the decisive elementary reaction, the continuity Eq. (130) for B is

$$\frac{\partial c_B}{\partial t} = -\text{div}\mathbf{j}_B + q_B \equiv -\text{div}\mathbf{j}_B + \nu_B \Re = -\text{div}\mathbf{j}_B + \nu_B(\vec{k}c_A^{\nu_A} - \overleftarrow{k}c_B^{\nu_B}) \quad (131)$$

Again we drop the tilde for simplicity. In the general case the problem depends on the rate constants of the association and dissociation processes. Since we assume local equilibrium (interaction much faster than transport) the situation simplifies considerably (only $K_{ass/diss}$ is included not the rate constants themselves). It would be wrong to believe that the second term in Eq. (131) can be neglected as a consequence of local equilibrium. It is true that the bracketed term in the formulation

$$\frac{\partial c_B}{\partial t} = -\text{div}\mathbf{j}_B + \nu_B \vec{k}c_A^{\nu_A}\left(1 - \frac{c_B^{\nu_B}}{c_A^{\nu_A}}\frac{\overleftarrow{k}}{\vec{k}}\right) \quad (132)$$

is close to zero because $c_B^{\nu_B}/c_A^{\nu_A} \simeq (\hat{c}_B^{\nu_B}/\hat{c}_A^{\nu_A}) = \vec{k}/\overleftarrow{k} = K$; however, the second part is not negligible in total in comparison with the flux divergence on account of the high values of the individual rate constants (see pre-factor).

It can now be shown that as far as the diffusion of certain ensembles, namely of the "conservative ensembles", is concerned, the source terms disappear. The resulting chemical diffusion coefficients then have to refer to this ensemble.

Let us consider an anti-Frenkel disordered material, taking into account both O_i'' and $v_O^{\bullet\bullet}$, but initially neglecting the occurrence of variable valence states. (In addition, we will assume a quasi one-dimensional situation.) Doing this we reduce the problem to a relatively trivial case. For it is immediately evident that the source terms disappear on consideration of the total ion flux density j (or current density i)

$$j_{O^{2-}} = j_{O_i'} - j_{v_O^{\bullet\bullet}} \qquad \text{or} \qquad i_{O^{2-}} = i_{O_i'} + i_{v_O^{\bullet\bullet}} \quad (133)$$

and the total electron flux

$$j_{e^-} = j_{e'} - j_{h^\bullet} \qquad \text{or} \qquad i_{e^-} = i_{e'} + i_{h^\bullet} \qquad (134)$$

In this sense $(c_{O_i'} - c_{v_O^{\bullet\bullet}})$ and $(c_{e'} - c_{h^\bullet})$ refer to "conservative ensembles". This is self-evident since all changes take place within these ensembles. Because

$$O_O + v_i \underset{\leftarrow}{\overset{\rightarrow}{}} v_O^{\bullet\bullet} + O_i'' \qquad (135)$$

and

$$\text{Nil} \underset{\leftarrow}{\overset{\rightarrow}{}} e' + h^\bullet \qquad (136)$$

it follows that $q_{v_O^{\bullet\bullet}} = q_{O_i'}$ and $q_{e'} = q_{h^\bullet}$ and, hence, $q_{O^{2-}} = q_{O_i'} - q_{v_O^{\bullet\bullet}} = 0$ and $q_{e^-} = q_{e'} - q_{h^\bullet} = 0$, if q represents the increase in concentration with time resulting from the defect chemical reactions. Since $\sigma_{O^{2-}} = \sigma_{O_i'} + \sigma_{v_O^{\bullet\bullet}}$ and $\sigma_{e^-} = \sigma_{e'} + \sigma_{h^\bullet}$, the flux equations, formulated in terms of O^{2-} and e^-, are formally the same as those given in Section VI.3.*iv*. (cf. Eq. 120a). This is, however, not the case when we evaluate them in terms of defect parameters. Rather it follows because of $\partial \ln a_{O^{2-}} = \partial \ln a_{O_i'} = -\partial \ln a_{v_O^{\bullet\bullet}}$, and $\partial \ln a_{e^-} = \partial \ln a_{e'} = -\partial \ln a_{h^\bullet}$ as well as $\partial c_{O^{2-}} = \partial c_{O_i'} - \partial c_{v_O^{\bullet\bullet}}$ and $\partial c_{e^-} = \partial c_{e'} - \partial c_{h^\bullet}$ the more general equation

$$D_O^\delta = \frac{RT}{4F^2} \frac{(\sigma_{v_O^{\bullet\bullet}} + \sigma_{O_i'})(\sigma_{e'} + \sigma_{h^\bullet})}{\sigma} \left(\frac{1}{c_{O_i'} + c_{v_O^{\bullet\bullet}}} + \frac{4}{c_{e'} + c_{h^\bullet}} \right) \equiv \frac{RT}{4F^2} \frac{\sigma^\delta}{c^\delta}$$

$$(137)$$

If we also allow for interactions between ions and electrons, the situation becomes qualitatively different (see Fig. 56) even on the level of electronic and ionic constituents. In such cases we introduce variable valence states by permitting O^- and O^0 as valence states, i.e.,

$O_i'', O_i', O_i^x,\ \ v_O^{\bullet\bullet}, v_O^\bullet, v_O^x$ as defects. Then the electronic and ionic ensembles $(O^2$ and $e^-)$ are no longer conservative but merely the combinations $\{O\}$ and $\{e\}$ as defined by Fig. 57. As can be derived from the reaction scheme, it follows that:

$$q_{\{o\}} \equiv q_{O^{2-}} + q_{O^-} + q_{O^x} = q_{O_i'} - q_{v_O^{\bullet\bullet}} + q_{O_i'} - q_{v_O^\bullet} + q_{O_i^x} - q_{v_O^x} = 0 \quad (138a)$$

and

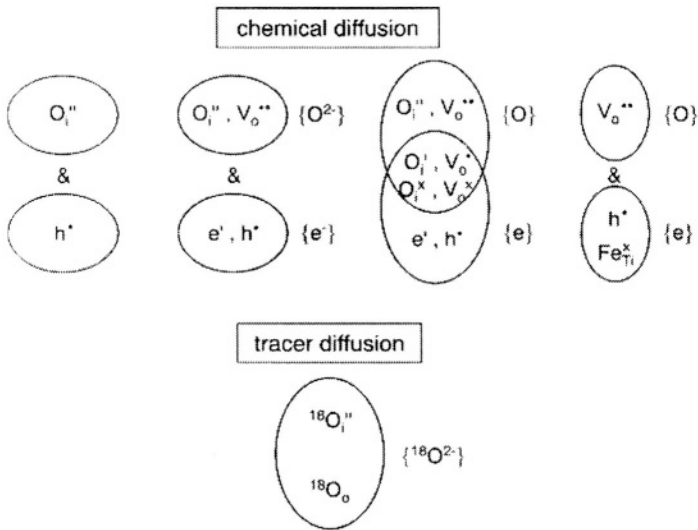$$q_{\{e\}} = q_{e'} - q_{h^\bullet} - q_{O_i'} + q_{v_O^\bullet} - 2q_{O_i^x} + 2q_{v_O^x} = 0 \qquad (138b)$$

Figure 57. Conservative ensembles in the case of complex defect chemistry for various examples discussed in the text.[233,234] (Reprinted from J. Claus, I. Denk, M. Leonhardt, and J. Maier, "Influence of Internal Reactions on Chemical Diffusion: Application to Fe-doped $SrTiO_3$.", *Ber. Bunsenges. Phys. Chem.* **101,** 1386-1392. Copyright © 1997 with permission from WILEY-VCH Verlag GmbH.)

This result is immediately understandable because the concentration of the oxygen ensemble so-defined (see Fig. 57, third arrangement in the upper row)

$$c_{\{O\}} = c_{O_i'} + c_{O_i} + c_{O_i^x} - c_{v_O^{\bullet\bullet}} - c_{v_O^{\bullet}} - c_{v_O^x} \tag{139a}$$

$$c_{\{e\}} = c_{e'} - c_{h^{\bullet}} - c_{O_i'} + c_{v_O^{\bullet}} - 2c_{O_i^x} + 2c_{v_O^x} = -2c_{\{O\}} \tag{139b}$$

obviously represents the deviation from the stoichiometric composition (δ), which is unchanged by the internal reaction. Eq. (138b) then follows as a consequence of the condition of electroneutrality ($-2c_{\{O\}} = c_{\{e\}}$).

For D^{δ}, now a structurally different expression is obtained after a more lengthy calculation:[231,232]

$$D_O^{\delta} = \frac{1}{4F^2}\left[2\sigma_{O^-} + 4s_{O^0} + \frac{(\sigma_{O^{2-}} + 2\sigma_{O^-})(\sigma_{e^-} - \sigma_{O^-})}{\sigma}\right]\frac{d\mu_O}{dc_O} \tag{140}$$

with the abbreviations $\sigma_{O^-} = \sigma_{O_i'} + \sigma_{v_O^{\bullet}}$ and $s_{O^0} = \dfrac{F^2}{RT}(D_{v_O^x}c_{v_O^x} + D_{O_i^x}c_{O_i^x})$. In a purely formal manner, the conductivity factor in Eq. (140) now permits oxygen permeation even for a zero partial electronic conductivity (as a result of the migration of neutral defects but also as a result of an ambipolar migration of $2O^-$ and O^2). The term $d\mu_O/dc_O$ takes another form as well when reformulated in terms of defects, e.g., in terms of the fully ionized particles:

$$\frac{d\mu_O}{dc_O} = RT\left(\frac{\chi_{O_i'}}{c_{O_i'}} + 4\frac{\chi_{h^{\bullet}}}{c_{h^{\bullet}}}\right) = RT\left(\frac{\chi_{v_O^{\bullet\bullet}}}{c_{v_O^{\bullet\bullet}}} + 4\frac{\chi_{e'}}{c_{e'}}\right) \tag{141}$$

The χ_k-terms refer to differential defect fractions and are defined via the corresponding conservative ensembles according to

$$\chi_k = \frac{\partial c_k}{\partial c_{\{k\}}} \tag{142}$$

whereby $c_{\{k\}} = c_{\{O\}}$ or $c_{\{e\}}$ in the case of the excess particles (O_i'', e'), or $-c_{\{O\}}$ and $c_{\{e\}}$ in the case of missing $(v_O^{\bullet\bullet}, h^{\bullet})$ particles, respectively. These can be calculated from the defect chemistry.

The comparison of Eq. (141) with Eq. (120) shows that under simplified conditions the χ-terms can also be considered to be activity corrections.

If we can neglect associates, a quick calculation yields

$$\chi_{O_i''}^{-1} = \frac{\partial c_{O_i''} - \partial c_{v_O^{\bullet\bullet}}}{\partial c_{O_i''}} = \frac{c_{O_i''} + c_{v_O^{\bullet\bullet}}}{c_{O_i''}} \tag{143}$$
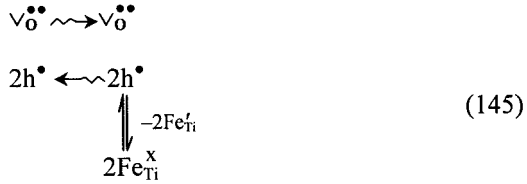
and we return to our simple result, namely to Eq. (137).

An example for which different valance states are important is[53] $YBa_2Cu_3O_{6+x}$. A more recent example refers to the transport of different valence states of hydrogen in oxides.[235]

Another one is Fe-doped $SrTiO_3$, which has already been discussed above (see Fig. 53b). Hence, effects on σ_O^δ are not relevant, but $\partial \mu_O / \partial c_O$ and hence c_O^{δ}[236] are markedly influenced. The internal source and sink reaction is the conversion of Fe^{3+} to Fe^{4+}, which we formulate as

$$Fe_{Ti}' + h^{\bullet} \underset{\longleftarrow}{\overrightarrow{}} Fe_{Ti}^{x} \tag{144}$$

in the high partial pressure regime. The mass action constant for Eq. (144) is well known as a function of temperature. The trapped hole states are not mobile but can supply mobile holes whenever necessary, hence strongly affecting the chemical capacitance $\partial c_O / \partial \mu_O$:

$$V_O^{\bullet\bullet} \rightsquigarrow V_O^{\bullet\bullet}$$

$$2h^\bullet \longleftarrow\!\!\!\rightsquigarrow 2h^\bullet$$

$$\Updownarrow {\scriptstyle -2Fe'_{Ti}}$$

$$2Fe_{Ti}^x \tag{145}$$

It is important to recognize that χ is a differential parameter, and the capacitance to be taken into account is a differential capacitance $(\partial c_O / \partial \mu_O)$. The electroneutrality relation yields $2[V_O^{\bullet\bullet}] \cong [Fe'_{Ti}] = C - [Fe_{Ti}^x]$ and $2\partial[V_O^{\bullet\bullet}] = -\partial\left([h^\bullet] + [Fe_{Ti}^x]\right)$. Owing to conservation of mass and ionic equilibrium the correction follows as

$$\chi_{h^\bullet} = \frac{\partial[h^\bullet]}{\partial[h^\bullet] + \partial[Fe_{Ti}^x]} = \frac{(1 + K_{ass}[h^\bullet])^2}{(1 + K_{ass}[h^\bullet])^2 + CK_{ass}} \tag{146}$$

The concentration $[h^\bullet]$ follows from the set of defect chemical equations as a function of P, T, C; the quantity $\chi_{h^\bullet}$ itself is, thus, a function of these three parameters, too.

Instead of Eq. (120c) we now have to write

$$D^\delta = \frac{\sigma_{h^\bullet}}{\sigma} D_{V_O^{\bullet\bullet}} + \frac{\sigma_{V_O^{\bullet\bullet}}}{\sigma} \chi_{h^\bullet} D_{h^\bullet} \tag{147}$$

The values derived according to Eq. (147) (without any adjusted parameter!) agree extraordinarily well with the experiments (see Fig. 58).

The importance of internal redox reactions is perhaps even clearer for $ZrO_2(Y_2O_3)$. Without taking internal reactions into account, the result is simply $D^\delta = D_{e'}$ or $D_{h^\bullet}$ (cf. Section VI.3.*iv.*), depending on the oxygen partial pressure region. When ignoring the above complications it is not evident that in view of the high Y-doping further minority doping would affect the diffusion coefficient. It would also not be understandable that great differences from material to material are found for the same Y content as well as astonishingly strong dependences of D^δ on oxygen partial pressure and temperature. Again it is the role of redox-active impurities with respect to the chemical capacitance which explains these apparent anomalies according to
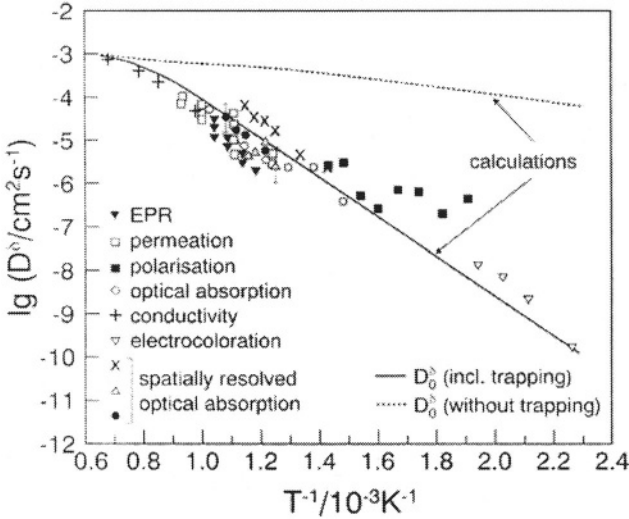
Figure 58. The chemical diffusion coefficient of oxygen in $SrTiO_3$ as a function of the temperature. The broken line includes the doping effect on σ^δ as determined by the ionization reaction (but in contrast to the continuous line ignores the effect on c^δ according to the χ-terms). The calculation applies to a doping content of 10^{19} cm^3 and an oxygen partial pressure of 10^5 Pa.[236] (Reprinted from J. Claus, I. Denk, M. Leonhardt, and J. Maier, "Influence of Internal Reactions on Chemical Diffusion: Application to Fe-doped $SrTiO_3$.", *Ber. Bunsenges. Phys. Chem.*, **101**, 1386-1392. Copyright © 1997 with permission from WILEY-VCH Verlag GmbH.)

$$D^\delta(T,P,C) = \chi_{h\bullet}(T,P,C)\, D_{h\bullet} \qquad (148)$$

(whereby $\chi_{h\bullet}$ is a well-defined function of the control parameters and $D_{h\bullet}$ is a weak function of temperature).[237]

In Fig. 59 χ is considered as a function of the parameter $r \equiv K_{ass}^{-1}[h^\bullet]^{-1}$. In the case of the association of an acceptor A' and a hole to the oxidized form A^x, r is identical with the redox ratio $[A']/[A^x]$. According to Eq. (146) and Fig. 59, the maximum effect

(minimum χ) does not lie at r = 0, but at r = 1 where the ratio[†] of oxidized and reduced species is unity (for minor redox-active doping). Obviously impurities are particularly relevant if their energy levels lie about in the center of the band gap (see Section IV.2) in the above cases, what reveals the similarity to static buffer effects in acid-base chemistry in aqueous solutions.[238]

The small maximum effect at r = 1 on the left-hand side of Fig. 59 is due to a small concentration of redox-active impurities. Plotting this maximum correction for r = 1, as a function of doping (r.h.s. of Fig. 59), shows that this "correction" can amount to several orders of magnitude.

Obviously, high D^δ values, e.g., as required for bulk conductivity sensors, demand materials that are free from redox centers, while the minimization of drift phenomena in boundary layer sensors demands just the opposite.[239]

The impact of internal equilibria on the evaluation of electrochemical measurement methods will be discussed in Part II.[1]

Let us now discuss the influence of variable valence states on the tracer (D^*) and charge diffusion coefficients (D^Q).

Here capacitance effects are absent and modifications are due to the different weight of the different charges. If we ignore correlation factors, the general result for the tracer diffusion coefficient is

$$D_O^* = \frac{RT}{4F^2} \frac{\sigma_{O^{2-}} + 4\sigma_{O^-} + 4s_{O^\circ}}{c_O} = \frac{1}{c_O}\Sigma_k[k]D_k \qquad (149)$$

whereby k indicates the individual ionic defects $(O_i'', O_i', O_i^x, \vee_O^{\bullet\bullet}, \vee_O^\bullet, \vee_O^x)$. Equation (149) can be re-formulated as

$$D_O^* c_O = [O^{2-}]D_{O^{2-}}^* + [O^-]D_{O^-}^* + [O^\circ]D_{O^\circ}^* \qquad (150)$$

[†] If the redox-active doping is in the majority, [h$^\bullet$] depends on K_{ass}, and the minimum is somewhat displaced (see Ref.[238] for more precise details).
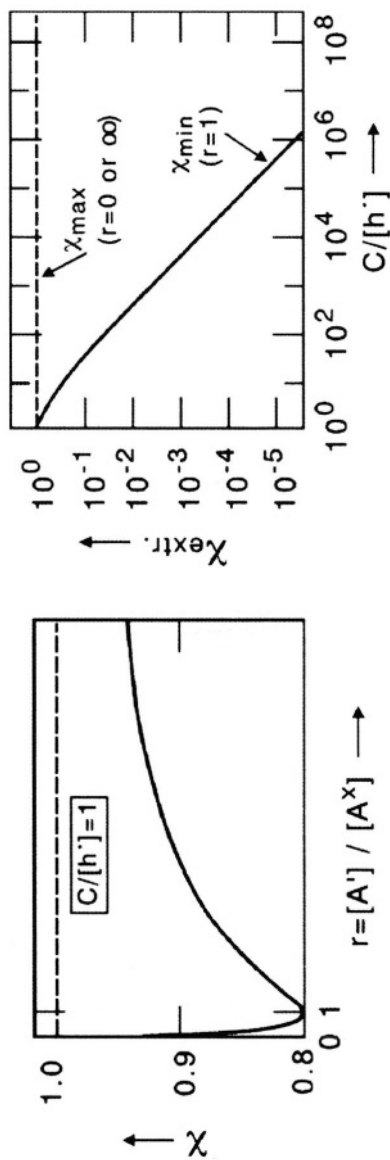
Figure 59. The χ factor of the holes as a function of the redox ratio r (left), if $[h^\bullet]$ can be regarded as independent of r. Maximum ($\chi = 1$) and minimum ($\chi = \chi_{min}$) values as a function of doping (right).[238] (Reprinted from J. Maier, "Trapping Effects on the Diffusion in Mixed Conductors and Solid Electrolytes: Application to $SrTiO_3$ and $ZrO_2(Y_2O_3)$," in: *Ionic and Mixed Conducting Ceramics* Vol.94-12, Ed. by T. A. Ramanarayanan, W. L. Worrell, and H. L. Tuller, The Electrochemical Society, Pennington, NJ, pp 542-551, Copyright © 1994 with permission from The Electrochemical Society, Inc.)

The complicated ratio of D_O^δ to D_O^* (cf. Eqs. 139 and 149) reduces to the thermodynamic factor for a predominant electronic conductor.

The effects on D^Q are different: (i) The unionized defect does not appear in the conductivity experiment; (ii) according to Eqs. (110) and (111) a constant charge number is used to convert $\sigma_{ion} = \sigma_{O^{2-}} + \sigma_{O^-}$ formally to D_O^Q; by using $z = 2$ as the effective valence,

$$D_O^Q = \frac{RT\,(\sigma_{O^{2-}} + \sigma_{O^-})}{4F^2 c_O} \tag{151}$$

is obtained.

(iii) Diffusion Involving Internal Boundaries

According to Section V boundary layers exert a double influence. In the structurally altered core regions of the interface the mobilities and, hence, the defect diffusion coefficients are modified. In the space charge region the mobility, parallel to the interface, is assumed to be invariant while, perpendicular to the interface, electrical field effects are only negligible in the case of high migration thresholds. The anisotropy is more relevant for the conductivity (D^Q), on account of the strong anisotropy of the concentration (Section V). Hence in the boundary controlled cases D^Q, D^δ, D^* are all expected to be strongly anisotropic.

While D^Q directly reflects the ionic conductivity measured in a steady state experiment, the relationships are more complex for chemical diffusion and tracer diffusion. For simplicity we assume that the transport is so slow that local relaxation effects occur instantaneously.[240]

We first consider the chemical transport of oxygen in an oxide along a highly conducting interface (see Fig. 60 r.h.s.). Now the flux lines are not parallel to the interface for the whole experiment since also gradients in the orthogonal direction occur and the problem becomes complicated even if space charge effects are negligible. For further details and a full treatment the reader is referred to the relevant

literature.[241] So long as ions and electrons are strictly coupled, tracer diffusion and chemical diffusion behave in an analogous way.

The treatment is greatly simplified, if the lateral diffusion into the bulk is absolutely negligible with respect to the boundary diffusion. The bulk transport then just takes place on a completely separate time scale; the effective diffusion length of the ceramic is the grain size (λ) rather than the sample size (L), but capacitive $(\propto 1/c^{\delta})$ and resistive terms $(\propto 1/\sigma^{\delta})$ are unchanged compared to the bulk values (cf. Section VI.3.*iv*.). In the case of the chemical experiment,

$$D_m^{\delta} = \frac{L^2}{\ell^2} D_{bulk}^{\delta} \propto \frac{L^2}{\ell^2} \frac{\sigma_{bulk}^{\delta}}{c_{bulk}^{\delta}} \qquad (152)$$

Donor-doped $BaTiO_3$ and $SrTiO_3$ are relevant examples. There bulk diffusion is very slow because of the very low $V_O^{\bullet\bullet}$ concentration and the low mobility of the metal vacancies. If a perovskite ceramic,
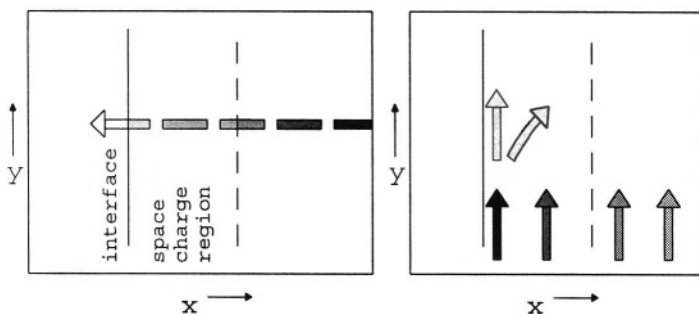

Figure 60. Diffusion across (left) and along (right) an interface (see text).

prepared under reducing conditions and exhibiting a high n-conductivity, is exposed to high partial pressures of oxygen, in-diffusion of oxygen takes place via the grain boundaries. As stated, bulk equilibration is very sluggish and only involves the upper layers of the grains. This leads to a ceramic material composed of highly conducting grains with insulating "skins", which exhibits very high effective (electrical) capacitances and finds application as a powerful capacitor material. [242]

In the case of chemical diffusion perpendicular to the interface, the complications are different ones (see Fig. 60, right). The problem is one-dimensional for reasons of symmetry, however, structural inhomogeneities (core versus bulk) and electrical field effects in the direction of transport are of importance here. Transfer processes through the interfacial core as well as through space charge zones have a profound influence on diffusion. In the instationary case the coupling of the partial fluxes according to Eq. (118) is violated and internal net fluxes occur also in the absence of external fluxes. Even though this complication disappears in the stationary state, the chemical diffusion coefficient is not a suitable transport coefficient any longer since ∇c_O is not a suitable driving force. It is important to note that–in addition to initially present equilibrium space charges–kinetic space charges build up during chemical diffusion in the general case (if oxygen diffusion into $SrTiO_3$ or SnO_2).[239,243]

Let us briefly highlight the effect of equilibrium space charges on the transport in our prototype oxide (with just O_i'' and $h^\bullet$ as defects).[244] The situation becomes particularly clear if we assume equal mobilities and equal bulk conductivities. Since in the case of chemical diffusion $\sigma_{O_i''}$ and $\sigma_{h^\bullet}$ are, as it were, in series, a space charge splitting according to the Gouy-Chapman situation always leads to a lowering of σ^δ and hence to a hindered chemical transport, while the sum of the conductivities increases and hence the electrical transport is facilitated (cf. Fig. 60). This slowing-down effect on D^δ explains the resistive impact of the Schottky boundary layer on the chemical diffusion in $SrTiO_3$; there, even both decisive charge carriers are depleted (see Section V.2). Figure 61 refers to such a bicrystal experiment measured by the optical technique described in Section VI.3.*iv*.

In a polycrystalline sample the situation is more complicated. Again, a simple result is only arrived at even if we assume extreme chemical resistance ratios for bulk and boundary values. Even if the

grain boundary resistance dominates completely, the thermodynamic factor is still determined by the bulk, provided the density of boundaries is not too great. In other words, the largest part of the stoichiometric change $(d\mu_O/dc_O)$ takes place there. In this case[‡] we obtain, for hardly permeable boundaries of thickness d_{gb}, the surprisingly simple relationship

$$D_m^\delta \propto \frac{\ell}{d_{gb}} \frac{\sigma_{gb}^\delta}{c_{bulk}^\delta} \qquad\qquad \ell \qquad\qquad (153)$$

as a counterpart to Eq. (152).[245] Note that $d_{gb}/\ell \propto \varphi_{gb}^\perp$. The proportionality factor in Eq. (153) is $RT/4F^2$.

The tracer diffusion is naturally influenced too by boundaries to be crossed. However, the situation is simpler here[§]. Since the tracer diffusion does not produce chemical or electrical effects, the tracer transport across a grain boundary, is characterized by the equilibrium O_i'' situation and similar to ionic conduction as described in Section V.2. It ought, in particular, to be added that, if the dominating charge carriers and $h^\bullet$ have the same mobility and the space charge potential is positive (negative), tracer diffusion is accelerated (retarded), while in chemical diffusion a retarding effect was to be expected for both signs. Just as for D^Q and D^δ, D^* is also subject to microstructural and bulk-crystallographic anisotropies, that endow the D values with tensor character (cf. again Fig. 60). In polycrystalline materials percolation processes via favorably orientated grains can be important.

[‡]This can be derived from the equivalent circuit shown in Section 6.7 (Fig. 69) for negligible C_{gb}^δ and dominating R_{gb}^δ.

[§] We neglect isotope effects on the mobility which is certainly incorrect in the case of the proton.
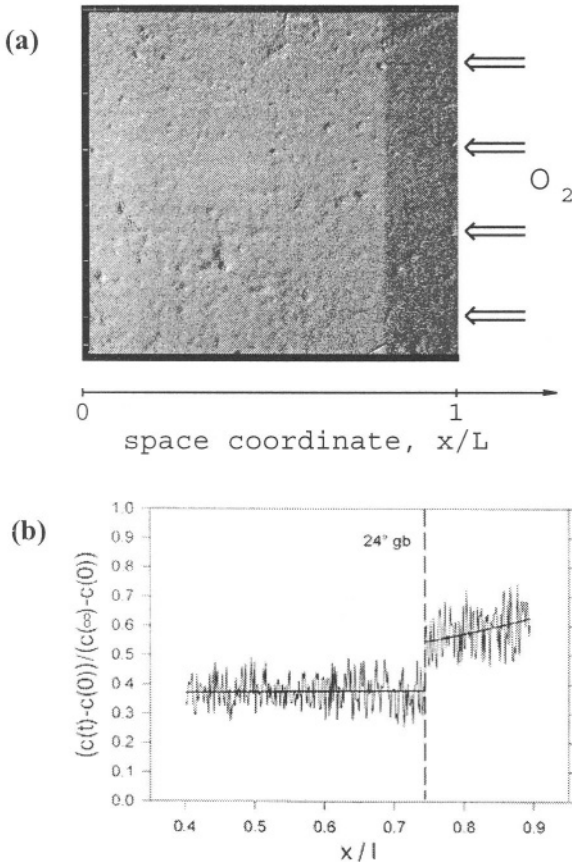
Figure 61. a) The figure shows the color change over a grain boundary of low symmetry (of a bicrystal of Fe-doped $SrTiO_3$) during the in-diffusion of oxygen through the right surface (partial pressure jump from 10^4 Pa to 10^5 Pa, T = 873 K, Fe concentration: $2.15 \times 10^{18} cm^{-3}$). The others are not activated ($24°$ tilt grain boundary, axis of rotation: [001], near Σ 13). According to Ref.[142]. b)Normalized vacancy profiles for low symmetry ($\sim\Sigma$ 13) as obtained from in situ measurements shown in a). According to Ref.[142]. Reprinted from M. Lionhardt, J. Jamnik and J. Maier, *Electrochem. Solid State Letter* **333-335**, 2. (Copyright © 1999 with permission from The Electrochemical Society, Inc.)

As far as the one-dimensional dislocations are concerned, possible blocking effects retreat, in contrast to interfaces, into the background, while they very frequently provide rapid diffusion paths as a result of core and space charge effects.[246]

As in the case of the conductivity experiments, current-constriction effects can occur in the diffusion experiments,[247] if lateral inhomogeneities are present. In this way resistivities occur that can be easily misinterpreted in terms of sluggish surface steps. A concise treatment of proper surface kinetics will be given now.

5. Surface Kinetics

Figure 62 gives a sketch of oxygen incorporation from the gas phase into a mixed conductor for the case of chemical incorporation. One recognizes a variety of elementary steps: Gas diffusion followed by gas adsorption, dissociation, ionization, transfer into the crystal, transport through the subsurface (space charge zone) and bulk transport. Lateral inhomogeneities can lead to parallel processes which will be neglected here. In the case of the tracer experiment the oxygen refers to a given isotope while the counter isotope undergoes exactly the opposite process. Electrons are not of explicit importance but implicitly necessary as regards individual steps; nonetheless, it is, in principle, possible for the electrons to be directly transferred between tracer atoms (e.g., $^{18}O_{ad} + {}^{16}O_{ad}^- \underset{\leftarrow}{\rightarrow} {}^{18}O_{ad}^- + {}^{16}O_{ad}$). Such a direct tracer mechanism may be of relevance in materials with extremely small concentrations of electronic carriers. In the electrical experiments the electrons stem from the electrode, and a fair comparison between e.g., tracer and electrical experiment needs to refer to a comparable phase distribution. Beyond these mechanistic differences manifested in the role of electrons, we also expect, similar as in the case of the diffusion coefficients, "conceptual" differences, i.e., differences that also occur even if we restrict ourselves to the case of the electron-rich electron conductor in which the mechanistic differences disappear.

A detailed treatment is given in Ref.[172] In the following we will assume two simplifying principles to be fulfilled. (1) The mechanism can be considered as a series mechanism in which one step has such small rate constants that it can be considered to be rate determining. (2) The storage of material in the surface during the diffusion experiments

$$\tfrac{1}{2}O_2 \rightleftharpoons \tfrac{1}{2}O_2 \rightleftharpoons \tfrac{1}{2}O_{2,\,ad}$$
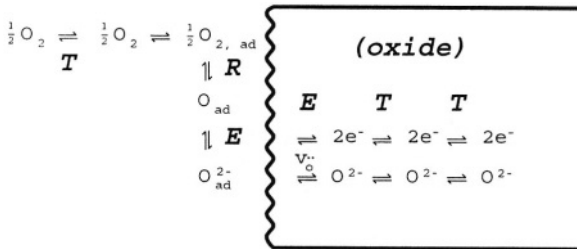
Figure 62. A selection of possible elementary steps for the incorporation of oxygen in an oxide. The surface reaction, in particular, is made up of complex individual steps. In reality the ionization degree of adsorbed atoms lies between zero and the bulk value (here –2). T: transport, R: chemical reaction, E: electrochemical reaction.

is assumed to be negligible compared to the material stored in the bulk (in other words: storage is small compared to flux divergence, and the flux is the same everywhere in the surface region). Then we neglect the chemical surface capacitances, and we only refer to surface resistances. Chemical capacitance effects will solely be determined by the bulk. In the case of the electrical experiment we refer to charge storage and hence to electrical capacitances that are, conversely, very substantial for interfaces. As the electrical experiment is not a diffusion experiment we will refer to it later (Section VI.6). Unlike electrode kinetics which is intensively considered in liquid electrochemistry, we will treat the surface part of the diffusion process—according to the great importance for the solid state—in more detail.

The inverse specific surface resistance, Λ_s, can be defined by the ratio of the flux and the affinity drop over the surface (A_s). Since the flux is the same everywhere and Λ_s by far takes its smallest value in the case of the rate determining step (*rds*), almost all the affinity drops over *rds:*

$$A_s = \Lambda_s^{-1} j_{O,s} = \Sigma_i \Lambda_{s,i}^{-1} j_{O,s} \simeq \Lambda_{rds}^{-1} j_{O,s} \simeq \Lambda_{rds}^{-1} j_{O,rds} \simeq A_{rds} \qquad (154)$$

(For simplicity we drop the tilde used in Section VI.2.) The comparison with Eq. (106) shows that Λ is identical with the exchange flux density $\overset{\circ}{j}_{rds}$ of the *rds*. The affinity of the surface process A_s refers to the negative change in the respective chemical potential of oxygen between gas phase and first layer where the bulk process starts. If we ignore space charges, as we will do in the following for simplicity, this locus is x = 0 (see, e.g., Fig. 63). (In the case of space charges $x \simeq 2\lambda$ is an appropriate coordinate.)
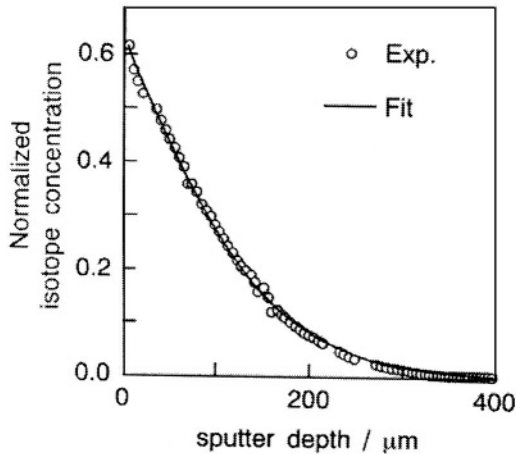

Figure 63. The kinetics in $La_{0.8}Sr_{0.2}CoO_{3-x}$, under the conditions given, is strongly influenced by the surface reaction. For pure diffusion control the normalized surface concentration would be unity.[207] (Reprinted from R. A. De Souza, J. A. Kilner, "Oxygen transport in $La_{1-x}Sr_xMn_{1-y}Co_yO_{3\pm\delta}$.", *Solid State Ionics,* **106,** 175-187. Copyright © 1998 wih permission from Elsevier.)

Since the chemical potential of oxygen (in the tracer case we refer to the chemical potential of the isotope) is spatially (Δ) constant in equilibrium, it holds that

$$j_{O,s} = -\Lambda_O \Delta\mu_O = -\Lambda_O \delta\mu_O(x = 0) \tag{155}$$

where, at the r.h.s., we refer to the deviation of μ from the final equilibrium state at $x = 0$. When investigating the time changes is of particular advantage to use concentration changes for the experimental detection. Then we rewrite Eq. (155) as

$$j_{O,s} = -\Lambda_O \frac{d\mu_O}{dc_O} \delta c_O(x = 0) \tag{156}$$

The thermodynamic factor $d\mu_O/dc_O$ refers to the bulk and reflects its (inverse) chemical capacitance. This term reduces to RTw_O/c_O for the chemical experiment and to RT/c_O for the tracer experiment. The pre-factor $\Lambda_O d\mu_O/dc_O$ evidently defines what is called effective rate constant $\bar{k}_O^\delta$ or $\bar{k}_O^*$:

$$j_{O,s} \equiv -\bar{k}_O \delta c_O(x = 0) \tag{157}$$

Note that $\delta c_O(x = 0) \neq c_O(g) - c_O(0)$. The transition from Λ to $\bar{k}$ is analogous to the transition from σ (or σ^δ) to D (or D^δ). Obviously

$$\bar{k}_O^\delta = \Lambda_O^\delta w_O / c_O, \quad \bar{k}_O^* = \Lambda^* / c_O \tag{158}$$

and

$$\bar{k}_O^\delta / \bar{k}_O^* = (\Lambda_O^\delta / \Lambda_O^*) w_O \tag{159}$$

As we will see, these $\bar{k}$-values can be easily measured with the help of diffusion experiments. In the case that the same mechanism applies, $\Lambda_O^\delta = \Lambda_O^*$ (see also below) and $\bar{k}_O^\delta / \bar{k}_O^* = w_O$.[248] By analogy to D^Q we can also define a $\bar{k}$-value for the electrical experiment according to

$$\bar{k}_O^Q \equiv \Lambda_O^Q / c_O \tag{160}$$

Let us consider the extreme cases and first lump together the surface reaction steps and also the individual bulk hopping steps and write the whole process in a two step form
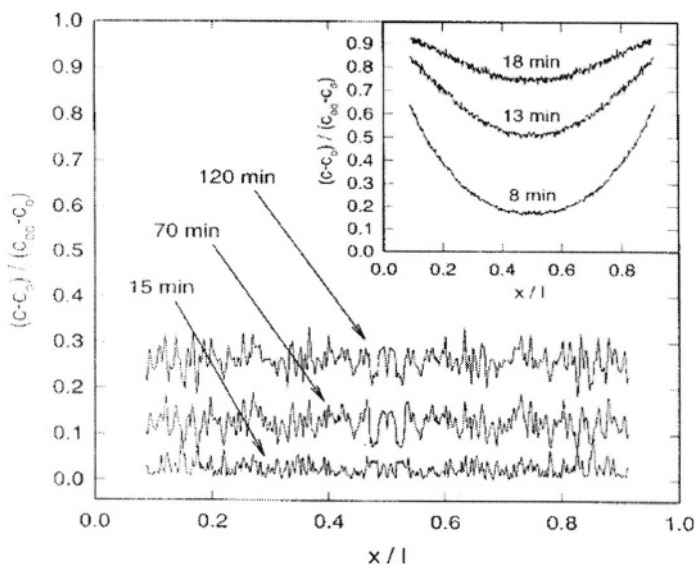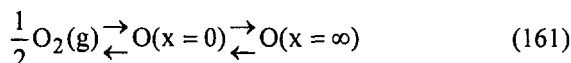
$$\frac{1}{2}O_2(g) \underset{\leftarrow}{\rightarrow} O(x=0) \underset{\leftarrow}{\rightarrow} O(x=\infty) \tag{161}$$

Figure 64. Normalized concentration profiles obtained from the spatially resolved in-situ technique (see Section VI.3.*iv.*) for Fe-doped SrTiO$_3$ samples (Fe content: **4.6 x 10^{19}cm^{-3}**) on rapid change of the gas atmosphere from 10^4 to 10^5 Pa at 923 K. The main diagram shows reaction control, the insert diffusion control. Both cases involve incorporation through a polished (100) surface. In the case of diffusion control a thin, porous Cr layer was used to activate the surface (according to Refs.[249,250]). (Reprinted from J. Maier, "Interfaces" in: *Oxygen Ion and Mixed Conductors and their Technological Applications,* Vol. 75-121, p. 368, Ed. by H. L. Tuller, J. Schoonman and I. Riess, NATO Science Series: E Applied Sciences, Kluwer Academic Publishers, Dordrecht, Copyright © 2000 with permission from Kluwer Academie Publishers B. V.)
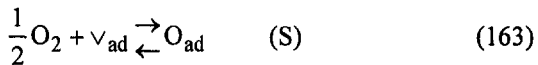
If the bulk step (second step in Eq. 161) is rate determining, $\mu_O(g) - \mu_O(x = 0) = 0$, i.e., $\delta\mu_O(x = 0) = 0$ and $\delta c_O(x = 0) = 0$, and the surface reaction is in equilibrium. This is the situation considered in the previous sections. Conversely, if the surface step (first step in Eq. 161) is rate determining, there is transport equilibrium in the bulk $\mu_O(x = 0) = \mu_O(x = \infty)$ and $c_O(x = 0) = c_O(x = \infty)$.   Then   the diffusion profiles are horizontal with intercepts determined by $c_O(t,x = 0)$. The flux into the bulk is determined by $-\bar{k}\delta c$ while the flux out of it is zero, leading to $\partial\delta c/\partial t \propto -\delta c$ and

$$\frac{c_O(t) - c_O(t = \infty)}{c_O(t = 0) - c_O(t = \infty)} = \exp-\frac{\bar{k}t}{L} \tag{162}$$

everywhere in the sample. Figure 64 shows almost horizontal profiles as predicted by Eq. (162) whose evaluation allows for an accurate determination of effective rate constants. Fig. 65 displays results of integral measurements. The exponential law for reaction control (Eq. 162) simplifies to a linear dependence for short times. As shown for the case of diffusion control in Section VI.3.*iv.* an exponential law is only valid for long times, while for short times a $\sqrt{t}$ -behavior is fulfilled. The latter is seen in the l.h.s. of the figure. The switch-over from reaction to diffusion control typically occurs for thick samples, high temperatures and/or for catalyzing surfaces.

So far we considered the surface process in the limit of proximity to equilibrium which is, for the relaxation experiments discussed, often a sufficient approximation. In order to extend the validity range but also to highlight the situation from a different point of view, let us apply chemical kinetics to the surface process which we now decompose into the individual steps of the reaction sequence.[23,24,172,248] The rate determining step is supposed to be one of these surface reaction steps.

For simplicity let us assume the model mechanism

$$\frac{1}{2}O_2 + v_{ad} \underset{\leftarrow}{\overset{\rightarrow}{\rightleftharpoons}} O_{ad} \qquad (S) \tag{163}$$

$$O_{ad} + v_O^{\bullet\bullet} + 2e' \underset{\leftarrow}{\overset{\rightarrow}{\rightleftharpoons}} O_O \qquad (T) \tag{164}$$

with Eq. (164) being the *rds*, and—in order to emphasize the general principle—first consider an electron-rich electron conductor. Since the overall rate is equal to $\mathfrak{R}_{rds}$, we can generally state ($\varepsilon = \delta, *, Q$)

$$\mathfrak{R}^{\varepsilon} = \vec{k}_T[v_O^{\bullet\bullet}] - \overleftarrow{k}_T[O_O] \tag{165}$$

Again, in order to simplify the notation, we suppress the tilde, even though the k's can contain electrical fields and do definitely so for $\varepsilon = Q$. The rate constant $\vec{k}_T$ contains also the constant electron concentration as well as the equilibrium concentration of the adsorbed species. (The appearance of the concentration of regular species in Eq. (165), even though not dilute, is justified, since it is constant in the cases $\varepsilon = \delta$ and $\varepsilon = Q$, while it refers to the ideal tracer concentration for $\varepsilon = *$.)

In the tracer case $[v_O^{\bullet\bullet}]$ is invariant and $[O_O]$ is perturbed, while exactly the inverse is true for chemical diffusion (as long as $[v_O^{\bullet\bullet}] << [O_O]$). The rate constants can also be considered to be invariant. However, in the electrical experiment, the latter are the variables of interest as they contain the driving force. Simplifying the notation by setting $v \equiv [v_O^{\bullet\bullet}]$, $O \equiv [O_O]$, $k' \equiv \vec{k}$, $k'' \equiv \overleftarrow{k}$, and using the arc to designate the state at $t \rightarrow \infty$, we can write with the help of Eq. (107)

$$\mathfrak{R}^{\varepsilon} = \begin{cases} -\mathfrak{R}^{\circ}\dfrac{\delta O}{\widehat{O}} & \text{tracer experiment} & (\varepsilon = *) \\[4mm] \mathfrak{R}^{\circ}\dfrac{\delta v}{\widehat{v}} & \text{chemical experiment} & (\varepsilon = \delta) \\[4mm] -\mathfrak{R}^{\circ}\left(\dfrac{\delta k'}{\widehat{k'}} - \dfrac{\delta k'}{\widehat{k''}}\right) & \text{electrical experiment} & (\varepsilon = Q) \end{cases} \tag{166}$$

with the exchange rate $\mathfrak{R}^{\circ}$ being $\widehat{k'v} = \widehat{k''O} = \sqrt{\widehat{k'v}\,\widehat{k''O}}$. Evaluating the last relation of Eq. (166), the Butler-Volmer equation originates. Linearization leads to Eq. (160). Apparently the other two relations represent similarly important rate equations for the surface processes of
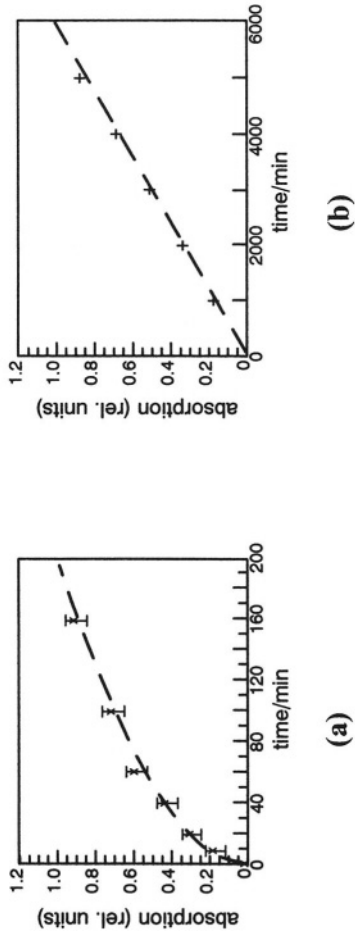
Figure 65. Results of the optical analysis of the incorporation of oxygen in SrTiO$_3$. Time course of the intergral optical absorption in the diffusion direction. a) diffusion control, b) reaction control.[251]

tracer and stoichiometry experiments from the linearization of which we derive Eq. (158).

If the compounds are no longer electron-rich, two difficulties are met. (i) The electron concentrations in the above equations may no longer be invariant in the chemical equations, and (ii) the experiments may be characterized by different mechanisms.

Let us assume identical mechanisms (cf. Eqs. 163 and 164). The changed electron budget only matters for $\varepsilon = \delta$ (for $\varepsilon = *$, Q the electron concentration is invariant). For the chemical process we find instead of Eq. (166) more generally

$$\Re^{\delta} = \Re^{\circ} \frac{\delta\left\{[e']^2 [v_O^{\bullet\bullet}]\right\}}{[\hat{e}']^2 [\hat{v}_O^{\bullet\bullet}]} \qquad (167)$$

which yields after linearization

$$\Re^{\delta} = \Re^{\circ} \left(\frac{\delta [v_O^{\bullet\bullet}]}{[\hat{v}_O^{\bullet\bullet}]} + 2 \frac{\delta [e']}{[\hat{e}']} \right) = \Re^{\circ} \left\{ \frac{1}{[\hat{v}_O^{\bullet\bullet}]} + 2 \frac{1}{[\hat{e}']} \frac{\delta [e']}{\delta [v_O^{\bullet\bullet}]} \right\} \delta [v_O^{\bullet\bullet}] \qquad (168)$$

$$= -\Re^{\circ} (w_O / c_O) \, \delta c_O (x = 0)$$

For a trap free situation the term $\delta [e'] / \delta [v_O^{\bullet\bullet}]$ simplifies to 2, otherwise to $2\chi_n$ (cf. Section VI.4.ii.).[175] The r.h.s. term in {} is obviously exactly the term w_O/c_O discussed for D^{δ}. Other mechanistic cases are more difficult to handle, especially if the rds does not refer to $x = 0$ and coupled equilibria have to be taken account of; however, the results are comparable.

This is shown in Refs.[24,172,248] in great detail. In agreement with the thermodynamic considerations we find in all cases close to equilibrium that

$$\bar{k}^{\delta} = \Re^{\circ\delta} (w_{O^{2-}} / c_{O^{2-}})_{bulk}$$

$$\bar{k}^{*} = \Re^{\circ*} / c_{O^{2-}_{bulk}} \qquad (169)$$

$$\bar{k}^{Q} = \Re^{\circ Q} / c_{O^{2-}_{bulk}}$$

where we now also distinguish between different exchange rates in view of the possibility that different mechanisms $\varepsilon = \delta, *, Q$ occur. The

molecularity of the *rds* can give rise to additional constant factors (ν) in Eq. (169). (This may occur, e.g., if the adsorption is rate determining. In the simplest case P_{O_2} appears as a factor with the exponent 1 in the kinetic ansatz leading to $\nu = 4$, whereas $\nu = 1$ results if $P_{O_2}^{1/2}$ enters the rate equation which is the case for a rapid predissociation.

The advantage of the kinetic treatment lies in the fact that (i) also solutions far from equilibrium can be handled and (ii) the range of validity of Eq. (169) can be given (similarly as in the diffusion case, cf. Section VI.2.*i*). Since in the above derivations bulk defect chemistry was assumed to be established at x = 0, the index "bulk" was used in Eq. (169) to allow for more general situations. Note that these explicit formulae predict defined dependencies on the control parameters which can be checked provided defect chemistry is known. For simple situations (see Refs.[252,253]) a power law relationship results (is a constant)

$$\bar{k}^{\varepsilon} = \alpha^{\varepsilon} P^{N^{\varepsilon}} \Pi_r K_r^{\gamma_r^{\varepsilon}} C^{M^{\varepsilon}} \tag{170}$$

describing the dependence on the control parameters temperature, component activity (partial pressure P) and doping content (C). The measurements of the dependencies provide extremely useful mechanistic information. Such dependencies and also the relationships between the $\bar{k}'s$ and the D's are discussed for specific cases in Refs.[252,253]

Let us turn to our $SrTiO_3$ (Fe-doped) example and to Fig. 66. The parameter $\bar{k}^{\delta}$ is indeed found to be markedly higher than $\bar{k}^{*}$ but less high than expected for $\mathfrak{R}^{\circ\delta} = \mathfrak{R}^{\circ*}$. In other words, $\bar{k}^{\delta} / w_O \ll \bar{k}^{*}$. Moreover, if we coat the surface with Pt we enhance $\bar{k}^{\delta}$ drastically while $\bar{k}^{*}$ remains unchanged. If this is indeed caused by different mechanisms is still under debate.

While a direct tracer exchange would not be substantially influenced by Pt, the Pt-coating makes the chemical measurement more similar to the electrical measurement as in both cases the electrons are
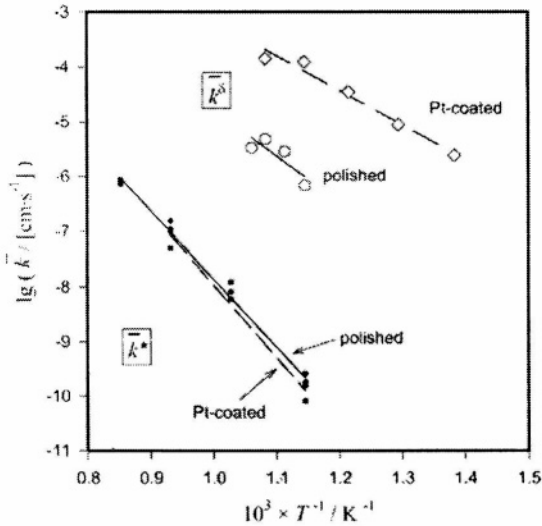
Figure 66. Chemical $\bar{k}'s$ $(\bar{k}^\delta)$ and tracer $\bar{k}'s$ $(\bar{k}^*)$ as a function of 1/T for differently prepared (100) surfaces of Fe-doped $SrTiO_3$.[250,254]

taken up from this metal. In this case $\bar{k}^\delta / w_O$ would approach $\bar{k}^Q \neq \bar{k}^*$. Such "surface Haven ratios" (cf. Eq. 127) are still to be verified. The respective mutual inter-dependencies of the $\bar{k}'s$ are displayed in Fig. 67 which may be compared to Fig. 52. There are almost no cases for which a clearcut mechanistic picture could be given, what is not surprising, in view of the manifold of possible reaction mechanisms. A comparatively well investigated process is chemical oxygen incorporation into $SrTiO_3$. By combining the knowledge of $\bar{k}^\delta$ (P,T,C) with experiments far from equilibrium and with UV-experiments that allow one to tune the concentration of electronic carriers, a mechanism could be made probable that involves (i) a first ionization of the adsorbed molecule by consuming a regular electron, (ii) a second ionization by consuming an energetically higher lying conduction electron; (iii) then the peroxide decomposes, finally
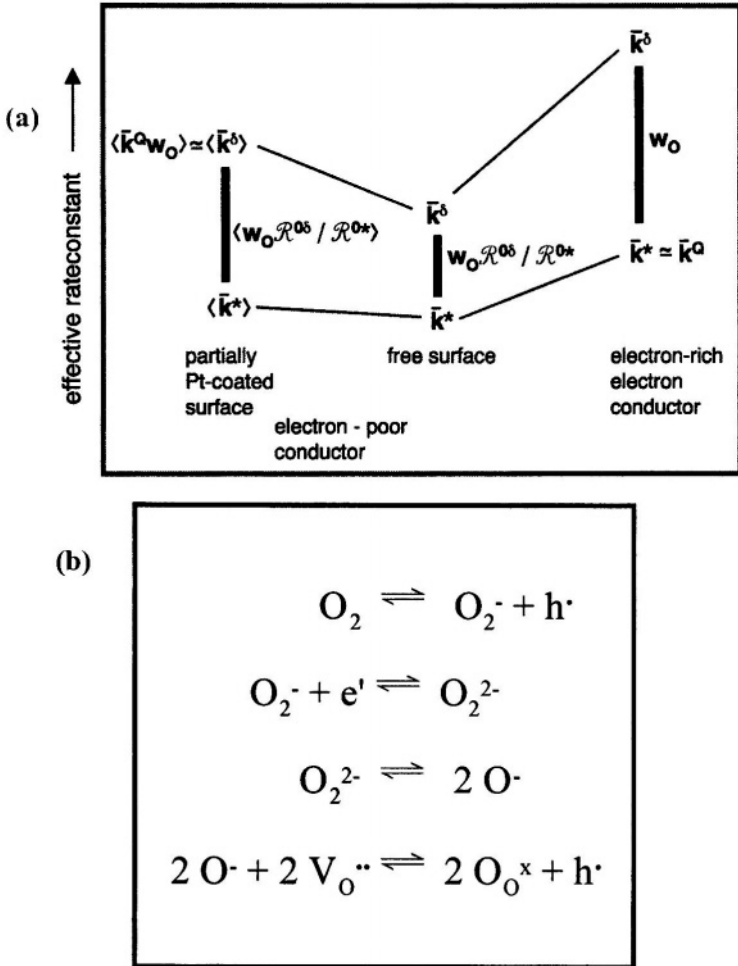
Figure 67. (a) Relation between the $\bar{k}'s$ for high electron concentration (r.h.s. column) and for low electron concentrations of the oxide. Free surface: center column, partial Pt coverage: left column. The brackets indicate averaging over the heterogeneous surfaces. There is a close correspondence to Fig. 52 (according to Ref.[248]) (b) Probable mechanism of oxygen incorporation in $SrTiO_3$ ($\bar{k}^\delta$). (Reprinted from J. Maier, "Interaction of oxygen with oxides: How to interpret measured effective rate constants?", *Solid State Ionics,* **135,** 575-588. Copyright © 2000 with permission from Elsevier.)

(iv) O^- enters the vacancy while being simultaneously fully ionized (see Fig. 67b).[255]

6. Electrode Kinetics

Now let us consider briefly electrode kinetics, i.e., $\overline{k}^Q$ or—since we have not involved any chemical capacitance effects—the exchange rate $\mathfrak{R}^{oQ}$. Let us follow the work by Wang and Nowick[256] on electrode kinetics of Pt, O_2/CeO_2 (doped) which was indeed invoking the model mechanism given by Eqs. (163) and (164). If the transfer step is assumed to be rate determining and the symmetry factors are set to 1/2, the exchange current density reads ($i^o \equiv zFj^o \propto \mathfrak{R}^{oQ}$)

$$i^o = zF\sqrt{\overline{\Theta(1-\widehat{\Theta})}}\sqrt{\widehat{\overrightarrow{k_T}}\,\widehat{\overleftarrow{k_T}}} \tag{171}$$

(Θ is the degree of coverage and refers, as the rate constants, to equilibrium values, i.e., bias free). The index T refers to the transfer reaction, while the index S refers to the sorption pre-equilibrium (cf. Eq. 163) characterized by the mass action constant K_s. Under Brouwer-like conditions (that is conditions necessary for Eq. 170 to apply) either $\widehat{\Theta}$ or $(1 - \widehat{\Theta})$ is unity. Since the adsorption enthalpy is smaller than zero for high temperatures and/or low P_{O_2}, for which $K_s P_{O_2}^{1/2} \ll 1$, it follows that $(\widehat{\Theta} \ll 1)$

$$\widehat{\Theta} = K_s P_{O_2}^{1/2} \tag{172}$$

The P_{O_2} - and T-dependencies of the exchange current density are then given by

$$\frac{\partial \ln i^o}{\partial \ln P} = 1/4$$
$$-R\frac{\partial \ln i^o}{\partial 1/T} = \frac{1}{2}\Delta H_s^o + \frac{1}{2}(\Delta \overrightarrow{H}_T^{\neq} + \Delta \overleftarrow{H}_T^{\neq}) \tag{173}$$
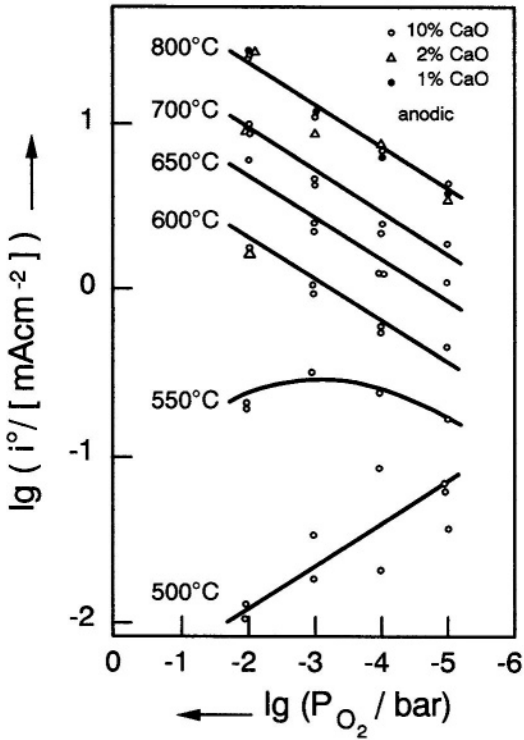
Figure 68. The exchange current density as a function of oxygen partial pressure for different temperatures confirming the electrode kinetical model given in the text.[256] (Reprinted from D. Y. Wang, A. S. Nowick, "Cathodic and Anodic Polarization Phenomena at Platinum Electrodes with Doped CeO_2 as Electrolyte. I. Steady-State Overpotential.", *J. Electrochem. Soc.,* **126,** 1155-1165. Copyright © 1979 with permission from The Electrochemical Society, Inc.)

In the other limit $K_s P^{1/2} \gg 1$ we obtain analogously

$$\frac{\partial \ln i^o}{\partial \ln P} = -1/4$$

$$-R \frac{\partial \ln i^o}{\partial 1/T} = -\frac{1}{2} \Delta H_s^o + \frac{1}{2}(\Delta \overrightarrow{H}_T^{\neq} + \Delta \overleftarrow{H}_T^{\equiv})$$

(174)

As σ in the bulk case, the exchange rate includes reaction and activation energies. The results shown in Fig. 68 as a function of P_{O_2} at different temperatures are consistent with these predictions. Not very many studies of electrode kinetics involving solid/solid contacts are known. What makes the treatment particularly complex are lateral inhomogeneities. A recent example which refers to the cathodic situation in high temperature fuel cells is given in Ref.[257].

7. Generalized Equivalent Circuits

In the framework of linear irreversible thermodynamics it is possible to handle responses to electrical and/or chemical driving forces, as could be seen from the previous sections, by what is called Nernst-Planck-Poisson set of equations plus rate equations of local reactions.[258-262] The transport and reaction coefficients are determined by inverse resistances and inverse capacitances. Hence it is, after all, not surprising that the situation can be mapped by generalized equivalent circuits. A recent general approach used network thermodynamics and is given in Ref.[263]. The treatment is partly based on earlier literature.[258,260,264] For the description three types of elements are needed. The first (i) is the electrochemical resistor ($\propto \sigma^{-1}$ or more generally $\propto \Lambda^{-1}$). As far as the resistor is concerned, we do not need to distinguish between chemical and electrical effects, since they refer to the same mechanism (cf. Nernst-Einstein-equation). This is different in the case of the capacitances. The chemical capacitance (ii) refers to a stoichiometry polarization, whereas the electrical capacitance as the third element (iii) refers to dielectric displacement. The equivalent circuits shown in Fig. 69 map the underlying equations 1:1. The horizontal axis refers to the positional coordinate while the orthogonal axis refers to the deviation from equilibrium. In this way complex
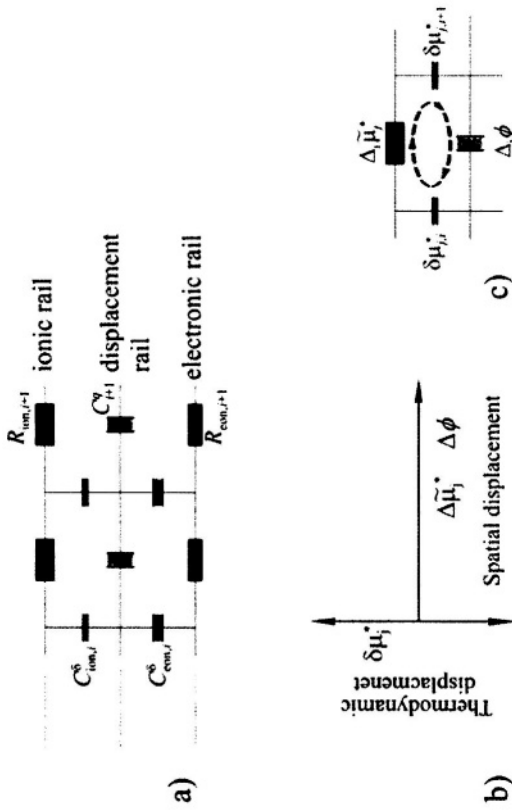
Figure 69. Equivalent circuit for the description of generalized electrochemical processes in linear systems (see text).[263] (Reprinted from J. Jamnik, "Impedance spectroscopy of mixed conductors with semi-blocking boundaries" *Solid State Ionics*, **157**, 19-28. Copyright © 2003 with permission from Elsevier.)

electrochemical phenomena can be handled, including the pure electric transport and pure chemical diffusion. An example of the latter, viz. chemical diffusion in a polycrystalline ceramic was addressed in Section VI.4.*iii.,* while electrochemical polarization effects are to be discussed in Part II.[1]

8. Solid State Reactions

Since the constituents are usually charged, the field of inorganic state reactions exhibits a substantial intersection with electrochemistry. The incorporation of a neutral component (e.g., O into an oxide) has already been considered as a most simple reaction. Here we concentrate on typical reactions that involve the formation of a new phase. Owing to the manifold of individual problems, a detailed treatment cannot be given here and only a few points relevant in our context shall be highlighted.

Let us consider the oxidation of a metal, e.g., Zn to ZnO.[4,75,265] The reaction starts with nucleation and early growth phenomena (lateral mass transport, tunneling, space charge phenomena). Usually at larger thicknesses the interface smoothens and at sufficiently large thicknesses the transport becomes controlled by chemical diffusion. Even though it is not clear whether the ion transport is due to oxygen vacancies or zinc interstitials, we will assume the second case ($\sigma_{ion} = \sigma_v$) without great restriction of generality. Then in the diffusion controlled regime the flux and thus the reaction rate is determined by $\sigma_O^\delta \nabla \mu_O$ (with $\sigma^\delta = \sigma_{eon} \sigma_{ion} / \sigma$ being the ambipolar conductivity, see Section VI.4.*ii*). Owing to its constancy the flux can be recast as $(1/L) \int \sigma_O^\delta d\mu_O$. Thus the growth rate measured by the thickness change $\dot{L}$ is inversely proportional to L and and the well-known square-root rate law ($L \propto t^{1/2}$) follows (see Fig. 70).

Since for ZnO, $\sigma_{eon} \gg \sigma_{ion}$, and thus $\sigma^\delta \simeq \sigma_{ion}$, the experimentally observed steep temperature dependence of the oxidation rate is explained by the activation enthalpy of σ_{ion}. Furthermore, the well-established doping effect[266] by Al^{3+} or Li^+ in depressing or enhancing the corrosion rate is immediately derived from the defect chemistry: $Al_{Zn}^\bullet$ defects decrease σ_{ion} by decreasing $[v_O^{\bullet\bullet}]$ (or $Zn_i^{\bullet\bullet}$) while the
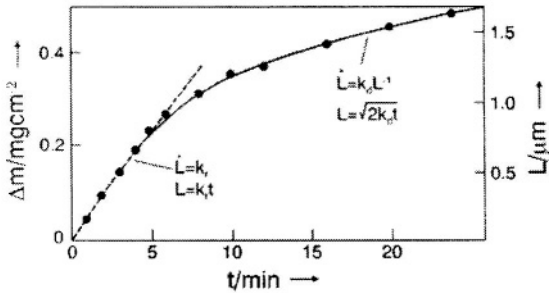
Figure 70. Change from reaction to diffusion control in a spinel formation reaction[4] indicated by the mass change. (Reprinted from H. Schmalz-ried, *Solid State Reactions,* Verlag Chemie, Weinheim. Copyright © 1981 with permission from WILEY-VCH Verlag GmbH.)

Li'_{Zn} defects increase σ_{ion}. The detailed partial pressure dependence follows through integration.

Figure 70 shows that the square-root law is preceded by a linear law for short times, which is indicative of a surface control. In the steady state of the surface control, $\dot{L}$ does not depend on t, neither explicitly or implicitly. (If $\Re$ is the rate of the surface reaction we may write $\dot{L} = f[L(t), \Re(t)]$, hence $\ddot{L} = \dfrac{\partial \dot{L}}{\partial L}\dfrac{dL}{dt} + \dfrac{\partial \dot{L}}{\partial \Re}\dfrac{d\Re}{dt} = 0$; the first term vanishes because $\partial \dot{L}/\partial L = 0$ and the second because of the steady state condition $d\Re/dt = 0$.) In the stage of early growth $\dot{L}$ depends also on L, and a more complicated law follows. Generally, the description of real solid state reactions can be awfully complicated owing to the role of the space coordinate in general, and the interfacial problems in particular.[4] Qualitatively speaking, it is clear from the above considerations that good contact, high conductivities (high T, appropriate doping), high driving forces and in particular small diffusion lengths are necessary to provide fast reaction.

Interrupting reading for a moment and looking around in the environment, tells us that there are essentially two categories of structures. Firstly, simple mostly planar geometries, particularly due to artificial architecture. There we rely on non-equilibrium processes such as cutting and polishing, the structure being maintained thanks to the extremely low diffusion constants. Secondly, complex interface morphologies, partly self-similar or self-affine, created under extreme conditions in the earth's history (e.g., rock-formation) and now frozen-in, or formed under mild in-situ conditions such as natural growth but still far from equilibrium. Such typical non-linear processes will be considered below. At this stage let us consider Fig. 71. It highlights that a planar interface may become unstable for kinetic reasons: If the diffusion of the metal M through the oxide is rate limiting for the corrosion of an M-N alloy (N: noble metal), any perturbation of the M, N/MO interface will be washed out (as shown in Fig. 71), but it will be augmented, possibly leading to dendrites, if the diffusion of M through the alloy is rate limiting.[265] In this case the noble metal will remain embedded in the oxide matrix. Local stability criteria like this may be extremely helpful even if they cannot predict the growth process.[177] (In the stable case the perturbation δL is positive, while the time change of it, $(\partial/\partial t)(\delta L)$, is negative; such a function guaranteeing stability is called a Ljapunow-function.)
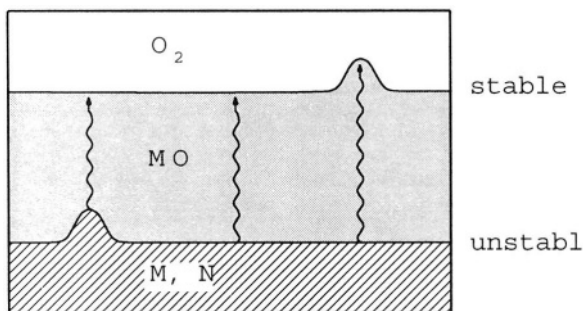

Figure 71. Morphological stability/ instability of the interfaces in a corrosion experiment.[265]

9. Non-linear processes

The vividness of our world does not rely on processes that are characterized by linear force-flux relations, rather they rely on the non-linearity of chemical processes. Let us recapitulate some results for proximity to equilibrium (see also Section VI.2.*ii*.): In equilibrium the entropy production (Π) is zero. Out of equilibrium, $\Pi \equiv T\delta_i S/\mathrm{I}\delta t > 0$ according to the second law of thermodynamics. In a perturbed system the entropy production decreases while we reestablish equilibrium ($\Pi < 0$), (Fig. 72). For the cases of interest, the entropy production can be written as a product of fluxes and corresponding forces (see Eq. 108). If some of the external forces are kept constant, equilibrium cannot be achieved, only a steady state occurs. In the linear regime this steady state corresponds to a minimum of entropy production (but non-zero). Again this steady state is stable, since any perturbation corresponds to a higher Π-value ($\delta\Pi > 0$) and $\Pi < 0$.[183] The linear concentration profile in a steady state of a diffusion experiment (described in previous sections) may serve as an example. With $\Pi \propto \int J\nabla c\, dV \propto \int (\nabla c)^2\, dV$. We argue as follows: The function c(x) satisfying this condition will be the same if we change the integrand of the variational problem to $(\nabla c)^2 + 1$ or even to $\sqrt{(\nabla c)^2 + 1}$. While the first point is trivial, the second one can be justified by Euler's variational theorem.[23]   Since $\int \sqrt{1 + (dc/dx)^2}\, dx = \int \sqrt{(dx)^2 + (dc)^2}$ $= \int$ (length element), the variational problem is obviously analogous to finding the curve of minimum length between two terminals, which is the line in the x-c-plane. Hence the linear profile of the steady state refers to a minimum entropy production. It is also straightforward to show that this is stable.

All this does no longer apply to non-linear systems,[183,267-270] there (if at all) only the part of Π that is caused by varying the forces, reaches a minimum. For those states, however, a stability is not guaranteed ($\delta_X \Pi \lessgtr 0$) (Fig. 72). Close to a steady state this partial variation of $\Pi = \Sigma_i \mathfrak{R}_i A_i$ is given by $\delta_X \Pi = \Sigma_i \mathfrak{R}_i^{ss} \delta A_i + \Sigma_i \delta\mathfrak{R}_i \delta A_i$ which reduces to

$$\delta_X \Pi = \Sigma_i \delta\mathfrak{R}_i \delta A_i \tag{175}$$

ENTROPY PRODUCTION CLOSE TO AND FAR FROM EQUILIBRIUM

EQUILIBRIUM

$\Pi \propto$ entropy - production

$\Pi = T d_i S/dt \geq 0$

$\dot{\Pi} \leq 0$

$\delta \Pi^{eq} \geq 0$

(prehistory unimportant, stable)
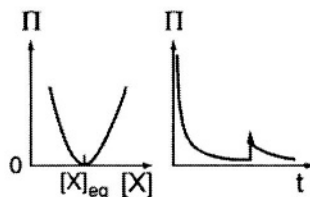
STEADY STATE CLOSE TO EQUILIBRIUM

$\Pi \geq \Pi^{ss} > 0$

$\dot{\Pi} \leq 0$

$\delta \Pi^{ss} \geq 0$

(prehistory unimportant, stable steady states)

STEADY STATE FAR FROM EQUILIBRIUM

$\Pi \geq 0$

$_x\dot{\Pi} \leq 0$

$\delta_x \Pi^{ss} \lesseqgtr 0$

(prehistory important, unstable steady states possible)
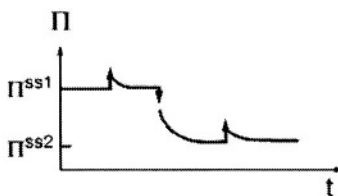
Figure 72. Entropy production close to and far from equilibrium

Table 7

Typical non-equilibrium phenomena far from equilibrium. [20,21]

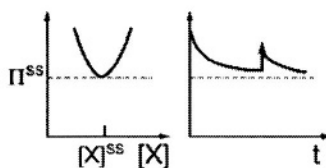|			
autocatalytic reaction	$A + X \longrightarrow 2X$	$[X]$ vs t	growth, positive feedback
autocatalytic + decay reaction	$A + X \underset{}{\overset{k_1}{\rightleftharpoons}} 2X$ $X \xrightarrow{k_2} Z$	$[X]$ vs t (ss)	growth or death
no selection pressure	$[A] = \text{const}$ $W_c = k_1[A] - k_2$	$[X]_{ss}$ vs $[A]$, with 0 and k_2/k_1	nonequilibrium phase transformation
autocatalytic + decay + selection pressure (+ perturbation)	$A + X \longrightarrow 2X$ $X \longrightarrow Z$ $[A] \neq \text{const}$ $W_c = f(t)$	$[X]$ vs t	competition selection mutation
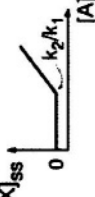
Table 7
Continuation

Lotka-Volterra reaction scheme	$A + X \rightleftharpoons 2X$ $X + Y \rightleftharpoons 2Y$ $Y \rightleftharpoons Z$		structurally unstable oscillation
Brusselator reaction scheme	$A \longrightarrow X$ $2X + Y \longrightarrow 3X$ $B + X \longrightarrow Y + D$ $X \longrightarrow Y$		limit cycle oscillation
or catalytic CO oxidation	$(CO + O \rightleftharpoons CO_2;$ $Pt_{hex} \rightleftharpoons Pt_{sq})$		symmetry breaking bifurcation deterministic chaos
above reaction scheme + diffusion	$(e.\,g.\ X \rightleftharpoons\rightleftharpoons X)$		compartmentation. dissipative structure in space
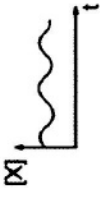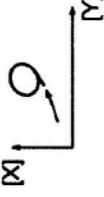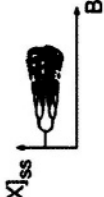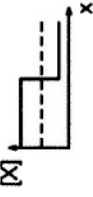
since the first order term must vanish for the steady state (ss).

A key ingredient of exciting reaction-schemes that drives reactions away from harmless states is autocatalysis. Let us consider the simplest autocatalytic reaction[270]

$$A + X \underset{\leftarrow}{\overset{\rightarrow}{}} 2X \tag{176}$$

and first neglect the back reaction. Owing to

$$\mathfrak{R} \propto d[X]/dt \propto [A][X] \tag{177}$$

the stationary (initial) state $[X] = 0$ is unstable, and any finite concentration of X leads to an exponential growth. Indeed the variation $\delta_X \Pi$ is negative ($\delta\mathfrak{R} \propto \delta[X], \delta A \propto -\delta[X]/[X]$ for ideal conditions; cf. Eq. 175). If the back reaction is taken account of, the system is driven towards equilibrium, as because of $\overleftarrow{\mathfrak{R}} \propto [X]^2$ the negative feedback becomes dominating. The final steady state is then stable because $\delta\mathfrak{R}$ is approximately $-[X]\delta[X]$ and $\delta_X\Pi > 0$.[269] If we return to the initial situation and add a decay reaction

$$X \rightarrow Z \tag{178}$$

to the growth reaction, i.e.,

$$\mathfrak{R} = (\overrightarrow{k}[A] - \overrightarrow{k'})\,[X] = W[X] \tag{179}$$

the situation is clearcut if the "food", i.e., [A] is constant. Then the bracketed term, i.e., W, determines whether X grows or decays. The situation becomes more interesting if [A] is exhaustible and one allows for similar parallel reactions that also involve A, to occur. This leads automatically to competition between the species and only one survives.[270] Tuning W leads to the possibility to decide about "dead or alive" (non-equilibrium phase transformation, cf. second row in Table 7). Introducing the possibility of fluctuations in k, automatically mutation and selection processes are obtained.[267,270] Marginally more complicated reaction mechanisms lead to oscillations or chaos, which can also affect the position coordinate if the processes are coupled to
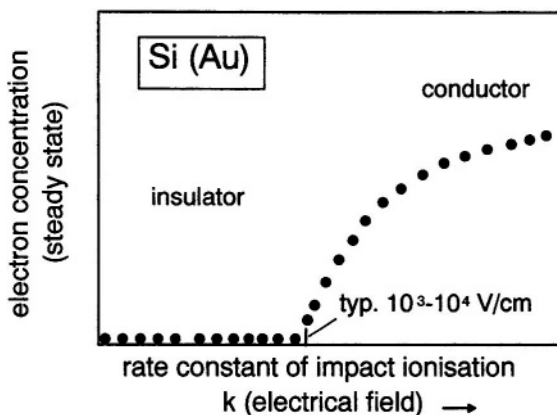
Figure 73. Non-equilibrium phase transition (insulator-conductor transition) in Au-doped silicon as a result of voltage variation in the nonlinear range.[271,272]

transport. Table 7 gives an overview. It is certainly not the place here to treat these phenomena in more detail. It is, however, clear that similar processes occur in solids, in particular if the interaction with electric field and/or electromagnetic waves are included.[271] An important autocatalytic charge carrier process in solids is impact ionization, crudely written as

$$e' \underset{\leftarrow}{\overset{\rightarrow}{\quad}} 2e' + h^\bullet \tag{180}$$

(The electron-hole annihilation serves as decay process.) Figure 73 refers to Au-doped silicon. If the rate constant is tuned by a bias one can switch from an insulating to a conductive behavior (cf. non-equilibrium phase transformation).

Figures 74 and 75 show oscillations, chaotic behavior and pattern formation observed in Ge under appropriate conditions.

Related phenomena are voltage oscillations at Ag/AgI contact observed in Ref.[275] periodic bands in precipitation reactions (Liesegang phenomenon)[177] or oscillations involving proton conductors.[276]
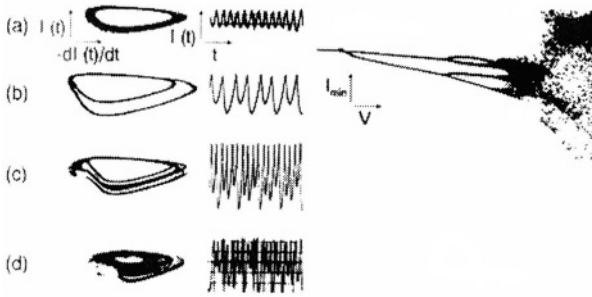
Figure 74. Periodic structures and chaotic behavior in Ge as a result of irradiation and voltage variation in the non-linear range (I: current, V: potential).[273] (Reprinted from S. W. Teitsworth, R. M. Westervelt, E. E. Haller, "Nonlinear Oscillations and Chaos in Electrical Breakdown in Ge." *Phys. Rev. Lett.,* **51,** 825-828. Copyright © 1983 with permission from the American Physical Society.)
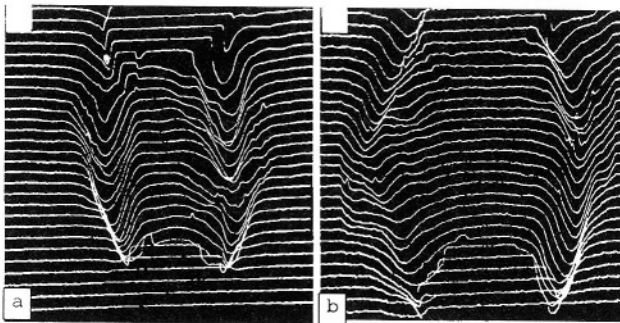
Figure 75. Current filaments in p-Ge at various voltages, made visible by the EBIC technique (electron beam induced currents). [274] (Reprinted from K. M. Mayer, R. Gross, J. Parisi, J. Peinke, R. P. Huebener, "Spatially Resolved Observation of Current Filament Dynamics in Semiconductors.", *Solid State Commun.,* **63,** 55-59. Copyright © 1987 with permission from Elsevier.)

The importance of the transport steps in the solid state has severe consequences: (i) Morphological questions are extremely relevant and can often be described by coupled diffusion reaction equations[183,277] (also the anisotropy of the surface energies is crucial here[278]). (ii) The "mean-field" character of the above reactions restricts the range of validity; more accurately inhomogeneities at the reaction centers[279] but also long range percolation phenomena have to be taken into account.[280]

A useful (also extreme) counterpart to the also idealized linear geometry is fractal geometry which plays a key role in many non-linear processes.[280,281] If one measures the length of a fractal interface with different scales, it can be seen that it increases with decreasing scale since more and more details are included. The number which counts how often the scale ε is to be applied to measure the fractal object, is not inversely proportional to ε but to a power law function of ε with the exponent d being characteristic for the self-similarity of the structure; d is called the Hausdorff-dimension. Diffusion limited aggregation is a process that typically leads to fractal structures.[283] That this is a non-linear process follows from the complete neglect of the back-reaction. The impedance of the tree-like metal in Fig. 76 synthesized by electrolysis does not only look like a fractal, it also shows the impedance behavior expected for a fractal electrode.[284]

Beyond that, fractal geometry is of direct relevance for the transport in inhomogeneous systems, since the percolation cluster (immediately at the percolation threshold, φ_c, c.f. Fig. 77) assumes a fractal shape. In two-phase mixtures of an insulating and a conducting phase this predicts a power law dependence of the conductivity on $\varphi - \varphi_c$ (φ: volume fraction).[281] A relevant example in the context of our considerations is the conduction behavior of $AgCl:\alpha\text{-}AgI$ composites.[118]

The present text could only address a few relevant topics within the rich field of solid state electrochemistry. It will have fulfilled its purpose if it not only convinces the reader of the diversity and colorfulness of the field, but also reveals to him or her the possibility of purposefully tuning electrochemical properties of solids.
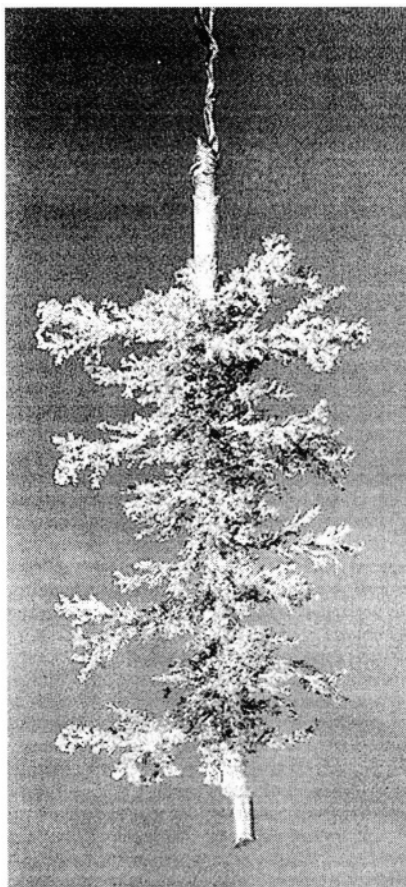
Figure 76. Electrode tree (Wood's metal). Its impedance corresponds to its fractal geometry.[282] (Reprinted from G. Daccord, R. Lenormand, "Fractal patterns from chemical dissolution.", *Nature,* **325,** 41-43. Copyright © 1987 with permission from Nature Publishing Group.)
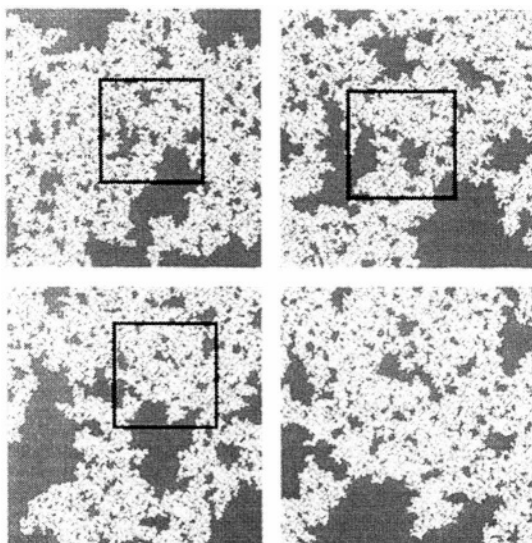
Figure 77. Selfsimilarity of a large percolation cluster at the critical concentration. The windows indicate the section which is enlarged in the respective succeeding figure.[281] (Reprinted from A. Bunde and S. Havlin, "Percolation I", in: *Fractals and Disordered Systems.* Ed. by A. Bunde and S. Havlin, Springer-Verlag, Berlin. Copyright © 1996 with permission from Springer-Verlag GmbH & Co. KG.)

ACKNOWLEDGMENT

SYMBOLS

C	doping content, capacitance
D	density of states, diffusion coefficient
E	electrical field
G	free enthalpy
ΔG^{o}	standard free energy of reaction
$\Delta G^{\neq}$	activation free enthalpy of reaction
H	Haven ratio, enthalpy
J	interaction term in the quasi-Madelung approach
K	mass action constant
L	cross coefficient, sample thickness
N	particle number
N_m	Avogadro's number
P	partial pressure
S	entropy
T	temperature
U	voltage
X	generalized force
a	activity, area
c	concentration (by volume)
f	activity coefficient, correlation factor
f^{c}	configurational activity coefficient
f^{nc}	non-configurational activity coefficient
g	free enthalpy per particle, nano-size factor, mismatch function
i	current density
j	flux density
k	rate constant
$\bar{k}$	effective rate coefficient
m	mass
n	mole number
$\bar{n}$	effective mole number of states
q	source term
t	transference number
u	mobility
v	stoichiometric number
x	mole fraction, position coordinate
z	charge number

Γ	jump frequency
Θ	degree of coverage
Λ	chemical permeability
Π	dissipation function
Σ	surface charge
α	symmetry factor
β	percolation parameter
ε	dielectric constant
ζ	$\equiv c / c_{\infty}$
ϑ	degree of influence
λ	Debye length
λ^*	Mott-Schottky length
μ	chemical potential
$\tilde{\mu}$	electrochemical potential
ξ	$\equiv x / \lambda$
σ	conductivity
σ_m	mean conductivity
τ	time constant
ϕ	electrical potential
φ	Madelung number, volume fraction
χ	differential defect fraction
ψ	wave function
$\vee$	vacancy
A	affinity
$\Re$	reaction rate
$\Re^o$	exchange rate

INDICES

$\sim$	electrochemical
$\frown$	equilibrium
$*$	tracer
$\perp$	perpendicular

‖	parallel
∞	bulk
⟶	forward
⟵	backward
Q	charge
i	interstitial site
δ	stoichiometry

REFERENCES

[1]J. Maier, in *Modern Aspects of Electrochemistry,* Ed. by B. Conway, C. G. Vayenas, R. E. White, Kluwer Academic/Plenum Press, to be published.

[2]F. A. Kröger, *Chemistry of Imperfect Crystals,* North Holland Publ. Comp., Amsterdam, 1964.

[3]H. Rickert, *Einführung in die Elektrochemie fester Stoffe,* Springer-Verlag, Berlin, 1973.

[4]H. Schmalzried, *Solid State Reactions,* Verlag Chemie, Weinheim, 1981.

[5]H. Schmalzried and A. Navrotsky, *Festkörperthermodynamik,* VCH, Weinheim, 1975.

[6]A. R. Allnatt, A. B. Lidiard, *Atomic Transport in Solids,* Cambridge University Press, Cambridge, 1993.

[7]A. B. Lidiard, in *Handbuch der Physik,* Ed. by S. Flügge, Springer-Verlag, Berlin, 1957, Vol. 20, pp. 246.

[8]P. Kofstad, *Nonstoichiometry, Diffusion and Electrical Conductivity in Binary Oxides,* John Wiley & Sons, New York, 1972.

[9]*Solid State Electrochemistry,* Ed. by P. Bruce, Cambridge University Press, Cambridge, 1994.

[10]T. Kudo and K. Fueki, *Solid State Ionics,* VCH, Tokyo-Kodansha, 1990.

[11]L. W. Barr, A. B. Lidiard in lit.[16]

[12]I. Riess, Solid State Ionics **157** (2000) 1.

[13]I. Riess, in *Encyclopedia of Electrochemistry,* Ed. by A. J. Bard and M. Stratmann, WILEY-VCH, Weinheim, Vol. 1 (E. Gileadi and M. Urbakh (eds.)) to appear.

[14]*CRC Handbook of Solid State Electrochemistry,* Ed. by P. J. Gellings and H. J. M. Bouwmeester, CRC Press, Boca Raton, 1997.

[15]J. Maier, *Solid State Phenomena* **39-40** (1994) 35.

[16]*Physical Chemistry, An Advanced Treatise,* Ed. by H. Eyring, D. Henderson, and W. Jost, Academic Press, New York, 1970, Vol. 10,

[17]J. Corish, and P. W. M. Jacobs, *Surf. Def. Prop. Solids* **2** (1973) 160; ibid. **6** (1976) 219.

[18]F. Aguillo-Lopez, C. R. A. Catlow and P. D. Townsend, *Point Defects in Materials,* Academic Press, New York, 1988.

[19]W. D. Kingery, H. K. Bowen, D. R. Uhlmann, *An Introduction to Ceramics,* John Wiley & Sons, New York, 1976.

[20]J. Maier and Angew. *Chem. Int. Ed. Engl.* **32** (3) (1993) 313.

[21]J. Maier and Angew. *Chem. Int. Ed. Engl.* **32** (4) (1993) 528.

[22]P. Knauth and H. L. Tuller, *J. Am. Ceram. Soc.* **85** (2002) 1654.

[23]J. Maier, *Physical Chemistry of Ionic Materials: Ions and Electrons in Solids,* John Wiley & Sons, Chichester, 2004.

[24]J. Maier, *Festkörper—Fehler und Funktion: Prinzipien der Physikalischen Festkörperchemie,* B. G. Teubner Verlag, Stuttgart, 2000.

[25]N. F. Mott, *Metal-Insulator Transitions,* Taylor & Francis, London, 1974.

[26]See textbooks of solid state physics and chemistry.

[27]G. Wulff and Z. Krist. **34** (1901) 449.

[28]R. Defay, I. Prigogine, A. Bellemans and H. Everett, *Surface Tension and Adsorption,* John Wiley & Sons, New York, 1960.

[29]F. A. Kröger and H. J. Vink, J. van den Boomgaard, *Z. phys. Chem.* **203** (1954) 1.

[30]W. Schottky, *Halbleiterprobleme I,* Ed. by W. Schottky, Vieweg, Braunschweig, 1954.

[31]R. Kirchheim, *Prog. Mater. Sci.* **32** (1988) 261.

[32]N. W. Ashcroft and N. D. Mermin, *Solid State Physics,* HRW Int. Ed., Philadelphia, 1976.

[33]H. Gerischer, in *Physical Chemistry, An Advanced Treatise,* Ed. by H. Eyring, Academic Press, New York, 1970.

[34]R. Memming, in *Comprehensive Treatise of Electrochemistry,* Ed. by B. E. Conway et al., Plenum Press, New York, 1983, Vol. 7, pp. 529.

[35]J. Maier, *Solid State Ionics* **143** (2001) 17.

[36]J. Maier, *Solid State Ionics* **157** (1-4) (2003) 327.

[37]J. Maier, *Z. Physik. Chem.* **217** (2003) 415.

[38]M. Born, *Z. Physik* **1** (1920) 45.

[39]W. Jost, *J. Chem. Phys.* **1** (1933) 466.

[40]N. F. Mott and M. J. Littleton, *Trans. Faraday Soc.* **34** (1938) 485.

[41]E. A. Guggenheim, *J. Phys. Chem.* **33** (1929) 842.

[42]G. Brouwer, *Philips Res. Repts.* **9** (1954) 366.

[43]C. G. Fonstad and R. H. Rediker, *J. Appl. Phys.* **42** (1971) 2911.

[44]J. Maier and W. Göpel, *J. Solid St. Chem.* **72** (1988) 293.

[45]J. Maier and Radiat. *Eff. Defects Solids* **158** (2003) 1.

[46]J. C. Philips, *Physics of High Temperature Superconductors,* Academic Press, New York, 1989.

[47]L. Heyne, M. Beekmans and A. de Beer, *J. Electrochem. Soc.* **119** (1972) 77.

[48]J. Maier and G. Schwitzgebel, *Mater. Res. Bull.* **18** (1983) 601.

[49]J. Teltow, *Ann. Phys.* **5** (1950) 63; *Z. phys. Chem.* **195** (1950) 213.

[50]J. Corish and P. W. M. Jacobs, *J. Phys. Chem. Solids* **33** (1972) 1799.

[51]C. G. Fonstad and R. H. Rediker, *J. Appl. Phys.* **42** (1971) 2911.

[52]J. G. Bednorz and K. A. Müller, *Z. Physik B* **64** (1986) 189.

[53]J. Maier and G. Pfundtner, *Adv. Mater.* **30** (1991) 292.

[54]G. M. Choi and H. L. Tuller, *J. Am. Ceram. Soc.* **71** (4) (1988) 201.

[55]S. Stotz and C. Wagner, *Ber. Bunsenges. Phys. Chem.* **70** (1966) 781.

[56]H. Iwahara, T. Esaka, H. Uchida and N. Maeda, *Solid State Ionics* **314** (1981) 259.

[57]R. Waser, *Ber. Bunsenges. Phys. Chem.* **90** (1980) 1223.

[58]Y. Larring and T. Norby, *Solid State Ionics* **77** (1995) 147.

[59]K. D. Kreuer, *Chem. Mater.* **8** (1996) 610.

[60]K.-D. Kreuer, E. Schönherr and J. Maier, *Solid State Ionics* **70/71** (1994) 278.

[61]W. Münch, K.-D. Kreuer, G. Seifert and J. Maier, *Solid State Ionics* **136-137** (2000) 183; M. Tuckermann, L. Laasonen, M. Sprik and M. Parrinello, *J. Phys.: Condens. Matter.* **6** (Supl. 23A) (1994) 99.

[62]A. S. Nowick, *Solid State Ionics* **77** (1995) 137.

[63]R. Waser, *J. Am. Ceram. Soc.* **74** (1991) 1934.

[64]D. M. Smyth, M. P. Harmer and P. Peng, *J. Am. Ceram. Soc.* **72** (1989) 2276.

[65]K. Sasaki and J. Maier, *J. Appl. Phys.* **86** (10) (1999) 5422.

[66]K. Sasaki and J. Maier, *J. Appl. Phys.* **86** (10) (1999) 5434.

[67]J. Maier, *Phys. Chem. Chem. Phys.* **5** (2003) 2164.

[68]I. Denk, W. Münch and J. Maier, *J. Am. Ceram. Soc.* **78**(12) (1995) 3265.

[69]N. Bjerrum, *Kgl. Danske Videnskab. Selskab. Mat. Fys. Medd.* **7** (1926) 3.

[70]P. Debye and E. Hückel, *Phys. Z.* **24** (1923) 185; 305.

[71]See textbooks on electrochemistry.

[72]J. B. Wachtman and W. C. Corvin, *J. Res. Nat. Bur. Std.* **69 A** (1965) 457.

[73]M. B. Armand, *Solid State Ionics* **9/10** (1983) 745; P. G. Bruce, J. Evans and C. A. Vincent, *Solid State Ionics* **28-30** (1988) 918.

[74]J. J. Markham, *F-Centres in Alkali Halides,* Academic Press, New York, 1966.

[75]S. M. Sze, *Physics of Semiconductor Devices,* Wiley-Interscience, New York, 1981.

[76]T. Bieger, J. Maier and R. Waser, *Ber. Bunsenges. Phys. Chem.* **97** (1993) 1098.

[77]J. Maier, *Chem. Eur. J.* **7** (22) (2001) 4762.

[78]W. Buckel, *Supraleitung,* VCH, Weinheim, 1990.

[79]J. O'M. Bockris and A. K. V. Reddy, *Modern Electrochemistry,* Plenum Press, New York, 1970.

[80]J. K. Aboague and R. S. Friauf, *Phys. Rev. B* 11(4) (1975) 1654; R. S. Friauf, *J. Phys. (Paris)* **38** (1977) 1077, *J. Phys. Paris Colloq.* **41** (1980) C6-97.

[81]N. Hainovsky and J. Maier, *Phys. Rev. B* **51**(22) (1995) 15789.

[82]J. Maier and W. Münch, *Z. Anorg. Allg. Chem.* **626** (2000) 264.

[83]A. R. Allnatt and M. H. Cohen, *J. Chem. Phys.* **40** (1964) 1860, 1871; R. A. Sevenich and K. L. Kliewer, *J. Chem. Phys.* **48** (1964) 3045; A. R. Allnatt, E. Loftus and L. A. Rowley, *Crystal Lattice Defects* **3** (1972) 77.

[84]J. G. Ghosh, *J. Chem. Soc.* **113** (1918) 707.

[85]N. H. March and M. P. Tosi, *J. Phys. Chem. Solids* **46** (1985) 757.

[86]F. Zimmer, P. Ballone, J. Maier and M. Parrinello, *J. Chem. Phys.* **112**(14) (2000) 6416.

[87]F. Zimmer, P. Ballone, M. Parrinello and J. Maier, *Solid State Ionics* **127** (2000) 277.

[88]R. Merkle and J. Maier, *Phys. Chem. Chem. Phys.,* **5**(11) (2003) 2297.

[89]The fact that attractive interaction can lead to phase transition is a well-established result of the theory of phase transition and has been referred to in the case of superionic free situations by a variety of authors.[285]

[90]E. F. Schubert, *Doping in III-V-Semiconductors,* Cambridge University Press, Cambridge, 1993.

[91]See e.g., H. Schilling, *Festkörperphysik,* Verlag Harri Deutsch, Thun, 1977.

[92]A direct proof of Eq. (67) for the case of ionic crystals is given in Ref.[286]. Mass action laws are locally still valid, since then the $\Delta\phi$-term in $\Sigma v_j\tilde{\mu}_j$ disappears because of

$$\Sigma_j v_j z_j = 0 \ .$$

[93]In the literature sometimes the statement is made that the Poisson-Boltzmann equation is only compatible with electrostatics if linearized, which is not correct. The argument refers to the superposition principle which relies on the presupposed linearity of Poisson's equation. Note, however, that Poisson's equation is not linear if the charge density depends on ϕ itself in a non-linear way as it is the case here.

[94]J. Maier, Prog. *Solid St. Chem.* **23**(3) (1995) 171.

[95]G. Gouy, *J. Physique* **9** (1910) 457; D. L. Chapman, *Phil. Mag.* **25** (1913) 475.

[96]D. C. Grahame, *Chem. Rev.* **41** (1947) 441.

[97]S. M. Sze, *Semiconductor Devices,* John Wiley & Sons, New York, 1985.

[98]G. E. Pike, *Phys. Rev. B* **30** (1984) 795; G. E. Pike and C. H. Seager, *J. Appl. Phys.* **50** (1979)3414.

[99]K. Bohnenkamp and H.-J. Engell, *Z. Elektrochem.* **61** (1957) 1184, VCH, Weinheim.

[100]I. Denk, J. Claus and J. Maier, *J. Electrochem. Soc.* **144**(10) (1997) 3526.

[101]J. Jamnik, *Appl. Phys.* **A55** (1992) 518.

[102]R. D. Armstrong and R. Mason, *J. Electroanal. Chem.* **41** (1973) 231.

[103]R. D. Armstrong and B. R. Horrocks, *Solid State Ionics* **94** (1997) 181.

[104]J. Jamnik, H.-U. Habermeier and J. Maier, *Physica B* **204** (1995) 57.

[105]S. Kim, J. Fleig and J. Maier, *Phys. Chem. Chem. Phys.* **5** (11) (2003) 2268.

[106]C. C. Liang, *J. Electrochem. Soc.* **120** (1973) 1298.

[107]K. Shahi, J. B. Wagner. *Appl. Phys. Lett.* **37** (1980) 757.

[108]J. Maier, *J. Electrochem. Soc.* **134** (1987) 1524.

[109]J. Maier, *J. Phys. Chem. Solids* **46** (1985) 309.

[110]Y. Saito, K. Hariharan and J. Maier, *Solid State Phenomena* **39-40** (1994) 235.

[111]A. Bunde, W. Dieterich and E. Roman, *Solid State Ionics* **18/19** (1986) 147; E. Roman, A. Bunde and W. Dieterich, *Phys. Rev. B* **34** (1986) 331; P Knauth, G. Albinet and J. M. Debierre, *Ber. Bunsenges. Phys. Chem.* **98**(7) (1998) 945; J. C. Wang, N. J. Dudney, *Solid State Ionics* **18/19** (1986) 112.

[112]J. Maier and B. Reichert, *Ber. Bunsenges. Phys. Chem.* **90** (1986) 666.

[113]J. Maier, Mater. *Chem. Phys.* **17** (1987) 485.

[114]U. Lauer and J. Maier, *J. Electrochem. Soc.* **139** (5) (1992) 1472.

[115]J. Maier, *Ber. Bunsenges. Phys. Chem.* **93** (1989) 1468; 1474.

[116]F. Croce, G. B. Appetecchi, L. Persi and B. Scrosati, *Nature* **394** (1998) 456; W. Wieczorek, Z. Florjanczyk and J. R. Stevens, *Electrochim. Acta* **40**(13-14) (1995) 2251. The effect can be even seen when the polymer is replaced by a liquid solvent ("soggy sand electrolytes") cf. Ref.[202].

[117]J. Maier, *Ber. Bunsenges. Phys. Chem.* **89** (1985) 355.

[118]U. Lauer and J. Maier, *Ber. Bunsenges. Phys. Chem.* **96** (1992) 111.

[119]N. Sata, K. Eberman, K. Eberl and J. Maier, *Nature* **408** (2000) 946.

[120]J. Maier, *Ber. Bunsenges. Phys. Chem.* **90** (1986) 26.

[121]J. Fleig and J. Maier, *Solid State Ionics* **86-88** (1996) 1351.

[122]A. S. Skapin, J. Jamnik and S. Pejovnik, *Solid State Ionics* **133** (2000) 129.

[123]Y. Saito and J. Maier, *J. Electrochem. Soc.* **142**(9) (1995) 3078.

[124]J. Maier, U. Lauer, *Ber. Bunsenges. Phys. Chem.* **94** (1990) 973.

[125]M. Holzinger, J. Fleig, J. Maier and W. Sitte, *Ber. Bunsenges. Phys. Chem.* **99**(11) (1995) 1427.

[126]*Sensors, A Comprehensive Study,* Ed. by W. Göpel, J. Hesse, J. N. Zemel, VCH, Weinheim, 1987.

[127]G. Simkovich and C. Wagner, *J. Catal.* **1** (1967) 340.

[128]J. Maier and P. Murugaraj, *Solid State Ionics* **40/41** (1990) 1017.

[129]F. Besenbacher, I. Chorkendorff, B. S. Clausen, B. Hammer, A. Molenbrock, J. K. Norskøv and I. Stensgaard, *Science* **279** (1998) 1913.

[130]G. C. Vayenas, S. Bebelis and S. Neophytides, *J. Phys. Chem.* **92** (1988) 5085.

[131]R. Hagenbeck and R. Waser, *Acta Mater.* **48** (2000) 797.

[132]Y.-M. Chiang and T. Tagaki, *J. Am. Ceram. Soc.* **73** (1990) 3278.

[133]R. Moos and K. H. Härdtl, *J. Appl. Phys.* **80** (1996) 393.

[134]X. Guo, J. Fleig and J. Maier, *J. Electrochem. Soc.* **148**(9) (2001) J50.

[135]X. Guo, W. Sigle and J. Maier, *J. Am Ceram. Soc.* **86**(1) (2003) 77.

[136]S. Kim and J. Maier, *J. Electrochem. Soc.* **149**(10) (2002) J73.

[137]N. M. Beekmans and L. Heyne, *Electrochim. Acta* **21** (1976) 303.

[138]S. H. Chu and M. A. Seitz, *J. Solid State Chem.* **23** (1978) 297.

[139]D. Bingham, P. W. Tasker and A. N. Cormack, *Philos. Mag. A* **60** (1989) 1.

[140]X. Guo, *Solid State Ionics* **96** (1997) 247.

[141]M. J. Verkerk, B. J. Middelhuis and A. J. Burggraaf, *Solid State Ionics* **6** (1982) 159.

[142]M. Leonhardt, J. Jamnik and J. Maier, *Electrochemical and Solid-State Letters,* **2** (1999) 333.

[143]J. Jamnik, X. Guo, J. Maier, *Appl. Phys. Lett.* **82**(17) (2003) 282.

[144]R. Hagenbeck and R. Waser, *J. Appl. Phys.* **83** (1998) 2083.

[145]J. Jamnik, J. Maier, S. Pejovnik, *Solid State Ionics* **75** (1995) 51.

[146]Structural changes, i.e., changes in the bond lengths can be of longer range in the case of hard materials and in the case of pronounced misfit, in particular for epitaxial films. Effects of longer range are also expected for polar surfaces.[147] Higher dimensional defects can largely contribute to the absorption of "mechanical" stress.

[147]E. Heifets, E. A. Kotomin, *J. Maier, Surf. Sci.* **462** (2000) 19; E. Heifets, R. I. Eglitis, E. A. Kotomin, J. Maier and G. Borstel, *Phys. Rev. B* **64** (2001) 23417.

[148]J. Maier, *Solid State Ionics* **23** (1987) 59.

[149]J. Maier, *Phys. Stat. Sol.* (a) **112** (1989) 115.

[150]J. Maier, *Solid State Ionics* **148** (2002) 367.

[151]J. Maier, *Solid State Ionics* **154-155** (2002) 291.

[152]J. Maier, *Proc. Electrochem. Soc.,* in press.

[153]Cubic clusters do usually not represent the equilibrium situation even for large crystals, nor is it represented by spheres. Owing to different free energies of crystallographically different interfaces or edges (more exactly interface and edge tensions γ_s, χ_t) the minimization of the total thermodynamic potential requires:[287]

$$\frac{1}{h_s}\left(\gamma_s + \Sigma_t \frac{\partial L_t}{\partial a_s} \chi_t \right) = \text{const.}$$

If we ignore edge tensions, the well-known Wulff-shape results for constant interfacial tensions.[27] This presumed constancy and the neglect of edges limits the validity of the Wulff-concept to small dimensions, while, for large crystals, a limit to its realization is given by the high kinetic demands. So it is not surprising that the Wulff-shape is not often found (not to mention the fact that contacts by condensed phases additionally change the thermodynamics).[288] In a polycrystal global morphological equilibrium is not established anyway, and we can only rely on local equilibration effects. If the anisotropy of the interfacial tensions is negligible, the equilibrium shape of a single crystal is a sphere, while in a "mean-field" ceramic the grain-shape is close to tetrakaidecahedron.[19] Its shape fulfills best the space requirements and the conditions of local equilibrium (e.g., contact angle of 120° at a three-grain contact). Since obviously more specific situations do not very significantly change the picture or lead to very individual corrections we go back to the simple bricklayer model and to Eq. (90). As far as the overall conductance effect is concerned, the bricklayer model also works surprisingly well for more complicated microstructures. For a consideration of its limits cf. Ref.[289,290]

[154]W. Puin, S. Rodewald, R. Ramlau, P. Heitjans and J. Maier, *Solid State Ionics* **131**(1, 2) (2000) 159.

[155]N. Sata, N. Y. Jin-Phillipp, K. Eberl and J. Maier, *Solid State Ionics* **154-155** (2002) 497.

[156]X. X. Guo, N. Sata and J. Maier, *Electrochim. Acta* **49**(7) (2004)1091.

[157]N. Y. Jin-Phillipp, N. Sata, J. Maier, C. Scheu, K. Hahn, M. Kelsch and M. Rühle, *J. Chem. Phys.* **120**(5) (2004) 2375.

[158]There are some reports on an enhanced ionic conductivity of nano-sized ZrO_2 films; whether this is due to mobility effects (core or elastic strain, in particular in epitaxial films) or to proton conductivity is to be clarified.[291]

[159]A. Tschöpe, E. Sommer and R. Birringer, *Solid State Ionics* **139** (2001) 255; A. Tschöpe, *Solid State Ionics* **139** (2001) 267, Y. Chiang, E. B. Lavik, I. Kosacki, H. L. Tuller and J. Y. Ying, *Appl. Phys. Lett.* 69 (1996) 8.

[160]R. A. De Souza, J. Fleig, J. Maier, O. Kienzle, Z. Zhang, W. Sigle, and R. Rühle, *J. Am. Ceram. Soc.* **86**(6) (2003) 922.

[161]J. Jamnik and J. Maier, *Phys. Chem. Chem. Phys.,* **5**(23) (2003) 5215.

[162]J. Schoonman, *Solid State Ionics* **135-137** (2000) 5.

[163]T. P. Martin, in *Festkörperprobleme,* Ed. by P. Grosse, Vieweg, Braunschweig, 1984, Vol. XXIV, pp. 1; *Phys. Reps.* **95** (1983) 167, Elsevier, Amsterdam.

[164]H. G. Fritsche, *Phys. Stat. Sol. (b)* **154** (1989) 603.

[165]R. J. Haug, K. von Klitzing, *FED--Journal* **6** (1995) 4; *Low Dimensional Structures Prepared by Epitaxial Growth or Growth on Patterned Substrates,* Ed. by K. Eberl and P. M. Petroff, Proc. NATO Advanced Res. Workshop, Ringberg, Kluwer, Dordrecht, 1995; *Growth and Characterisation of Semiconductors,* P. C. Klipstein and R. A. Stradling, Hilger, Bristol, 1990; K. Ploog, in *Semiconductor Interfaces: Formation and Properties,* Ed. by G. LeLay, J. Denien, and N. Boccara (Hrsg.), Springer-Verlag, Berlin, 1987.

[166]I. Lubomirsky, J. Fleig and J. Maier, *J. Appl. Phys.* **92** (2002) 6819.

[167]E. L. Brus, J. Chem. Phys. 80 (1984) 4403.

[168]R. Lipowsky, *Phasenübergänge an Oberflächen* (IFF-Ferienkurs), Forschungszentrum Jülich GmbH, 1993, pp. 9.1; *Springer Tracts in Mod. Phys.,* Vol. 127; R. Lipowsky, *J. Appl. Phys.* **55** (1984) 2485.

[169]J.-S. Lee, St. Adams and J. Maier, *Solid State Ionics* **136-137** (2000) 1261.

[170]P. Poizot, S. Laruelle, S. Grugeon, L. Dupont and J. M. Tarascon, *Nature* **407** (2000) 496.

[171]H. Li, G. Richter and J. Maier, *Adv. Mater.* **15** (2003) 736.

[172]J. Maier, *Solid State Ionics* **112** (1998) 197.

[173]C. Wagner, *Prog. Solid St. Chem.* **10** (1975) 3.

[174]L. Heyne in *Solid Electrolytes* Ed. by S. Geller, Springer-Verlag, Berlin, 1977, pp. 137.

[175]J. Maier, *J. Am. Ceram. Soc.* **76(5)** (1993) 1212, 1218, 1223, 1228.

[176]R. A. Marcus, *Ann. Rev. Phys.* **15** (1964) 155; *J. Phys. Chem.* **95** (1991) 2010.

[177]H. Schmalzried, *Chemical Kinetics of Solids,* VCH, Weinheim, 1995.

[178]L. Onsager, *Phys. Rev.* **37** (1931) 405; **38** (1931) 2265.

[179]Note that a charge free zone between x and x′ leads to a linear course of $\phi(x)$ owing to Poisson's equation.

[180]R. Parsons, *Trans. Faraday Soc.* **47**(1951) 1332.

[181]W. Nernst, *Z. phys. Chem.* **2** (1888) 613.

[182]T. de Donder, *Bull. Acad. Roy. Belg. (Cl. Sc.)* **28** (1942) 496; S. R. de Groot, *Thermodynamics of Irreversible Processes,* North Holland Publ., Amsterdam, 1951.

[183]I. Prigogine and P. Glansdorff, *Structure, Stability and Fluctuations,* Wiley, London, 1971. Care has to be taken with respect to the definition of the boundary conditions (see Ref.[23]). The principle refers to the value intergrated over a volume at the boundary surfaces of which the μ^ρ's are kept constant.

[184] G. H. Weiss, in *Fractals in Science,* Ed. by A. Bunde and S. Havlin, Springer-Verlag, Berlin, 1994; G. Daccord, R. Lenormand, *Nature* **325** (1987) 41.

[185] A. D. Le Claire and A. B. Lidiard, *Phil. Mag.* **1** (1956) 1; A. D. LeClaire, *Brit. J. Appl. Phys.* **14**(1963)351.

[186] P. Müller, *phys. stat. sol.* **12** (1965) 775.

[187] L. W. Stock, *Z. phys. Chem.* **B25** (1934) 441; R. Cava, F. Reidinger, B. J. Wuensch, *Solid State Commun.* **24** (1977) 411.

[188] B. Ma, J. P. Hodges, J. D. Jorgensen, D. J. Miller, J. W. Richardson Jr and U. Balachandran, *J. Solid State Chem.* **141** (1998) 576.

[189] Data complied by K. Sasaki after: T. Kudo and K. Fueki, *Solid State Ionics,* Kodansha, 1990, and references therein; A. Rabenau, *Solid State Ionics* **6** (1982) 277; K. D. Kreuer, Chem. Mater. **8** (1996) 610 and references therein; K. D. Kreuer, Th. Dippel, J. Maier, in Proc. Electrochem. Soc., Pennington (NJ), 1995, Vol. PV 95-23, pp. 241; K. Schmidt-Rohr, J. Clauss, B. Blümich and H. W. Spiess, *Magn. Reson. in Chem.* **28** (1990) 3; K. D. Kreuer, *Solid State Ionics* **97** (1997) 1; H. Iwahara, T. Esaka, H. Uchida and N. Maeda, *Solid State Ionics* **3/4** (1981) 539; B. C. H. Steele, *Solid State Ionics* **75** (1995) 157; T. Takahashi, H. Iwahara and T. Esaka, *J. Electrochem. Soc.* **124** (1977) 1563; T. Ishihara, H. Furutani, H. Nishiguchi and Y. Takita, in *Ionic and Mixed Conducting Ceramics III,* Ed. by T.A. Ramanarayanan, W.L. Worrell, H.L. Tuller, M. Mogensen, and A.C. Khandkar, The Electrochemical Society, Pennington (NJ), 1994, Vol. PV 94-22, pp. 834; T. Ishihara, H. Matsuda and Y. Takita, *J. Am. Ceram. Soc.* **116** (1994) 3801; J. B. Goodenough, J. E. Ruiz-Diaz and Y. S. Zhen, *Solid State Ionics* **44** (1990) 21; I. Kontoulis, Ch. P. Ftikos and B. C. H. Steele, *Mater. Sci. Eng.* **B22** (1994) 313; H. L. Tuller, *Solid State Ionics* **94** (1997) 63; J. T. Kummer, *Prog. Solid St. Chem.* **7** (1972) 141; G. Farrington, B. Dunn, *Solid State Ionics* **7** (1982)287.

[190] S. Chandra, *Superionic Solids,* North-Holland, Amsterdam, 1981; *Superionic Solids and Solid Electrolytes,* Ed. by S. Chandra and A. S. Laskar, Academic Press, New York, 1989.

[191] O. Yamamoto, Y. Takedo and R. Kanno, *Kagaku* **38** (1983) 387, Kagaku-Dojin Publishing Company, Kyoto.

[192] K. D. Kreuer, W. Münch, U. Traub and J. Maier, *Ber. Bunsenges. Phys. Chem.* **102** (1998) 552.

[193] C. A. Vincent, *Chemistry in Britain,* April, 1981, pp. 391.

[194] B. Scrosati, in *Lithium Ion Batteries,* Ed. by M. Wakihara and O. Yamamoto, VCH, Weinheim, 1998.

[195] H. J. van Daal, *Solid State Commun.* **6** (1968) 5, Elsevier, Amsterdam.

[196] R. J. Cava, R. B. van Dover, B. Batlogg and E. A. Rietman, *Phys. Rev. Lett.* **58** (1987) 408, The American Physical Society, College Park (MD).

[197] J. C. Philips, *Physics of High Temperature Superconductors,* Academic Press, New York, 1989.

[198] C. A. Beevers and M. A. R. Ross, *Z. Krist.* **95** (1937) 59; J. T. Kummer, *Prog. Solid St. Chem.* **7** (1972) 141.

[199] K.-D. Kreuer, A. Fuchs, M. Ise, M. Spaeth and J. Maier, *Electrochim. Acta* **43**(10-11) (1998) 1281.

[200] P. Maass, M. Meyer, A. Bunde and W. Dieterich, *Phys. Rev. Lett.* **77** (1996) 1528; P. Pendzig, W. Dieterich and A. Nitzan, *J. Non-Cryst. Solids* **235-237** (1998) 748.

[201] M. B. Armand, *Ann. Rev. Mat. Sci.* **6** (1986) 245; M. A. Ratner and D. F. Shriver, *Mater. Res. Bull.* **14** (1989) 39.

[202] A. Bhattacharyya and J. Maier, *Advanced Materials,* in press.

[203]O. Madelung, *Introduction to Solid State Theory,* Springer-Verlag, Berlin, 1978.

[204]R. E. Peierls, *Quantum Theory of Solids,* Clarendon Press, Oxford, 1955.

[205]J. R. Manning, *Diffusion Kinetics for Atoms in Crystals,* Van Nostrand, Princeton, 1968; A. D. Le Claire and A. B. Lidiard, *Phil. Mag.* **1** (1956) 1.

[206]R. Dieckmann and H. Schmalzried, *Ber. Bunsenges. Phys. Chem.* **81** (1977) 344.

[207]R. A. De Souza and J. A. Kilner, *Solid State Ionics* **106** (1998) 175.

[208]J. Maier, in preparation.

[209]Since we only allow for small driving forces $\Delta\mu_O$, this implies large chemical capacitances $\partial c_O / \partial \mu_O$; a relevant example is the high temperature superconductor $YBa_2Cu_3O_{7-\delta}$.

[210]R. Metselaar and P. K. Larsen, *J. Phys. Chem. Solids* **37** (1976) 599.

[211]K. Sasaki and J. Maier, *Phys. Chem. Chem. Phys.* **2** (2000) 3055; K. Sasaki and J. Maier, *Solid State Ionics* **134** (2000) 303.

[212]I. Denk, U. Traub, F. Noll and J. Maier, *Ber. Bunsenges. Phys. Chem.* **99** (1995) 798; M. Leonhardt, Ph D thesis, University of Stuttgart, 1999.

[213]H. S. Carslaw and J. C. Jäger, *Conduction of Heat in Solids,* Clarendon Press, Oxford, 1959.

[214]I. Denk, Ph D thesis, University of Stuttgart, 1995; I. Denk, F. Noll and J. Maier, *J. Am. Ceram. Soc.* **80** (2) (1997) 279.

[215]G. Pfundtner, Ph D thesis, University of Tübingen, 1993.

[216]M. Spaeth, K. D. Kreuer, C. Cramer and J. Maier, *J. Solid St. Chem.* **148** (1999) 169.

[217]K. Funke and I. Riess, *Z. phys. Chem. Neue Folge* **140** (1984) 217; K. Funke, *Solid State Ionics* **94** (1997) 27.

[218]K. Funke, Prog. *Solid St. Chem.* **22** (1993) 11.

[219]K. Funke, R. D. Banhatti, S. Brückner, C. Cramer, C. Krieger, A. Mandanici, C. Martiny and I. Ross, *Phys. Chem. Chem. Phys.* **4** (14) (2002) 3155.

[220]W. Dieterich and P. Maass, *Chem. Phys.* **284** (2002) 439.

[221]J. A. Bruce and M. D. Ingram, *Solid State Ionics* **9/10** (1983) 717.

[222]G. V. Chandrashekar and L. M. Foster, *Solid State Commun.* **27** (1978) 269.

[223]P. K. Davies, G. I. Pfeiffer and S. Canfield, *Solid State Ionics* **18/19** (1996) 704.

[224]M. Tatsumisago, Y. Akamatsu, T. Minami, *Mater. Sci. Forum* **32-33** (1988) 617.

[225]H. Hrugchka, E. E. Lissel and M. Jansen, *Solid State Ionics* **28-30** (1988) 159

[226]J. A. Bruce, R. A. Howic and M. D. Ingram, *Solid State Ionics* **18/19** (1986) 1129, Elsevier, Amsterdam.

[227]M. Meyer, V. Jaenisch, P. Maass and A. Bunde, *Phys. Rev. Lett.* **76** (1996) 2338.

[228]A. Bunde, *Solid State Ionics* **105** (1981) 1; A. Bunde, M. D. Ingram, P. Maass, *J. Non-Cryst. Solids* **172/174** (1994) 1222.

[229]S. Rodewald and J. Maier, unpublished.

[230]M. Martin and H. Schmalzried, *Solid State Ionics* **20** (1986) 75; H. I. Yoo, H. Schmalzried, M. Martin and J. Janek, *Z. phys. Chem. Neue Folge* **168** (1990) 129.

[231]J. Maier, *J. Am. Ceram. Soc.* **76** (1993) 1223.

[232]J. Maier, G. Schwitzgebel, *phys. stat. sol. (b)* **113** (1982) 535.

[233]This representation of "Conservative Ensembles" was used by M. H. R. Lankhorst, H. J. M. Bouwmeester and H. Verweij, in *Electroceramics IV,* Ed. by R. Waser, S. Hoffmann, D. Bonnenberg, Ch. Hoffmann, Augustinus Buchhandlung, Aachen, 1994, Vol. II, pp. 697.

[234]J. Claus, I. Denk, M. Leonhardt and J. Maier, *Ber. Bunsenges. Phys. Chem.* **101**(9) (1997) 1386.

[235]M. Widere, W. Münch, Y. Larring and T. Norby, *Solid State Ionics* **154-155** (2002) 669.

[236] J. Claus, I. Denk, M. Leonhardt and J. Maier, *Ber. Bunsenges. Phys. Chem.* **101** (1997) 1386.

[237] R. I. Merino, N. Nicoloso, J. Maier, in *Ceramic Oxygen Ion Conductors and Their Technological Applications,* Ed. B. C. H. Steele, British Ceram. Proc., The Institute of Materials, Cambridge, 1996, pp. 43; K. Sasaki and J. Maier, *Solid State Ionics* **134** (2000) 303.

[238] J. Maier, in *Ionic and Mixed Conducting Ceramics,* Ed. by T. A. Ramanarayanan, W. L. Worrell and H. L. Tuller, The Electrochemical Society, Pennington (NJ), 1994, Vol. PV 94-12, pp. 542; J. Maier and W. Münch, *J. Chem. Soc. Faraday Trans.* **92**(12) (1996) 2143.

[239] J. Jamnik, B. Kamp, R. Merkle and J. Maier, *Solid State Ionics,* **150** (2002) 157.

[240] H. Schmalzried and J. Janek, *Ber. Bunsenges. Phys. Chem.* **102** (1998) 127.

[241] R. T. Whipple, *Phil. Mag.* **45** (1954) 1225; A. D. LeClaire, *Brit. J. Appl. Phys.* **14** (1963) 351; Y.-Ch. Chung and B. J. Wuensch, *J. Appl. Phys.* **79** (1996) 8323; O. Preis and W. Sitte, *J. Appl. Phys.* **79** (1996) 2986.

[242] J. Daniels, K. H. Hardtl, D. Hennings and R. Wernicke, *Philips Res. Repts.* **31** (1978) 489.

[243] R. Meyer and R. Waser, *J. Eur. Ceram. Soc.* **21**, (2001)1743.

[244] J. Jamnik and J. Maier, *Ber. Bunsenges. Phys. Chem.* **101**(1) (1997) 23; J. Jamnik and J. Maier, *J. Phys. Chem. Solids* **59**(9) (1998) 1555.

[245] J. Jamnik, in *Solid State Ionics: Science & Technology,* Ed. by B. V. R. Chowdari, K. Lal, S. A. Agnihotry, N. Khare, S. S. Sekhon, P. C. Srivastava and S. Chandra, World Scientific Publishing Co., Singapore, 1998, pp. 13.

[246] J. D. Eshelby, C. W. A. Newey, P. L. Pratt and A. B. Lidiard, *Phil. Mag.* **3**(25) (1958) 75; A. Atkinson, *Adv. Ceram.* **23** (1987) 3; *Solid State Ionics* **28-30** (1988) 1377.

[247] J. Jamnik, J. Fleig, M. Leonhardt and J. Maier, *J. Electrochem. Soc.* **147** (8) (2000) 3029.

[248] J. Maier, *Solid State Ionics* **135**(1-4) (2000) 575.

[249] J. Maier, in *Oxygen Ion and Mixed Conductors and their Technological Applications,* Ed. by H. L. Tuller, J. Schoonman and I. Riess, NATO Science Series: E Applied Sciences, Kluwer Academic Publishers, Dordrecht, Vol. 368, (2000) pp. 75.

[250] M. Leonhardt, Ph D thesis, Stuttgart, 1999.

[251] T. Bieger, J. Maier and R. Waser, *Ber. Bunsenges. Phys. Chem.* **97** (1993) 1098.

[252] J. Maier, *Solid State Ionics* **112** (1998) 197.

[253] J. Maier, *Mat. Res. Soc. Proc.* **548** (1999) 415.

[254] M. Leonhardt, R. A. De Souza, J. Claus and J. Maier, *J. Electrochem. Soc.* **149**(2) (2002) J19; R. A. De Souza, J. Fleig, R. Merkle, and J. Maier, *Z. Metallkd.* **94**(3) (2003) 218.

[255] R. Merkle and J. Maier, *Phys. Chem. Chem. Phys.* **4**(17) (2002) 4140.

[256] D. Y. Wang and A. S. Nowick, *J. Electrochem. Soc.* **126** (1979) 1155; D.Y. Wang and A. S. Nowick, *J. Electrochem. Soc.* **126** (1979) 1166.

[257] V. Brichzin, J. Fleig, H.-U. Habermeier and J. Maier, *Electrochemical and Solid-State Letters* **3** (9) (2000) 403.

[258] R. P. Buck and C. Mundt, *Electrochim. Acta* **44** (1999) 1999.

[259] D. R. Franceschetti, *Solid State Ionics* **70/71** (1994) 542.

[260] G. C. Barker, *J. Electroanal. Chem.* **41** (1973) 201; T. R. Brumleve and R. P. Buck, *J. Electroanal. Chem.* **126** (1981) 73.

[261] J. R. Macdonald, *J. Chem. Phys.* **58** (1973) 4982.

[262] J. R. Macdonald and D. R. Franceschetti, *J. Chem. Phys.* **68** (1978) 1614.

[263]J. Jamnik and J. Maier, *Phys. Chem. Chem. Phys.* **3** (2001) 1668; J. Jamnik, *Solid State Ionics* **157** (2003) 19.

[264]J. Maier, *Z. Physik Chemie N. F.* **140** (1984) 191.

[265]C. Wagner, *J. Electrochem. Soc.* **103** (1956) 571.

[266]C. Gensch and K. Hauffe, *Z. phys. Chem.* **196** (1951) 427.

[267]W. Ebeling, *Strukturbildung bei irreversiblen Prozessen,* B. G. Teubner, Leipzig, 1976.

[268]J. Meixner, *Z. Naturforschung* **4A** (1949) 594; G. Nicolis and I. Prigogine, *Self-Organisation in Non-Equilibrium Systems,* John Wiley & Sons, New York, 1971.

[269]M. Eigen, P. Schuster, *The Hypercycle,* Springer-Verlag, Heidelberg, 1979.

[270]M. Eigen, *Naturwiss.* **58** (1971) 465.

[271]E. Schöll, *Phase Transitions in Semiconductors,* Springer-Verlag, Berlin, 1987.

[272]S. H. Koenig, R. D. Brown and W. Schillinger, *Phys. Rev.* **128** (1962) 1668; M. E. Cohen and P. T. Landsberg, *Phys. Rev.* **154** (1967) 683; A. E. McCombs and A. G. Milnes, *Int. J. Electron.* **32** (1972) 361.

[273]S. W. Teitsworth, R. M. Westervelt and E. E. Haller, *Phys. Rev. Lett.* **51** (1983) 825.

[274]K. M. Mayer, R. Gross, J. Parisi, J. Peinke and R. P. Huebener, *Solid State Commun.* **63** (1987) 55.

[275]J. Janek and S. Majoni, *Ber. Bunsenges. Phys. Chem.* **99** (1995) 14.

[276]E. D. Wachsman, *J. Electrochem. Soc.* **149** (2002) A242.

[277]H. Meinhard and A. Gierer, *J. Cell. Sci.* **15** (1974) 312; H. Haken, *Synergetik,* Springer-Verlag, Berlin, 1990.

[278]T. Ihle and H. Müller-Krumbhaar, *Phys. Rev. E* **49** (1994) 2972.

[279]E. Kotomin and V. Kuzovkov, *Modern aspects of diffusion controlled reactions,* Elsevier, Amsterdam, 1996.

[280]B. Mandelbrot, *The Fractal Geometry of Nature,* Freeman, San Francisco, 1982.

[281]A. Bunde and S. Havlin, *Fractals and Disordered Systems,* Springer-Verlag, Berlin, 1996.

[282]G. Daccord and L. Lenormand, *Nature* **325** (1987) 41.

[283]J. Nittmann and H. E. Stanley, *Nature* **321** (1986) 663.

[284]E. Chassaing and B. Sapoval, *J. Electrochem. Soc.* **141** (1994) 2711; G. Daccord and R. Lenormand, *Nature* **325** (1987) 41.

[285]R. A. Huberman, *Phys. Rev. Lett.* **32** (1974) 1000; A. Bunde, *Z. Physik B* **36** (1980) 251; H. Schmalzried, *Z. phys. Chem. NF* **22** (1959) 199 and others.

[286]K. L. Kliewer and J. S. Koehler, *Phys. Rev. A* **140** (1965) 1226.

[287]A. I. Rusanov, *Phasengleichgewichte und Grenzflächenerscheinungen,* Akademie-Verlag, Berlin, 1978.

[288]R. Kaischew, *Bull. Acad. Bulg. Sci. Phys.* **1** (1950) 100; **2** (1951) 191.

[289]J. Fleig and J. Maier, *J. Electrochem. Soc.* **145** (6) (1998) 2081.

[290]T. Mason, *Mat. Res. Soc. Proc.,* in press.

[291]I. Kosacki, B. Gorman and H. U. Anderson, in *Ionic and Mixed Conductors,* Ed. by T. A. Ramanarayanan, W.L. Worrell, H. L. Tuller, M. Mogensen, and A. C. Khandkar, The Electrochemical Society, Pennington, NJ, 1998, pp. 631; I. Kosacki, talk given at EURODIM 2002, Wrocaw, Poland.